RECONSTRUCTING DYSOXIA IN THE GULF OF ALASKA AND THE EASTERN NORTH PACIFIC: SEVERITY, DURATION, AND DRIVERS

A Dissertation

by

SHARON

Submitted to the Office of Graduate and Professional Studies of
Texas A&M University
in partial fulfillment of the requirements for the degree of

DOCTOR OF PHILOSOPHY

Chair of Committee,	Christina Belanger
Committee Members,	Leah Levay
	Franco Marcantonio
	Brendan Roark
Head of Department,	Julie Newman

August 2021

Major Subject: Geology

ABSTRACT

High resolution paleoenvironmental studies in the Gulf of Alaska (GoA) were previously restricted to the last ~17,000 years, limiting our knowledge of oxygenation in the high latitude North Pacific. In this work, I develop a ~54,000 year-long record of co-registered benthic foraminiferal assemblages and redox sensitive metal concentrations (Mo/Al and U/Al) at Site U1419 in the upper OMZ of GoA to reconstruct the history of OMZ extent and intensity at multi-centennial resolution. Using multivariate analyses of total benthic foraminiferal assemblages, I develop quantitative dissolved oxygen estimates that are robust against differences in the benthic foraminiferal size fraction analyzed, replicate modern oxygenation patterns in the GoA, and are cross validated by redox sensitive metal concentrations. Two dysoxic events of comparable severity to the Bolling-Allerod were found during MIS 3.

On comparing taxonomically standardized benthic foraminiferal data across four sites in the North Pacific, I found that dysoxic events occurred basinwide around similar time intervals across the North Pacific and may have been linked to global climatic changes. In addition, the differences in the relative severities of dysoxia at different sites were enhanced by regional factors. GoA which is generally a better oxygenated site did become as dysoxic as the southern sites which are known for their lower oxygen. These studies are important because if happened in the past it may occur in the future of GoA as well.

Using paleoenvironment proxies to understand the relationship between different drivers and oxygen we found that dysoxia in the GoA during the glacial interval may have been associated with both surface productivity and warming/meltwater. The relationship between dysoxia and drivers during the deglacial was confounded by the influence of glacial-interglacial changes. However, it is possible that the similar drivers of dysoxia may have led to dysoxia during the deglacial as in the glacial interval. The Holocene in GoA has high relative abundances of opportunistic taxa which represent high surface productivity, if sufficient meltwater is introduced severe dysoxia can develop here. Quantitative estimates of paleo-oxygenation, such as those possible with benthic foraminiferal assemblages, are important for forecasting future oxygenation changes in OMZs and their potential impacts on the marine ecosystems.

DEDICATION

I would like to dedicate this PhD to my parents, my dad up in heaven Mr. Satwant Singh and my mother Mrs. Sheela Devi. They have always showered me with unconditional love, support, and comfort to make me what I am today.

ACKNOWLEDGEMENTS

I would like to sincerely express my gratitude to my mentor Dr. Christina Belanger for providing me with the opportunity to work with her; and guiding, encouraging, and inspiring me in every step of my PhD. I learned a lot from her and am very grateful for her time and effort. I would also like to thank my committee members Dr. Leah Levay, Dr. Franco Marcantonio, and Dr. Brendan Roark for their support and feedback on my work.

Also, I am deeply thankful to my father Mr. Satwant Singh and my mother Mrs. Sheela Devi for making me who I am today and for always encouraging me to work and study hard. My father always challenged me to grow and reach for the stars. Unfortunately, he passed away in September 2019, but his words gave me the strength to never give up what I began.

I would also like to thank my best friend, family, refuge, and emotional support in the States Dr. Hari Chapagain who was with me every step of my PhD journey. It would have not been possible without him. I am very grateful to my best friends Akriti Sharma, Rashid Khan and other friends in India who always inspired strength in me during my tougher times. I would also like to thank my brother Solomon and my little sister Sarah for being supportive siblings. In addition, I would like to sincerely thank my extended family in India who supported us so much after my dad passed away. I would also like to thank all my friends in the States who helped me on several occasions.

I would also like to thank the faculty and staff at Department of Geology at Texas A&M University (TAMU) and South Dakota School of Mines and Technology (SDSM&T). Special thanks to all the undergraduates at TAMU, SDSM&T and Oregon State University (OSU) who helped with the data collection. Thanks to National Science Foundation (NSF) for funding my PhD project and Integrated Ocean Discovery Program Expedition 341 team for providing the study cores.

Finally, I am grateful to Dr. Alan C. Mix and Dr. Jianghui Du of OSU for their contributions. I would also like to thank Jesse Muratli from the W.M. Keck Collaboratory for Plasma Spectrometry of OSU for assistance with digesting sediment samples and analyzing metal concentrations. I would also like to thank June Padman, Jennifer McKay, and Andy Ross for assistance with stable isotope analyses. Perry Chesebro, Ozlem Orhun, Adrian Sweeney, and Christopher Schiller at SDSM&T; and Pablo Cavazos and Calie Payne at TAMU assisted with fossil sample preparation. I am also thankful to two anonymous reviewers whose suggestions improved the manuscript included as chapter 2 in this work.

CONTRIBUTORS AND FUNDING SOURCES

Contributors

This dissertation work was supervised by the committee chair Dr. Christina Belanger of the Department of Geology at TAMU. Other committee members included Dr. Franco Marcantonio, Dr. Leah Levay from the Department of Geology and Dr. Brendan Roark of the Department of Oceanography.

The geochemical trace metal data analyzed for Chapter 2 was provided by Dr. Alan C. Mix and his student Dr. Jianghui Du of OSU. Part of the fossil sample preparation was done by Perry Chesebro, Ozlem Orhun, Adrian Sweeney, and Christopher Schiller at SDSM&T; and Dr. Christina Belanger, Pablo Cavazos and Calie Payne at TAMU.

All other work conducted for this dissertation was completed by the student independently.

Funding Sources

This work was supported by NSF 1502746 and 1801511 to Christina L. Belanger of TAMU and NSF 1360894 and 1502754 to Alan C. Mix of OSU.

TABLE OF CONTENTS

Page

LIST OF FIGURES

Page

LIST OF TABLES

Page

1. INTRODUCTION

Declining oxygen levels in the world oceans is becoming a major concern as it can be detrimental for the ecosystem and our society. Studying paleo-oxygenation and paleoenvironments can give us insights into what may occur in the future of our oceans. If low-oxygen (dysoxic) occurred in the past it may occur in the future if similar environmental drivers arise. Therefore, it is very important to study paleo-oxygenation. Previous studies in the Gulf of Alaska (GoA) record two dysoxic events in the deglacial during the Bølling-Allerød (B-A; 14.7-12.9 ka) and early Holocene (11.5-10.5 ka). These studies recorded the oxygenation history for ~17,000 years record in the GoA near the upper limit of the oxygen minimum zone (OMZ; Davies et al., 2011; Praetorius et al., 2015). Several hypotheses for the drivers of these dysoxic events were also introduced, however no clear causes of dysoxia were concluded. Here, I extend this record to ~54,000 years using samples collected by IODP Expedition 314 at Site U1419. High sedimentation rates allowed for excellent preservation of benthic foraminifera which can be used as a proxy to reconstruct paleo-oxygenation. In addition to benthic foraminifera, geochemical trace sensitive metals (Mo and U) data are also used to reconstruct low-oxygen events.

The main goal of the study in Chapter 2 is to determine whether dysoxic events also occurred during the glacial interval. If they did, were they as extreme as the deglacial dysoxic events? In Chapter 3, I compare the relative severity of dysoxic events that occurred around similar times across several sites in the eastern North Pacific. In Chapter

4, I determine whether the environmental drivers led to dysoxia in GoA were different in the glacial and deglacial intervals.

In Chapter 2, I reconstruct paleo-oxygenation for the whole ~54,000 year-long record using a multiproxy approach that used both benthic foraminiferal faunal methods and geochemical trace sensitive metals. I examine the relative abundances of benthic foraminifera in the >63 μm size fraction and use multivariate ordination analyses to identify the major gradients in faunal composition. Further, I develop a new quantitative metric for paleo-oxygenation which improves upon previous efforts by Ohkushi et al. (2013). I find several dysoxic events in the glacial interval and two were as severely dysoxic as the B-A and early Holocene dysoxic events. I also test whether the test size of the benthic foraminifera used in the analysis can affect the results of paleo-oxygenation reconstruction and found that size does affect the ordination analyses and the relative abundances of species indicative of high productivity, however species sensitive of oxygenation gradients reconstructed similar oxygenation trends in both the >63 μm size fraction and the >125 μm size fraction.

In Chapter 3, I compare the relative severity of dysoxic events across different sites in the eastern North Pacific. Here I examine which sites were the most dysoxic and place the deoxygenation at GoA into a broader context. I taxonomically standardize benthic foraminiferal data for four sites including GoA (U1419), Santa Barbara Basin (MD02-2303 and MD02-2304), and MD02-2508 in Baja Sur California and analyze all the data in a single ordination analyses, thus placing all samples on a common oxygenation scale for comparison. Interestingly, these faunal analyses demonstrate that GoA did become as

dysoxic as the southern sites nearer to the Eastern Tropical North Pacific OMZ. Placing the sites on a common scale also leads to reinterpretation of previously published records and I find that MD02-2508 stayed dysoxic throughout the 60,000-year record, contrary to the occasionally oxic conditions determined by the original authors (Tetard et al., 2017). The SBB sites record intermittent severe dysoxia but also had better oxygenated conditions similar to GoA during Younger Dryas and MIS 2 and MIS 3, consistent with previous authors (Cannariato et al., 1999).

In Chapter 4, I divide the 54, 000 years GoA record into two subsets to determine whether the drivers of dysoxia differed between the deglacial and glacial intervals. I use Pearson correlation and multi-regression techniques to understand the relationships between major gradients in faunal composition and independently measured environmental proxies representing temperature, salinity, oxygenation, and carbon cycle process. I further examine the relationships between paleo-oxygen proxies and other paleoenvironmental proxies to determine the best supported environmental predictors for changes in oxygenation. I find that dysoxia was related to high temperatures, low salinity, and high productivity, but that neither condition alone was sufficient to drive dysoxia – instead the interaction of warm, potentially fresher water, high productivity conditions drove low-oxygen conditions. These relationships are more evident in the glacial data than in the younger data set where large-scale environmental changes related to the glacial-interglacial transition confounded the relationships with temperature and productivity.

In summary, GoA had dysoxic events of similar severity during the glacial and deglacial intervals and oxygenation levels become as low as in the southern sites that are

known for developing severe dysoxia during the deglacial and during interstadial events during the glacial. The dysoxic events in the GoA during the glacial were likely caused by a combined effect of high productivity and warm temperatures. If conditions that are similar to the dysoxic events of the glacial interval occur in the present or future of GoA, dysoxic event as severe as the B-A can occur, which will be detrimental for the regional ecosystem and impact the fisheries that GoA communities highly rely upon. The faunal analyses herein show that high seasonal productivity that contributed to past dysoxic events currently occur in the modern GoA, thus only the increase in temperature would be necessary to trigger severe dysoxia.

2. RECONSTRUCTING PALEO-OXYGENATION FOR THE LAST 54,000 YEARS IN THE GULF OF ALASKA USING CROSS-VALIDATED BENTHIC FORAMINIFERAL AND GEOCHEMICAL RECORDS*

2.1. Introduction

Low-oxygen conditions occur naturally in fjords, upwelling zones, restricted basins, and at intermediate ocean depths within oxygen minimum zones (OMZs). The intensity and spatial extent of OMZs vary with changes in global climate, ocean circulation, and nutrient availability (Helly and Levin, 2004; Keeling et al., 2010; Deutsch et al., 2011). Since at least the 1960's, the global ocean oxygen inventory has declined, including within OMZ cores, and upper OMZ boundaries have shoaled (Whitney et al., 2007; Bograd et al., 2008; Pierce et al., 2012; Schmidtko et al., 2017; Ito et al., 2017). This expansion and intensification of OMZs are a major threat to ecosystem health (Helly and Levin, 2004; Diaz and Rosenberg, 2008; Gilly et al., 2013). In addition, changes in OMZ size and extent affect nutrient and carbon cycle processes with particular effects on deep-sea carbon storage with global climate consequences (Keeling et al., 2010; Gray et al., 2018).

The North Pacific contains the most extensive modern OMZ and the lowest minimum oxygen values in the ocean due to the longer circulation paths (Paulmier & Ruiz-

---

* An edited version of this paper was published by AGU. Copyright 2020 by American Geophysical Union. Sharon et al., (2021), Reconstructing Paleo-oxygenation for the Last 54,000 Years in the Gulf of Alaska Using Cross-validated Benthic Foraminiferal and Geochemical Records. *Paleoceanography and Paleoclimatology*, 36, e2020PA003986, DOI: 10.1029/2020PA003986. To view the published open abstract, go to https://doi/org/10.1029/2020PA003986.

Pino, 2009). North Pacific paleoceanographic records document changes in the extent of its OMZs since the Late Pleistocene including sites in Baja California, the California Margin, Santa Barbara Basin, East and South China Seas, Sea of Japan, Sea of Okhotsk, Bering Sea, the Cascadia Margin, and the southeastern margin of Alaska (Cannariato et al., 1999; Cannariato and Kennett, 1999; Mix et al., 1999; McKay et al., 2005; Shibahara et al., 2007; Cartapanis et al., 2011; Davies et al., 2011; Ohkushi et al., 2013; Bubenshchikova et al., 2015; Moffitt et al., 2014; Praetorius et al., 2015; Takahashi et al., 2016; Tetard et al., 2017; Li et al., 2018; Belanger et al., 2020; Saravanan et al.; 2020, Zou et al., 2020). In many of these records, low-oxygen events correspond to warmer periods, such as the Bølling-Allerød (B/A) and interstadials during glacial conditions. Proposed proximal drivers of deoxygenation during these events include decreased oxygen solubility directly related to warming, enhanced productivity, and thus respiration, due to changes in nutrient supply, and decreased intermediate water ventilation (Jaccard and Galbraith, 2012; Moffitt et al., 2015; Praetorius et al., 2015; Gray et al., 2018).

Previous studies of low-oxygen events in the southeastern margin of Alaska are restricted to the last ~17,000 years (Davies et al., 2011; Addison et al., 2012; Praetorius et al., 2015). These paleoceanographic records suggest OMZ expansion and strengthening in the Gulf of Alaska (GoA) during B/A interstadial (14.7-12.9 ka) and the early Holocene; 11.5-10.5 ka. However, the frequency and severity of hypoxia for glacial intervals are not documented for this region as they have been elsewhere in the North Pacific. This paleoceanographic gap in the high-latitude North Pacific is largely due to poor preservation of microfossils in corrosive bottom waters. Paleoceanographic records for

the past ~54,000 years are obtainable in the GoA, though, due to high sedimentation rates that led to the excellent preservation of foraminifera (Gulick et al., 2015).

Combined sedimentary, faunal, and geochemical approaches are important for resolving oxygenation records because each proxy has limitations. The presence of laminations indicates the absence of bioturbation due to severe low-oxygen conditions (van Geen et al., 2003; Moffit et al., 2015). However, these sedimentary structures are easily overprinted by later bioturbation when oxic conditions return, especially if sedimentation rates are low. Redox-sensitive metal accumulations (including Mo and U) are instrumental in reconstructing dysoxia (<0.5 ml/L O_2), including in the North Pacific (Zheng et al., 2002; Davies et al., 2011; Jaccard and Galbraith, 2013; Moffitt et al., 2015; Praetorious et al., 2015). However, processes like post-diagenetic reworking, re-oxidative burn down, bioturbation, sedimentary dilution, and diffusion within the sediments can overprint oxygenation histories based on redox-sensitive metals (Calvert and Pedersen, 1993; Tribovillard et al., 2006; Zindorf et al., 2020). This may lead to imprecise interpretations of paleoenvironmental conditions like the severity, duration, and timing of the events.

Benthic foraminifera are particularly useful for studying oxygenation because some species rapidly respond to changes in oxygenation but are insensitive to oxygenation differences above 1 or 2 ml/L (Murray et al., 2001; Moffitt et al., 2015). Like sedimentary proxies, bioturbation can mix foraminifera accumulated under different environmental conditions across environmental changes leading to time-averaged assemblages in the sediment core (Fürsich and Aberhan, 1990). This time-averaging can dampen the signal

of low-oxygen events but, unlike redox-sensitive metals, foraminifera are not necessarily removed from the sediments. However, many environmental factors can influence the distribution of benthic foraminifera including organic carbon flux, salinity, current velocity, temperature, and substrate characteristics, and thus, can confound paleo-oxygen reconstruction, especially when based on only a few index species (Jorissen et al., 2007). Thus, cross-validation across sedimentary, faunal, and geochemical proxies is important for reconstructing paleo-oxygenation.

Like index taxon approaches, paleoenvironmental reconstructions based on benthic foraminifera restricted to larger (>125 μm) sizes may also exclude species and overlook some environmental information, especially in low-oxygen or eutrophic environments (Sen Gupta et al., 1987; Schroeder et al., 1987; Schönfeld et al., 2012; Weinkauf and Milker, 2018). However, separating smaller foraminifera from sediments is time-intensive and they are more difficult to identify thus, some studies exclude them for efficiency (Schroeder et al., 1987; Weinkauf and Milker, 2018). Therefore, we must also consider the sensitivity of foraminiferal assemblage-based paleo-oxygenation proxies to taxonomic and size inclusion.

In this study, we use both benthic foraminiferal assemblages and redox sensitive metals as proxies for pore-water oxygenation and assess their correspondence in reconstructing a quantitative oxygenation history of the upper OMZ in GoA. We develop a new method for calculating oxygenation values from total benthic foraminiferal assemblages, which is not limited to taxa with known physiological tolerances. Further, we examine the influence of faunal size-fraction on this correspondence and on the

resulting paleoxygenation reconstructions. With these data, we reconstruct an oxygenation history over the last ~54,000 years at ~200 year resolution to test the hypotheses that: a) hypoxia occurred in both glacial and interglacial intervals in the GoA b) the duration and severity of hypoxia are independent of whether the event occurred during glacial or interglacial times, and c) ecologically relevant changes in oxygenation can occur on multi-centennial timescales in GoA.

2.2. Materials and Methods

Integrated Ocean Drilling Program (IODP) Site U1419, jumbo piston core EW0408-85JC and an adjacent multicore EW0408-84MC are located on the Khitrov Bank in the GoA at 697 and 682 m water depth, respectively, and underlie North Pacific Intermediate Water (NPIW; Figure 2.1; Jaeger et al., 2014). The modern OMZ core in GoA is at ~ 670 – 1,060 m (~0.45 ml/L O_2; Paulmier and Ruiz-Pino, 2009), thus this site lies within the upper OMZ. The central GoA is a high nutrient low chlorophyll (HNLC) area and micronutrients, like iron, limit productivity (Stabeno et al., 2004). Nitrates and phosphates are generally transported from the subsurface ocean (Childers et al., 2005), while iron comes from fluvial sources (Stabeno et al., 2004). The availability of sunlight is the main limiting factor for the primary productivity in the GoA, and productivity is low in winters and comparatively high in early summer (Stabeno et al., 2004). Early spring may have large algal blooms due to availability of ample sunlight and nutrients (Stabeno et al., 2004).

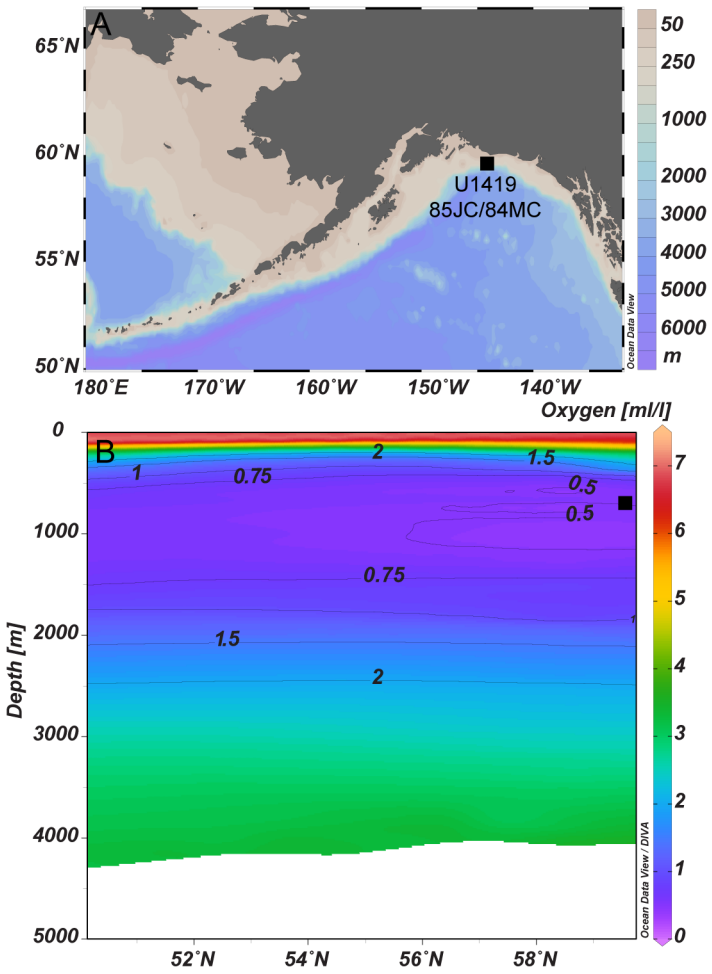

Figure 2.1 Study site locations. (A) Map showing the location of sites EW0408-85JC, EW0408-84MC and Site U1419 in the Gulf of Alaska. (B) Meridional cross section (144^{O}W) of the oxygen concentration in the modern Eastern Pacific Ocean, showing location of site with respect to the oxygen minimum zone. Oxygenation data are from the World Ocean Atlas 2013 (Garcia et al., 2013) and both panels were constructed in Ocean Data View (Schlitzer, 2018). OMZ, oxygen minimum zone.

Site U1419 was drilled to ~177 m below the seafloor with an overall core recovery of 82% (Jaeger et al., 2014). The chronology for Site U1419 is based on a Bayesian age model using 250 ^{14}C values from separately analyzed benthic and planktonic foraminiferal samples that were calibrated using the Marine13 calibration curve (Walczak et al., 2020). The base of the stratigraphic splice among holes at U1419 is ~55 ka. Sedimentation rates

at Site U1419 average ~50 cm/ka over the past 12 ka, are as high as 800 cm/ka during the deglacial interval, and average ~200 cm/ka during the glacial portion of the record (Walczak et al., 2020). These high sedimentation rates led to exceptional preservation of carbonate, including foraminiferal fossils (Gulick et al., 2015).

The width of the continental shelf in SE Alaska is ~25 km near Kayak Island with shelf break at 220 m water depth (Molnia, 1983; Dobson et al., 1998). As a result, lithology in the continental shelf varies from hemipelagic muds to glacial diamictites, and glacial-marine sand and silt (Carlson, 1989; Penkrot et al., 2018). The dominant lithofacies recorded in the Site U1419 core is clast poor diamict, and facies ranged from massive bioturbated mud to laminated diamicts (Penkrot et al., 2018). Laminations occur during the deglacial, similar to site survey core EW0408-85JC (Davies et al., 2011), but also within the glacial interval (Penkrot et al., 2018).

We sampled 2-3 cm-wide intervals (5-40 cc) with a median age resolution of 127 years (interquartile range, IQR = 73-201 years) based upon the age model from Walczak et al. (2020). Sample ages and depths are calculated from the midpoint of sample width. Approximately 2 cc of each sample was reserved for redox metals analyses and the remainder was disaggregated for faunal analyses.

2.2.1. Multivariate Faunal Analysis

Sediment samples for faunal analysis were weighed after freeze-drying, disaggregated in deionized water, and wet-sieved at 63 μm. After air-drying, the coarse fraction (>63 μm) was weighed and used to calculate the proportion of sand and silt. Coarse fractions were split with a microsplitter to obtain at least 150 benthic foraminifera

specimens >63 μm in each sample. Samples with a high proportion of sand-sized sediment grains often had fewer specimens due to sedimentary dilution and samples with as few as 50 individuals in the >63 μm fraction were retained for analysis. The median number of individuals we obtained per sample is 268 (IQR = 159-404). While previous work estimates 300 individuals are needed for statistical analyses of diversity metrics (Buzas, 1990), more recent studies suggest that multivariate analyses of assemblage composition are stable with as few as 58 individuals (Forcino et al., 2015). Foraminifera were picked and identified to species-level within four size fractions (>355, 355-250 μm, 125-250 μm, 63-125 μm) to retain size information (Supplemental Table 2.1). Species that were rare and occurred infrequently were often grouped at the genus-level for counts. Only those species and generic groups that occurred in more than one sample and comprised >2% of individuals in at least one sample were included in analyses.

We use the multivariate ordination method Detrended Correspondence Analysis (DCA) to reduce the dimensionality of our faunal data set and extract major gradients in faunal composition. DCA, which uses the chi-square dissimilarity among the relative abundances of taxa to define assemblage differences, is commonly used in paleoecological analyses and is preferred when the research emphasis is on finding a single faunal gradient reflective of environmental gradients (McCune and Grace, 2002; Scarponi and Kowalewski, 2004; Bush and Brame, 2010; Belanger and Villa Rosa Garcia, 2014). We then test the hypothesis that oxygenation influences the primary axes of faunal variation by comparing by DCA species scores of taxa with different environmental preferences in the modern (Supplemental Table 2.2). DCA analyses are performed using the “decorana”

function with its defaults in vegan package of the R programming language (R core team, 2016; Oksanen et al., 2017). We calculate the proportion of variance summarized by each axis using the Pearson correlation between the Euclidean dissimilarity of the DCA sites scores and the Bray-Curtis dissimilarity of the faunal abundances for each site with the *mantel* function in the "ecodist" package ("after the fact method" of McCune and Grace, 2002).

To test the hypothesis that different benthic foraminiferal size fractions reconstruct the same environmental gradients, we perform DCA analyses on three size fractions (>63 μm, >125 μm, 63-125 μm) separately. Subsetting the data by size fraction necessarily reduces the number of individuals per sample, thus, these analyses contain samples with fewer than the typically recommended 300 to 58 individuals per sample (Table 2.1). We do not perform DCA analyses using subsets focused on the larger size fractions alone because we obtained fewer than 50 individuals larger than 250 μm in ~90% of samples (median = 12 individuals >250 μm). We use the Mantel correlation among sample ordination scores to test whether the resulting ordination structures are significantly different. Similarly, we use the Mantel test to compare the similarity of species positions in ordination space. Mantel tests were performed using *mantel* function in the "ecodist" package in R (Goslee and Urban, 2007).

Table 2.1 Comparison of ecological analyses on benthic foraminiferal assemblages using three size fractions (>63 µm, >125 µm and 63-125 µm). *Note*: For Spearman correlations, rho-values are reported; for Mantel correlations, r-values are reported. 95% confidence intervals for each correlation are in parentheses.
***=p<0.05; **=p<0.01, ***=p<0.001, ns=non-significant.**

Size fractions used →	>63 µm	>125 µm	63-125 µm
Total number of taxa	74	67	67
Number of taxa used in analyses (>2%)	48	46	47
Median number of individuals per sample (Interquartile Range; IQR)	268 (159-404)	81 (46-141)	175 (85-265)
DCA Axis 1, proportion of variance summarized	55%	51%	52%
DCA Axis 2, proportion of variance summarized	16%	6%	19%
Spearman rho DCA 1 vs. Mo/Al	0.45 (0.35-0.55)***	0.45 (0.35-0.54)***	0.43 (0.33-0.53)***
Spearman rho DCA 1 vs. U/Al	0.61 (0.54-0.69)***	0.58 (0.50-0.66)***	0.59 (0.51-0.66)***
Spearman rho DCA 2 vs. Mo/Al	-0.33 (-0.42 -0.25)***	0.01 (-0.10-0.12)ns	-0.06 (-0.17- 0.04)ns
Spearman rho DCA 2 vs. U/Al	-0.14 (-0.23 - -0.04)*	0.28 (0.18-0.37)***	-0.18 (-0.29 - -0.08)***
Mantel correlation Faunal vs Mo, U dissimilarity	0.47 (0.46 -0.49)**	0.42 (0.41 -0.43)**	0.39 (0.38 -0.41)**

2.2.2. Redox Sensitive Metals

Authigenic accumulations of Molybdenum (Mo) and Uranium (U) are commonly used as paleo-oxygen proxies. In sulfidic environments, Mo solubility decreases, thus the concentration of authigenic Mo can serve as a geochemical tracer of severely dysoxic (<0.5 ml/L O_2) conditions (Crusius et al., 1996; Zheng et al., 2000; McManus et al., 2006). Accumulation of authigenic U in sediments typically occurs at similar redox condition as the reduction of iron oxyhydroxides and thus indicates less severe, suboxic (<1.4 ml/L O_2) conditions (Klinkhammer and Palmer, 1991; McManus et al., 2006; Tribovillard et al., 2006). Thus, when used together, U and Mo allow differentiation of suboxic and sulfidic conditions respectively, increasing the quantifiably of paleo-oxygen reconstructions.

Mo and U were measured in bulk sediment samples (~50 – 100 mg) and digested using a mixture of HF-HCl-HNO_3 in a CEM MARS-6 microwave oven (Muratli et al., 2012). Mo and U concentrations were analyzed on a quadrupole ICP-MS in the W.M. Keck Collaboratory for Plasma Spectrometry of Oregon State University. Samples, calibration standards, and blanks were spiked with internal standards (^{103}Rh and ^{209}Bi). Procedural blanks of the entire process were corrected for and were 0.8±0.3 (1σ) % for Mo and 0.03±0.01 (1σ) % for U. Repeated analysis of sediment reference material PACS-2 produced a Mo concentration of 5.70±0.23 (1σ, n=58) ppm, agreeing well with the certified value of 5.43±0.14 (1σ) ppm. Repeated analysis of the USGS rock reference material AGV-1 resulted in U concentration of 1.900±0.049 (1σ, n=3) ppm, also in agreement with the literature value of 1.903±0.010 ppm (Jochum et al., 2016). Repeated

analysis of an in-house marine sediment standard yielded long-term (over 3 years) reproducibility (1 relative standard deviation [SD], n=57) of ~4% of measured values for Mo and of ~6% of measured values for U.

We report Mo and U as Element/Aluminum (Al) ratios to distinguish authigenic accumulation from the terrigenous background (Muratli et al., 2010; Cartapanis et al., 2011). Al was analyzed using an ICP-OES at the same lab. Repeated analysis of the sediment reference material PACS-2 gave an Al concentration of 6.45±0.16 (1σ, n=58) wt% consistent with the certified value of 6.62±0.16 (1σ) wt%. Procedural blanks of Al were negligible (<0.1%). Long-term (over 3 years) reproducibility (1 relative standard deviation, n=57) of Al were ~2%. The choice of terrigenous normalization is however not essential given that Al and Ti, two most widely used elements for terrigenous background, at both sites varied little (<5%) during the entire record, suggesting that the variabilities of Mo and U concentrations were dominated by authigenic accumulation.

2.2.3. Correspondence between faunal changes and redox-sensitive metals

We obtained redox sensitive metal concentrations and benthic foraminiferal faunal counts from the same samples, making it possible to quantitatively compare the two types of data. In total, we have 355 samples with both faunal and redox metals data (Supplemental Table 2.1). We use the Mantel correlation to test the hypothesis that samples that are most dissimilar in faunal composition are also most dissimilar in their concentrations of redox metals. For these analyses, we calculated Bray-Curtis dissimilarity among samples using the proportional abundances of species and the Euclidean dissimilarity among samples using the z-score transformed redox metals data (Mo/Al,

U/Al); the Euclidean dissimilarity metric accommodates negative values unlike the Bray-Curtis dissimilarity, which is most appropriate for faunal abundances (McCune and Grace, 2002). Z-score transformations were performed using the *scale* function of the "base" package in R (R Core Team, 2016).

Each redox sensitive metal has different threshold sensitivity to changes in oxygenation and, thus, may have a different relationship to the faunal gradients. To test if Mo/Al and U/Al differ in the strength of their correlation to the primary axis of faunal variation, we calculate the Spearman correlation between faunal DCA Axis 1 scores and individual redox-sensitive metal concentrations. All correlations were also performed for each size fraction separately to test the hypotheses that faunal variation is similarly associated with differences in redox metals concentrations regardless of the size fraction.

2.2.4. Quantifying dissolved oxygen concentrations from faunal assemblages

Further, we quantitatively estimate oxygenation values from benthic foraminiferal faunal assemblages using the Behl dissolved oxygen (BDO) index following Ohkushi et al. (2013). However, in its original implementation, this index was restricted to the 19 species for which the authors acquired oxygen tolerances reported in the literature (Ohkushi et al., 2013). Of these 19 species, we found 14 in our samples and used these species to calculate a "literature-based" BDO estimate comparable to this previous work (Supplemental Table 2.2). In order to instead use all species in our analyses, we also calculate a modified BDO using the covariation of species with known oxygenation tolerances in DCA ordination spaces to place unassigned species into dysoxic (>1.83 DCA species scores), suboxic (-0.39 to 1.83), or weakly hypoxic to oxic (< -0.4) categories (see

Section 2.3.3). To assess whether the faunal size fraction examined can affect these calculated oxygenation values, we compare BDO results using the >63 μm size fraction and the >125 μm size fraction.

2.2.5. Comparing fossil assemblages to modern surface sediment assemblages

We further compare our fossil assemblages (>63 μm size fraction) to 225 benthic foraminifera assemblages collected from sediment surface samples following Belanger et al. (2016) to identify fossil assemblages indicative of oxygenation values outside the range of modern spatial variability in GoA. Samples were compiled from Bergen and O'Neil (1979), Echols and Armentrout (1980) and from EW0408 and IODP Expedition 341 coretops (Belanger et al., 2016). The data set includes at least 13 samples from within the modern oxygen minimum zone. As in previous work, we consider a fossil sample to have no modern analog if its nearest-neighbor Spearman rho coefficient is less than 0.1285, which we calculated from the 95th percentile of the dissimilarity among modern-modern sample pairs (Belanger et al., 2016). We use Spearman rho because it considers only the rank abundance of taxa and, thus, minimizes the dissimilarity due to differences in the proportional abundances of species. Fossil assemblages for which we identify analogs are also assigned to a primary environment (i.e., slope or shelf) based upon the environment of their nearest modern analog.

Modern species represented in the fossil data set were assigned to the same oxygen categories as in the fossil calculations. The twenty-seven modern species not found in the fossil data set were assigned to oxygen categories based upon the correlation between their relative abundances in a modern sample and the modern oxygen values of the collection

site estimated from the World Ocean Atlas (WOA) 2013 (Garcia et al., 2014). Species with a positive correlation with oxygen concentrations were assigned to the oxic category and species with a negative correlation to the suboxic category (Supplemental Table 2.3). Samples with flagged WOA data for oxygenation were excluded from analyses requiring oxygen concentrations leaving 208 modern samples with modern oxygen measurements.

2.2.6. Identifying the occurrence, severity, and duration of hypoxic events

To quantitatively distinguish low-oxygen events from background conditions, we extract the most extreme values for each oxygenation proxy (DCA Axis 1 score, Mo/Al, and U/Al) in our time series using the 95th, 95-90th, and 80-90th upper quantiles where the 95th upper quantile represents data in the highest 5% of values. We focus on the change in DCA Axis 1 because this Axis summarizes the majority of our faunal variation and is well related to oxygenation (see section 3.1). This method ensures that all proxies yield the same number of potential low-oxygen events. Further, we used the BDO values calculated from >63 μm dataset to operationally categorize the events into dysoxic (< 0.5 ml/L), suboxic (0.5 - 1 ml/L) and weakly hypoxic to oxic (>1 ml/L) conditions. Because we are primarily interested in identifying low-oxygen events and the BDO index is known to underestimate oxygenation at higher values, we conservatively define the threshold between suboxic and weakly hypoxic to oxic conditions at 1 ml/L instead of the 1.4 ml/L used by others (Ohkushi et al., 2013; Moffitt et al. 2015). Using these data, we can then ask whether proxies agree or disagree on the presence, duration, and relative severity of a low-oxygen event.

2.2.7. Rates of faunal and environmental change

DCA axes are scaled in units of standard deviations of total faunal variation (McCune and Grace, 2002), thus we can use DCA Axis 1 scores to quantify rates of ecological change as in other paleoecological studies (Correa-Metrio et al., 2012). We also calculate the rate of change in oxygenation using our modified BDO values. We recalculate the rate of BDO change after removing shelf analogs to provide a more conservative rate estimate that accounts for potential downslope transport and faunal changes due to major sedimentation changes.

2.3. Results

In total, we identified 74 species and congeneric groups of benthic foraminifera in the >63 μm size fraction. Of the 74 species, 26 comprised less than 2% of any one sample and, thus, were removed from the analyses leaving 48 species. From the full faunal list, 67 species occur in the 63-125 μm size fraction and 67 species occur in the >125 μm size fraction (Table 2.1). The most frequently observed species regardless of size fraction are *Cassidulina reniforme, Epistominella pacifica, Uvigerina peregrina, Islandiella norcrossi, Elphidium clavatum, Alabaminella wedellensis,* and *Epistominella exigua* and together they often comprise the majority the assemblage in the >63 μm size fraction (Figure 2.2 (A) and 2.2 (B)). Only 9% of the taxa present in the >63 μm size fraction are absent from the >125 μm size fraction. Some species, including *Bolivina earlandi, Loxostomum minuta, Bolivina decussata, A. wedellensis,* and *E. exigua,* are abundant in the 63-125 μm size fraction and are rare to absent in the >125 μm fraction (Supplemental Table 2.1). For example, *A. wedellensis* and *E. exigua,* which are used as proxies of

organic carbon fluxes (Gooday, 1993; Sun et al., 2006; Gooday, 2012), comprised up to 76% of the assemblage in the 63-125 μm size fraction but are less than 6% of the assemblage in the >125 μm size fraction (Figure 2.7).

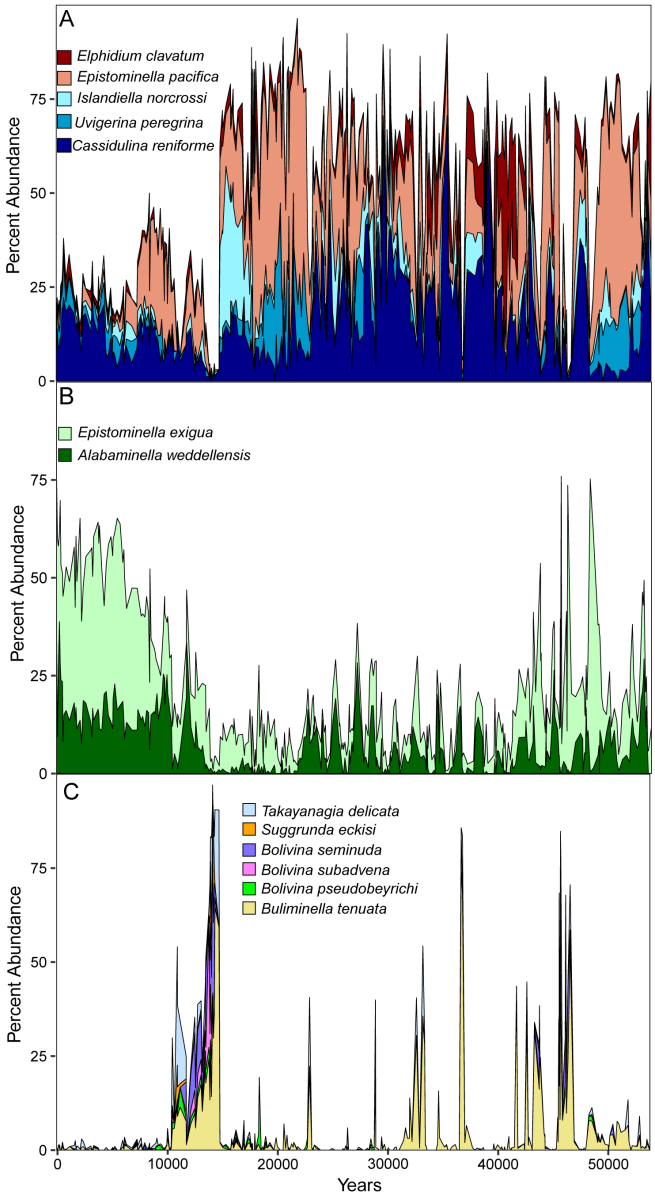

Figure 2.2 Relative abundance of numerically and ecologically significant benthic foraminiferal species in the >63 μm size fraction. (A) Five of the most frequently occurring species that are also have high abundances in the glacial. (B) Opportunistic species. (C) Six species with reported oxygen tolerances <0.1 ml/L.

2.3.1. Primary gradients in faunal composition

DCA Axis 1 summarizes 51-55% of the faunal variation whereas DCA Axis 2 summarizes 6-19% of the faunal variation depending on the size fraction analyzed (Table 2.1). The position of samples in the total DCA space (axes 1-4) has a strong positive Mantel correlation among all three size-fractions; sample position along DCA Axis 1 alone is also similar among size fractions (Table 2.2). Species positions in total DCA space are also positively correlated among size fractions, but with weaker associations among size fractions than for site positions in DCA space (Table 2.2). Given these similarities among the ordinations and their temporal patterns regardless of size fraction (Figure 2.3; Supplemental Table 2.4), we will only discuss the DCA results using the >63 µm data set.

Table 2.2 Pairwise Mantel correlations between DCA site scores for the three benthic foraminiferal size fractions (>63 µm, >125 µm and 63-125 µm). *Note*: Mantel r-values are reported with 95% confidence intervals for each correlation in parentheses. *=p<0.05; **=p<0.01.

DCA score comparison	>63 µm and >125 µm	>63 µm and 63-125 µm	>125 µm and 63-125 µm
DCA Axes 1-4 sample scores	0.82 (0.81-0.83)**	0.80 (0.79-0.80)**	0.58 (0.57-0.60)**
DCA Axis 1 sample scores	0.82 (0.81-0.82)**	0.93 (0.93-0.94)**	0.76 (0.75-0.77)**
DCA Axes 1-4 species scores	0.28 (0.24-0.33)*	0.50 (0.47-0.55)**	0.18 (0.14-0.22)*
DCA Axes 1 species scores	0.65 (0.62-0.70)**	0.83 (0.82-0.85)**	0.47 (0.43-0.53)**

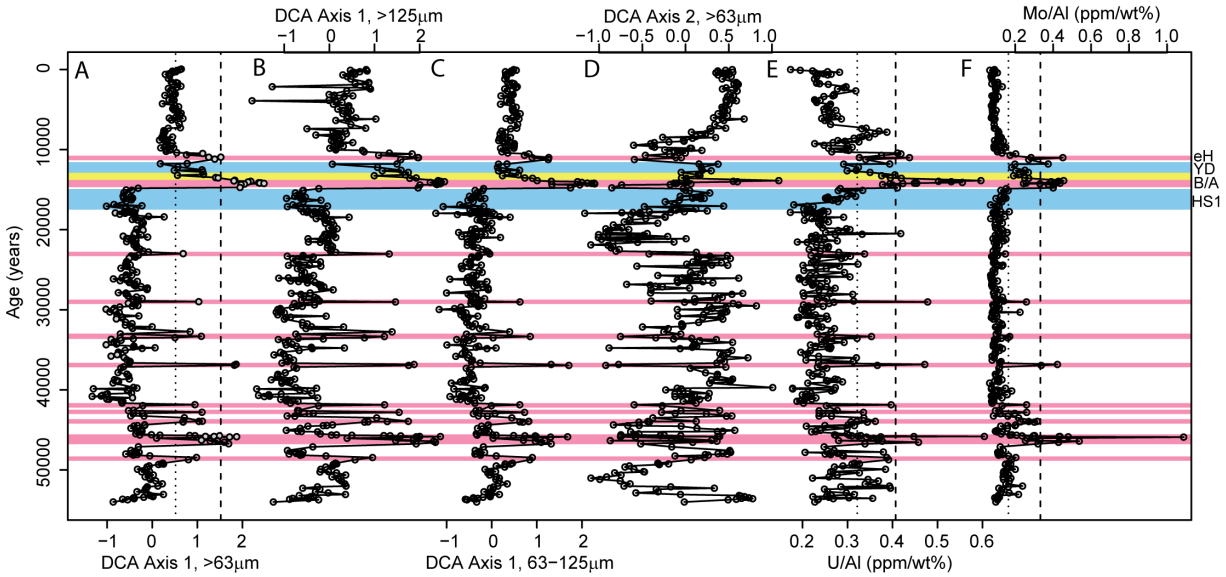

Figure 2.3 Ecological and environmental proxies for Site U1419 in the Gulf of Alaska for the last 54 ka. A -- C Detrended Correspondence Analysis (DCA) Axis 1 scores of benthic foraminiferal assemblages using each of three size fractions (>63 µm, >125 µm, and 63-125 µm). In (A) assemblages with no modern analog are indicated with gray-filled symbols. (D) DCA Axis 2 scores for the >63 µm size fraction. Redox metal values from the same samples: (E), U/Al, (F), Mo/Al. Vertical dashed line in (A), (E), and (F) represents the upper 95th upper quantile and the dotted line represents upper 80th upper quantile of the data distribution. Climate intervals indicated as eH: early Holocene; YD: Younger Dryas; B/A: Bølling-Allerød and HS1: Heinrich Stadial 1. Pink bars represent dysoxic events discussed in the text, blue bars are oxic intervals discussed in the text. The Allerød is distinguished from the Bølling in yellow.

Species with the most positive DCA Axis 1 scores include *Buliminella tenuata*, *Takayanagia delicata, Bolivina seminuda, Bolivina subadvena, Bolivina pseudobeyrichi,* and *Suggrunda eckisi* (Figure 2.4; Supplemental Table 2.5); these taxa are common in dysoxic to suboxic settings (Schmiedl et al., 2003; Ohkushi et al., 2013; Tetard et al., 2017; Erdem and Schonfeld, 2017) and sometimes dominate our assemblages (Figure 2.2 (C)). Species with strong negative DCA Axis 1 scores include *I. norcrossi, Stainforthia*

complanata, *Astrononion gallowayi, Nonionella digitata, Triloculina trihedra, E. clavatum, Quinqueloculina* spp*., Virgulina* spp., *Stainforthia fusiformis*, a phytodetritus-feeding opportunist related to ephemerally low-oxygen environments (Alve, 2003), has a low negative DCA Axis 1 score. Other opportunistic species sensitive to the seasonality of productivity and flux of fresh phytodetritus including *A. wedellensis* and *E. exigua* (Gooday, 1993; Sun et al.; 2006; Gooday 2012), have low positive (*A. wedellensis*) and high positive (*E. exigua*) DCA Axis 1 scores and dominate assemblages in the Holocene interval of our record (Figure 2.2 (B)). Species associated with glacial conditions, including *E. pacifica* and *C. reniforme* (Ohkushi et al., 2003), and oxic settings, such as *Pyrgo* spp. and *Quinqueloculina* spp. (Ohkushi et al., 2013), have negative DCA 1 Axis scores. *Nonionellina labradorica*, categorized by others as a taxon that favors oxic environments (Ohkushi et al., 2013), has a low positive DCA Axis 1 score in our analyses.

Species with positive DCA Axis 2 scores include phytodetritus sensitive taxa such as *N. labradorica, S. fusiformis, A. wedellensis* and *E. exigua* (Cedhagen, 1991; Sun et al., 2006); these species are dominant in some samples with DCA Axis 2 scores >0.5 (Figure 2.4; Supplemental Table 2.5). Other species with positive DCA Axis 2 scores include *Bolivina decussata, Trifarina angulosa, B. subadvena*, *T. trihedra, Nonion grateloupii, Valvulineria* spp*., C. reniforme and Cassidulina* spp. Some low-oxygen tolerant taxa, including *B. seminuda*, *S. eckisi*, and have positive DCA Axis 2 scores, however other low-oxygen tolerant taxa including *T. delicata*, *B. tenuata*, and *B. pseudobeyrichi* have negative DCA Axis 2 scores.

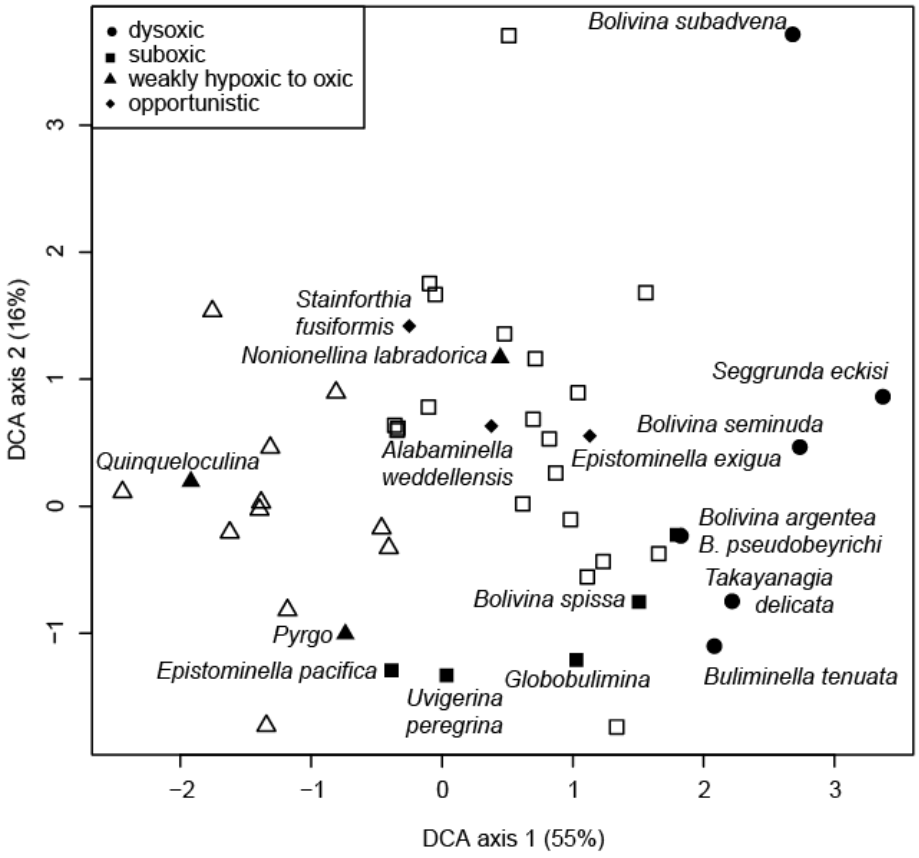

Figure 2.4 Detrended Correspondence Analysis (DCA) species scores for benthic foraminiferal assemblages from the >63 µm size fraction. Circles indicate species with a lowermost oxygen tolerance below 0.1 ml/L O_2, squares indicate species with a lowermost oxygen tolerance of 0.1-0.5 ml/L O_2, and triangles indicate those with a lowermost oxygen tolerance above 0.5 ml/L O_2 based upon published tolerances (Supplemental Table 2.2). Diamonds denote opportunistic taxa, which are also inferred to tolerate suboxic conditions. Filled symbols indicate species for which environmental preferences were obtained from the literature and are labeled with species names. Open symbols denote species assigned to a category based on its DCA Axis 1 score.

2.3.2. Correspondence between faunal and redox metal variation

Samples that are most dissimilar in their faunal composition are also most dissimilar in their redox metal concentrations in all three size-fractions we tested (Mantel

correlations, Table 2.1). Individual redox-sensitive metal concentrations (Mo/Al and U/Al) and the primary gradient of faunal composition (DCA Axis 1 scores) also positively covary regardless of size fraction (Table 2.1), such that samples with higher DCA Axis 1 scores have higher redox metal concentrations. This is consistent with the positive DCA Axis 1 scores of low-oxygen tolerant species. U/Al has a stronger positive correlation (Spearman's rho=0.61) with DCA axis 1 scores as compared to Mo/Al (Spearman's rho=0.45). In contrast to DCA Axis 1, DCA Axis 2 has weaker correlations with redox metal concentrations and no systematic relationship with low-oxygen tolerant species (Table 2.1; Figure 2.4).

2.3.3. Quantifying oxygenation from faunal assemblages

Published oxygen tolerances indicate 6 species associated with dysoxic conditions (lowermost oxygen tolerances <0.1 ml/L O_2) and 5 species associated with suboxic conditions (lowermost oxygen tolerances 0.1-0.5 mL/L O_2) are present in our data set (Supplemental Table 2.2). Following previous studies using similar methods (Ohkushi et al., 2013; Tetard et al., 2017), only three "weakly hypoxic to oxic" species (*N. labradorica*, *Pyrgo* spp., and *Quinqueloculina* spp.) are used in our "literature-based" BDO calculations. Using this subset of 14 species produces BDO values between 0.10-1.25 ml/L (Figure 2. 5 (A), Supplemental Table 2.4).

All species designated as dysoxic in the literature have DCA Axis 1 scores greater than or equal to 1.83. Species categorized as suboxic indicators in the literature have with DCA Axis 1 scores between -0.39 and 1.83, thus we assign species without literature-based oxygen tolerances that fall within this range of DCA Axis 1 scores to the suboxic

category. We categorize all species without published oxygen tolerances with DCA Axis 1 scores less than -0.4 as weakly hypoxic to oxic, consistent with the DCA Axis 1 scores of *Pyrgo* spp., and *Quinqueloculina* spp. (Figure 2.4, Supplemental Table 2.3). Oxygen values calculated using the >63 µm data set produce values between 0.12 and 1.40 ml/L O_2; restricting to foraminifera >125 µm produces values from 0.11-1.50 ml/L O_2 (Figure 2.5 (B) and 2.5 (C)).

On average, BDO calculations using only those species with published oxygen tolerances reconstruct oxygen values 0.30 ml/L O_2 (IQR =0.15 - 0.43) lower than calculations using all species in the >63 µm size fraction (Figure 2.6). Oxygen estimates from the literature-based calculations tend to frequently produce values of ~0.5 ml/L O_2 whereas calculations for these same samples are 0.5 to 1.2 ml/L O_2 using the total fauna. In contrast, oxygen calculations using the >125 µm size fraction are similar on average to the >63 µm size fraction (median difference= 0.05 ml/L, IQR = -0.04 to 0.10; Figure 2.6).

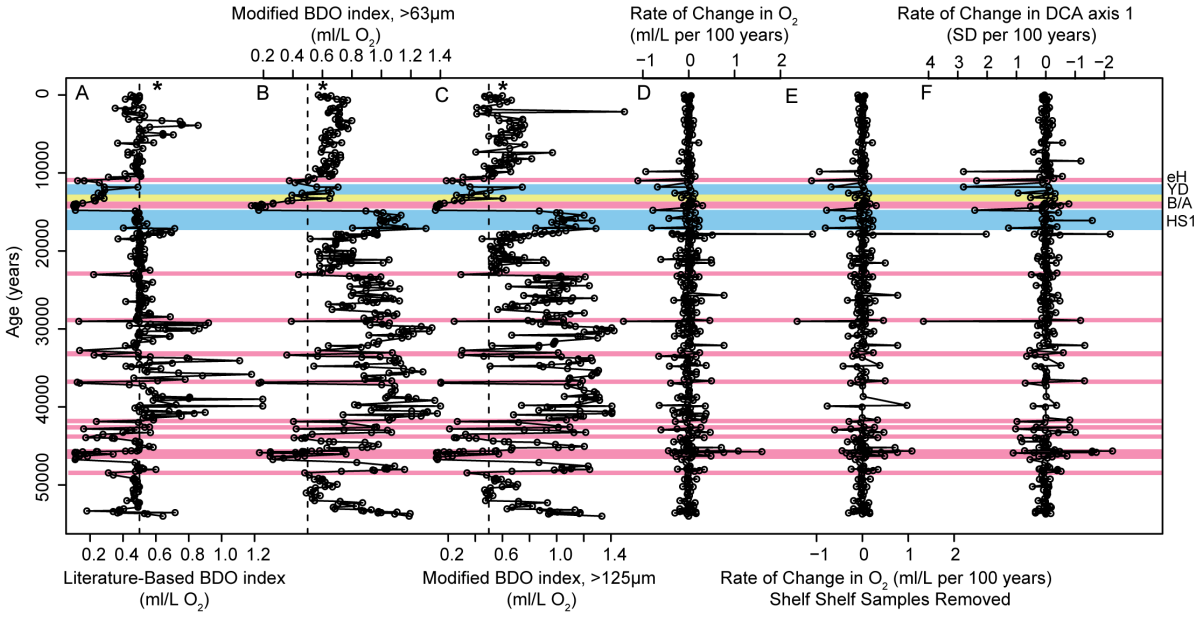

Figure 2.5 Rates of oxygenation and ecological change. (A) Dissolved oxygen values calculated using the BDO index and only species whose oxygen tolerances are known from the literature. (B) Dissolved oxygen values calculated using the total assemblage and (C) using the >125 µm size fraction. (D) Rate of oxygenation change per 100 years using all samples. (E) Rate of change in oxygenation per 100 years with shelf analogs removed. (F) Rate of change in DCA Axis 1 scores per 100 years using all samples. All metrics are derived from the >63 µm size fraction unless otherwise specified. Dashed lines in A -- C indicate 0.5 ml/L are dysoxic-suboxic O_2 threshold. Climate intervals indicated as eH: early Holocene; YD: Younger Dryas; B/A: Bølling-Allerød and HS1: Heinrich Stadial 1. Pink bars represent low oxygen events discussed in the text, blue bars are the oxic events. Allerød is distinguished from the Bølling in yellow.

2.3.4. Oxygen estimates from modern faunas

Core top assemblages from Site U1419 and EW0408-84MC have an average BDO estimate of 0.60 ml/L O_2 using the full fauna (>63 µm size fraction), similar to the 0.59 ml/L O_2 estimates for the modern site derived from the WOA (Supplemental Table 2.6). Oxygen calculations from our modified BDO index and the modern measured oxygen concentrations have a strong positive correlation (Spearman rho=0.81, $p << 0.001$), but the values are different in scale (Figure 2.6 (C)). The calculated oxygen estimates are higher than measured values when WOA values are <0.5 ml/L (median difference = 0.26 ml/L, IQR = 0.15 - 0.39), similar for WOA values 0.5 - 1.5 ml/L (median difference = -0.09 ml/L, IQR = -0.17 to 0.09) and lower than measured values when WOA values are >1.5 ml/L (median difference = -5.29 ml/L, IQR = -5.49 to -4.34).

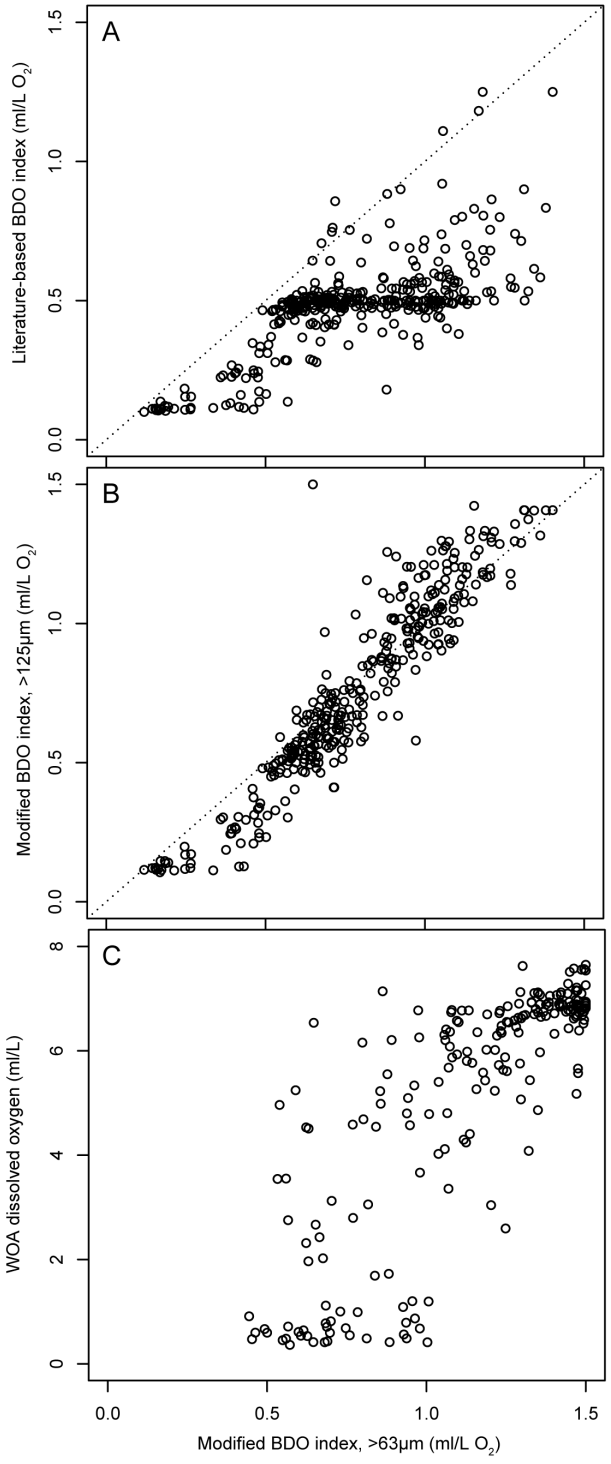

Figure 2.6 Relationships among dissolved oxygen calculations for (A) fossil assemblages using only 14 species with published oxygen tolerances and fossil assemblages using all 48 species in the >63 µm size fraction, (B) fossil assemblages

from the >63 µm size fraction and fossil assemblages from the >125 µm size fraction, (C), modern assemblages in the >63 µm size fraction and measured dissolved oxygen values from the World Ocean Atlas 2013 (Garcia et al., 2013). In (A) and (C), BDO values are the same as in Figure 2.5 A -- C and dotted lines are 1:1 lines.

2.3.5. Defining the occurrence and duration of low-oxygen events

Of the 355 samples we analyzed, 129 have at least one low-oxygen proxy (DCA Axis 1 score, U/Al or Mo/Al) that exceeds the 80th upper quantile of the data for that variable (Figure 2.3). In total, we found 71 samples in which all the proxies suggest low-oxygen conditions. For the majority of the record, all three faunal size fractions indicate similar DCA Axis 1 excursions with minor differences in the relative severity (Figure 2.3). During the mid-Holocene (~6.8 ka) to present, many samples have DCA Axis 1 scores in the upper 80 - 90th quantile, but these samples do not have correspondingly high redox metal concentrations (Figure 2.3). Similarly, some Holocene samples from 8.5 to 7.4 ka and MIS 3 samples from 53.5 to 49.2 ka have redox metal concentrations in the 80th upper quantile without corroborating DCA Axis 1 scores. However, these are exceptions and the majority of samples that have high positive DCA Axis 1 scores have high redox metal concentrations.

High DCA Axis 1 scores and high concentrations of redox metals also generally correspond to low BDO estimates. All samples with either DCA Axis 1 scores or redox metals concentration in the 80th upper quantile have BDO values suggesting dysoxic or suboxic conditions. Most of the severe dysoxic events with <0.5 ml/L BDO estimates contain fewer than 5% oxic species. Mo/Al values in the 95th upper quantile correspond to median BDO values of 0.23 ml/L (IQR = 0.18 - 0.40), significantly lower than DO

estimates of 0.41 ml/L for samples with Mo/Al values in the 90-95th upper quantile (Mann-Whitney U=258, p=0.0013; Table 2.3). Similarly, Mo/Al values in the 90-95th upper quantile have BDO estimates that are significantly lower than the median BDO estimates of 0.59 ml/L in the 80-90th upper quantile (U=1188, p<0.0001, Table 2.3). Increasing U/Al values also correspond with increasing faunal DO estimates. The BDO estimates in samples with U/Al in for the >95th upper quantile (Mann-Whitney U=76, p=0.0034) are significantly lower than for samples in than 90-95th U/Al quantile (Mann-Whitney U=244, p=0.0049) and 80-90th quantile (Mann-Whitney U=1079, p<0.0001; Table 2.3).

The lowest BDO estimates occur during the B/A and during discrete intervals in MIS 3 as indicated by both the faunal and redox sensitive metals. DCA Axis 1 scores (>63 μm data set) exceeding the 95th and 90th upper quantile of the faunal data occur in samples from the Bølling (14.7-13.8 ka) and the Allerød (13.8 to 12.9 ka), respectively (Table 2.3). The B/A interval had the lowest calculated DO values (0.12 ml/L from modified BDO >63 μm) in the ~54 ka record with a median value = 0.20 ml/L; IQR = 0.16 - 0.37. The B/A is also corroborated by redox metal values in the 80th upper quantile. Within the B/A, the Bølling had lower BDO values (0.12-0.26 ml/L) and most samples have redox values in the 95th upper quantile. In the Allerød, however, BDO estimates were greater than 0.26 ml/L and redox values where in the 80 - 90th upper quantile (Figure 2.3 and 2.5). DCA Axis 1 scores and redox metal concentrations are also in the upper 90th quantile from 46.7 to 45.7 ka with median BDO estimates of 0.42 ml/L (IQR= 0.25 - 0.46 ml/L; Figures 2.3 and 2.5).

Table 2.3 Upper quantile values for faunal and geochemical oxygenation proxies. *Note*: Faunal dissolved oxygen estimates are from the BDO index using the full fauna in the >63 µm size fraction. Interquartile ranges on the medians are in parentheses.

	Proxy Value Range	**Median Faunal >63 Dissolved Oxygen Estimate (ml/L)**
Mo/Al (ppm/wt%)		
95th upper quantile	0.34-1.09	0.23 (0.18-0.40)
90-95th upper quantile	0.25-0.33	0.41 (0.37-0.46)
80-90th upper quantile	0.16-0.25	0.59 (0.50-0.68)
U/Al (ppm/wt%)		
95th upper quantile	0.41-0.60	0.30 (0.18-0.45)
90-95th upper quantile	0.37-0.41	0.49 (0.40-0.63)
80-90th upper quantile	0.32-0.37	0.55 (0.43-0.68)
DCA Axis 1 (sample scores)		
95th upper quantile	1.52-2.50	0.19 (0.16-0.26)
90-95th upper quantile	1.05-1.51	0.42 (0.39-0.47)
80-90th upper quantile	0.52-1.05	0.60 (0.52-0.64)
75-80th upper quantile	0.44-0.52	0.68 (0.64-0.71)

In addition to the excursions in the B/A and MIS 3 discussed above, shorter duration excursions occur during MIS 3. DCA scores >1.52 occur in two adjacent samples at ~36.9 ka with BDO value of 0.18 ml/L and are corroborated by Mo/Al values in the 95th upper quantile and U/Al values in the upper 80th quantile. BDO estimates as low as 0.38

ml/L occur from 11.2 to 10.9 ka during the early Holocene and are associated with DCA Axis 1 scores in the upper 90th quantile and redox metal values in the upper 80th quantile. Faunal assemblages and both redox sensitive metals also have values in the upper 80th quantiles in single samples at 23 ka, 29 ka, 33.3 ka, 41.8 ka and 42.8 ka and in a sample pair at ~48.5 ka. These shorter (<150 yrs) events have BDO values ranging from 0.36 - 0.44 ml/L. In addition, five consecutive samples from 44-43.5 ka have scores in the 80-95th upper quantile with BDO values ranging from 0.40-0.53 ml/L (Figure 2.5). All of these shorter MIS 3 events are corroborated by Mo/Al and U/Al values in the upper 80th quantile with the exception of the 23 ka event where U/Al is not in the upper 80th quantile.

When proxy values are less extreme, correspondence becomes less common. For example, DCA Axis 1 scores in the 80-95th upper quantile (scores 0.52 - 1.51) occur immediately following the B/A event between 13.6 and 11.7 ka, similar in timing to the Younger Dryas (YD; 12.9 - 11.7 ka). These YD samples also have Mo/Al values in the upper 80th quantile, however only two of five samples have U/Al values in the upper 80th quantile. In the younger record from ~7 ka to present, DCA Axis 1 scores are in the 75-90th upper quantile with the median BDO values of 0.68 ml/L (IQR = 0.64 - 0.72 ml/L), but both redox sensitive metals have values below the 80th quantile for the entire interval. Further, during MIS 3, samples from ~53 to 48 ka have redox metals values in the upper 80th quantiles, however, with the exception of two samples, DCA Axis 1 scores are below the upper 80th quantile (median BDO= 0.72 ml/L; IQR= 0.58 - 0.98 ml/L).

2.3.6. Rates of faunal and environmental change

Changes in faunal composition along DCA Axis 1 are minor between sequential samples with a median absolute ecological change between samples of 0.11 SDs per 100 years (IQR = -0.11 to 0.12). Changes in DCA Axis 1 sample scores exceeding 1 SD/100 years toward higher scores occur 11 times in the record and 12 times toward lower scores; changes exceeding 2 SD/100 years occur 5 times toward higher DCA Axis 1 scores and thrice toward lower scores (Figure 2.5). The most rapid faunal shift toward higher DCA Axis 1 scores occurs at 29 ka with additional changes >2 SD/100 years at 9.8, 11.0, 11.8 and 14.8 ka. Similarly, changes in oxygenation values calculated using the modified BDO index (>63 μm size fraction) are generally low between adjacent samples with a median absolute change of 0.07 (IQR = 0.03 - 0.17) ml/L per 100 years. However, changes in oxygenation exceeding 0.5 ml/L per 100 years occurs 18 times and changes exceeding 1 ml/L per 100 years occurs five times in our record (Figure 2.5). Of these, 10 are decreases in oxygenation and 8 are increases in oxygenation. The most rapid oxygenation changes co-occur with rapid changes in DCA Axis 1 scores (Figure 2.5).

Of the 355 fossil assemblages, 50 are most similar to samples from the modern shelf (Supplemental Table 2.7). Thus, we reevaluated changes in oxygenation after removing all the samples that are most similar to the shelf samples to reduce the potential influence of downslope transport on the abruptness of faunal changes. All retained fossil samples had modern analogs from water depths greater than 473 m. Some abrupt changes in DCA Axis 1 scores are diminished as faunal shifts are now stretched over greater potential time or are offset to occur earlier (Figure 2.5). In this restricted set of calculations, the median absolute change in oxygenation is 0.06 (IQR = 0.02 - 0.16) ml/L

per 100 years. Changes in oxygenation exceeding 0.5 ml/L per 100 years occur 15 times and changes exceeding 1 ml/L per 100 years occur four times (Figure 2.5).

2.4. Discussion

2.4.1. Primary determinant of faunal composition is oxygenation

Benthic foraminifera are commonly used as marine paleo-oxygenation proxies, however confounding environmental factors such as organic carbon availability can complicate their use (Jorrissen et al., 2007; Gooday, 1993; Gooday, 2012). In our approach to reconstructing the oxygenation history of GoA, we first use multivariate analyses of species-level faunal assemblages to detect faunal gradients and cross-validate the gradients using concentrations of redox-sensitive metals measured on the same sediments from which we collected the foraminifera. We find that the redox-sensitive metal concentrations generally increase with increasing DCA Axis 1 scores, suggesting that, while these co-registered proxies are independently measured, they reflect a similar oxygenation gradient. This interpretation is further supported by high positive DCA Axis 1 scores for species associated with dysoxic conditions in modern environments. The stronger association between DCA Axis 1 and U/Al than between DCA Axis 1 and Mo/Al suggests that benthic foraminiferal assemblage composition is sensitive to oxygen variation at suboxic levels and is not simply responding to a threshold condition such as the presence or absence of sulfidic conditions.

The positive association between redox sensitive metal concentrations and the position of samples in the overall faunal ordination space further underscores the

importance of oxygen in structuring the GoA assemblages. Species known to respond positively to phytodetritus input have the most influence on DCA Axis 2 scores, suggesting that this secondary, orthogonal, axis reflects differences in organic carbon availability. Unlike DCA Axis 1, species with known tolerances for low-oxygen conditions have both positive and negative DCA Axis 2 scores, suggesting little direct influence of oxygenation on DCA Axis 2. Our previous analysis of benthic foraminiferal faunas at two sites in GoA extending to ~23 ka also found that variation in oxygen-sensitive and productivity-sensitive components of the fauna were separated on different ordination axes (Belanger et al., 2020). The separation of oxygen-sensitive and productivity-sensitive components of the faunal variation in our GoA records on orthogonal axes strengthens our ability to use DCA Axis 1 scores as the basis for estimating quantitative oxygenation changes.

2.4.2. Sensitivity of faunal and environmental gradients to size fraction

Inconsistencies in the faunal size fraction examined among studies can pose a challenge for comparisons among regions and could inadvertently bias the reconstructed oxygenation histories (Schönfeld et al., 2012; Weinkauf and Milker, 2018). While some studies suggest using only individuals >125 μm is more efficient and does not strongly affect environmental or ecological interpretations (Bouchet et al., 2012; Schönfeld et al., 2012), the smaller size fractions (63-125 μm) may contribute important faunal variation in eutrophic or low-oxygen settings (Schönfeld et al., 2012; Gooday and Goineau, 2019). In addition, comparisons of the >125 μm and >150 μm size fractions show that subtle

variations between size fractions can contribute significant variations in assemblage counts and subsequent multivariate analyses (Weinkauf and Milker, 2018).

Comparisons among analyses using different size fractions herein, however, suggest that faunal variation is similarly captured regardless of size fraction (Figure 2.3). While the majority of foraminiferal individuals are in the 63-125 μm size fraction in the GoA dataset, the taxonomic composition is similar among size fractions. Further, faunal variation is partitioned similarly among DCA axes in each size fraction and the position of samples in DCA space is similar between the analyses. However, the position of species in DCA space is not as well correlated among size fractions, suggesting that species positions in ordination space are not as stable as sample positions, which incorporate the relative abundances of all species. Together, these comparisons suggest that analyses using total faunas are likely to replicate similar ecological and environmental gradients regardless of size fraction, but size-fraction choices may affect analyses that rely on index taxa.

2.4.3. Quantifying paleo-oxygenation in the Gulf of Alaska

Differences in the taxa incorporated into oxygen reconstructions could also affect the perceived severity of low-oxygen events in paleoceanographic records, however index taxon methods prevail in the literature, even among studies incorporating multivariate faunal analyses (e.g., Ohkushi et al., 2013; Tetard et al., 2017). For the GoA, BDO calculations restricted to literature-derived oxygen tolerances reconstruct significantly lower oxygen concentrations than the full fauna; the disproportionate inclusion of species at the low-oxygen end of the faunal gradient in the literature-based calculations likely

drives this bias (Figure 2.6 (A)). In contrast, there is no systematic difference between oxygenation values calculated using all taxa in the >63 μm size fraction compared to all taxa in the >125 μm size fraction (Figure 2.6 (B)). Thus, taxonomic inclusion affects these oxygen calculations, but, when using all observed species, size fraction choices introduce no systematic bias for the GoA record Figure 2.6.

For the GoA site, our modified BDO index accurately reconstructs the modern measured oxygen concentrations using the full fauna from modern surface sediment samples, suggesting our assignment of taxa to oxygenation categories reflects the foraminiferal tolerances well. Further, the dissolved oxygen calculations for the modern assemblages are positively related to the modern measured oxygen values suggesting that the faunas successfully record relative differences in oxygenation. However, the BDO values severely underestimate oxygen concentrations above 1.5 ml/L (Figure 2.6 (C)). This limitation is expected given the equation is restricted to producing values between 0.1 and 1.5 ml/L. Further, foraminiferal assemblages do not tend to vary in response to oxygenation above >1 or 2 ml/L (Murray, 2001; Moffit et al., 2015), but modern oxygen concentrations in the data set exceed 7 ml/L. Ohkushi et al. (2013) further suggested that the BDO index overestimates the lowest oxygen values. This is reflected in GoA in the overestimate of modern oxygenation for sites with WOA oxygen concentrations <0.5 ml/L (Figure 2.6 (C)). Differences between the measured dissolved oxygen and the BDO values may also occur because the WOA values are from near-bottom waters rather than at the sediment-water interface or within pore waters where benthic foraminifera reside. Our modified BDO index is not systematically biased for modern oxygen concentrations

between 0.5 ml/L and 1.5 ml/L and, thus, may be most reliable for observed oxygen values in that range. Despite these potential inaccuracies, calculated BDO values <0.45 ml/L occur when Mo/Al values are in the 90th upper quantile of our data set, consistent with measurable Mo accumulation occurring at O_2 values <0.51 ml/L (Zheng et al., 2000). Further, samples with the highest Mo/Al values (upper 95th quantile of our data) have a median BDO value of 0.23 ml/L, consistent with the interpretation that the presence of authigenic Mo suggests bottom water oxygen values <0.22 ml/L (Zheng et al., 2000). Mo/Al values as low as 0.25 ppm/wt% also straddle the dysoxic-suboxic boundary reconstructed by the faunal assemblages while lower Mo/Al values correspond to the more oxic faunas. Thus, the oxygenation values reconstructed by the faunas are consistent with the known redox behavior of Mo. Similarly, higher U/Al values correspond tend to correspond with lower BDO estimates from the faunas.

Given the faunal-based BDO calculations herein tend to overestimate oxygenation at the lowest values, and low BDO estimates are strongly associated with the highest Mo/Al values, we are confident that when the calculation produces oxygen concentrations <0.5 ml/L, the conditions were indeed dysoxic. Using these methods, we find either 21 or 32 fossil samples that indicate lower oxygen conditions in the past 54 ka than present in the modern GoA data set based upon WOA-derived data (minimum of 0.36 ml/L O_2) or the BDO estimates using modern benthic foraminiferal assemblages (minimum of 0.44 ml/L O_2), respectively. This suggests that this upper oxygen minimum zone site experienced lower oxygen conditions in the past than anywhere in the modern GoA. While benthic foraminiferal proxies primarily reflect pore water oxygenation, previous studies

have related low (<5%) abundances of oxic taxa to I/Ca values from epifaunal benthic foraminifera that suggest dysoxic bottom waters (Taylor et al., 2017). In our record, species assigned to the weakly-hypoxic to oxic category make up fewer than 5% of individuals in samples with the lowest BDO values. Thus, when our benthic foraminiferal faunas indicate extreme dysoxia in the pore waters, oxygen was likely also low in the bottom waters.

The environmental tolerances of benthic foraminifera most abundant in our lowest oxygen samples also support past low-oxygen conditions with no modern analog in the GoA. Species that dominate our lowest oxygen assemblages, such as *B. tenuata*, *B. seminuda, and B. argentea,* are rare in the modern GoA samples. These species are known to perform complete denitrification, to have a metabolic preference for nitrate as an electron acceptor, or are associated with denitrifying chemosymbionts (Piña-Ochoa et al., 2010; Bernhard et al., 2012; Glock et al., 2019). The presence of these species with metabolic adaptations for living in oxygen-depleted sediments further indicates the presence of no-analog low-oxygen conditions in our record.

These low-oxygen conditions in GoA that favor benthic foraminifera able to use nitrate-based metabolisms suggest that metazoan species would be extirpated during the dysoxic events. Median lethal dissolved oxygen concentrations from a study of benthic crabs, fish, bivalves and gastropods is ~1.2 ml/L (Vaquer-Sunyer and Duarte, 2008), which is far better oxygenated than we infer during dysoxic intervals. Laminated muds also occur in this record, particularly during the deglacial and at ~29, 36, and 43 ka (Davies et al., 2011; Penkrot et al., 2018), further suggesting that oxygen levels were occasionally

low enough to exclude or reduce the activity of metazoans. Metazoan meiofauna (such as some nematodes) are more tolerant of low-oxygen conditions (Gallo and Levin, 2016), thus sediments under suboxic conditions, even if previously laminated during preceding dysoxia, may still have bioturbation due to the activities of those specialists.

2.4.4. Occurrence and duration of low oxygen events

Previous work in the GoA recognized low-oxygen events during the last deglacial using redox sensitive metals and selected index taxa from jumbo piston core and adjacent multicore (Davies et al., 2011; Praetorious et al., 2015) and using whole faunal assemblage analyses based on foraminiferal proxies at Site U1419 over the past 54 ka at much lower temporal resolution (Belanger et al., 2016). In the present study, using much higher resolution, we recognize low-oxygen events from whole assemblage analyses in interglacial, deglacial, and glacial conditions that are supported by enrichments in redox sensitive metals. While we base our faunally derived oxygenation history below on the >63 μm size fraction, the occurrence of events does not differ significantly when considering only the >125 μm size fraction (Figure 2.3).

2.4.4.1. Low-oxygen events in MIS 2 to the Holocene

Analyses of modern assemblages from the site indicate suboxic conditions, as expected from the site's position in the upper OMZ. Our high-resolution faunal analysis recognizes severe dysoxic events in the earliest Holocene and during the B/A interstadial. Between 14.7 and 13.8 ka, modified BDO values are sustained below 0.27 ml/L O_2 with redox metals values frequently in the upper 90^{th} upper quantile of the data. This dysoxic event is followed by a better-oxygenated interval (BDO: 0.4 - 0.7 ml/L) from 13.2 - 11.8

ka, overlapping the YD. BDO estimates below 0.50 ml/L O_2 then reoccur in the early Holocene immediately following the YD along with elevated concentrations of Mo/Al and U/Al. In total, this deglacial low-oxygen interval lasts for ~4 ka in our GoA record, with a brief interruption during the YD, and corroborates previous work at the site (Davies et al., 2011; Praetorious et al., 2015; Du et al., 2018). Overall, redox sensitive metals corroborate the BDO estimates, especially during the extreme low-oxygen events in the deglacial.

Deglacial dysoxia during the B/A is also well recorded elsewhere in the North Pacific margin, but the proposed drivers vary (Moffitt et al., 2015). At ODP Site 1017, on the slope near Point Conception on the California margin, local productivity may have driven pore-water deoxygenation during the Bølling whereas incursion of low-oxygen intermediate waters may have contributed to dysoxia during the Allerød (Taylor et al., 2017). OMZ intensification on the Cascadia Margin also occurred during the B/A following a dramatic increase in primary productivity related to intense upwelling driven by changes in the California Undercurrent (McKay et al., 2005; Saravanan et al., 2020). High productivity has also been reported during the B/A in the Bering Sea and during the Allerød in the Okhotsk Sea (Max et al., 2014). The Bering and Okhotsk Seas are potential sources of NPIW during the glacial while the Okhotsk Sea is the primary source of NPIW in the modern (Rella et al., 2012; Max et al., 2014; Knudson and Ravelo, 2015; Ohkushi et al., 2016). NPIW extends to the eastern parts of the North Pacific and low-oxygen conditions in Okhotsk Sea Intermediate Water (OSIW) influence the GoA and the eastern North Pacific margin (Max et al., 2014; Ohkushi et al., 2016). Local factors, such as

organic carbon export, may then contribute to further deoxygenation of these source-waters.

Better-oxygenated intervals occur in our record during Heinrich Stadial (HS) 1 and the YD, consistent with previous GoA studies (Davies et al., 2011; Praetorious et al., 2015; Du et al., 2018; Belanger et al., 2020) and other North Pacific records. For example, increased oxygenation during HS1 in our record (17-15 ka, BDO >0.99 ml/L) coincides with oxygenation >1.5 ml/L Santa Barbara Basin (SBB) (Cannariato et al., 1999; Ohkushi et al., 2013) and with a well-ventilated interval in the Okhotsk Sea (Max et al., 2014; Ohkushi et al. 2016) and Okinawa Trough (Zou et al., 2020). During the YD, intermediate depths on the eastern and western Pacific margins were also better-oxygenated (Cannariato et al., 1999; Cannariato and Kennett, 1999; McKay et al., 2005; Max et al., 2014; Tetard et al., 2017; Taylor et al., 2017; Zou et al., 2020). This relaxation of severe low-oxygen conditions is consistent with enhanced NPIW ventilation during the YD suggested by records near Hokkaido, Japan (Ikehara et al., 2006; Shibahara et al., 2007; Ohkushi et al., 2016). Thus, better ventilation and decreased biological productivity during colder periods in the OSIW had broad effects on oxygenation in the GoA and California margin (Shibahara et al., 2007; Ohkushi et al., 2016). However, a decrease in primary productivity locally may also contribute to the increase in oxygenation on the California margin (Taylor et al., 2017).

Following the YD, oxygenation declined in GoA during the early Holocene (11.2 - 10.9 ka). A similarly timed low-oxygen event occurred near Vancouver Island from ~11 - 10 ka, potentially driven by decreased ventilation and increased productivity (McKay et

al., 2005). In addition, dysoxic foraminifera increased in abundance during the early Holocene along the California margin to Baja California and in the western subtropical North Pacific (Cannariato and Kennett, 1999; Tetard et al., 2017; Zou et al., 2020), suggesting this low-oxygen event was also widespread. After this early Holocene deoxygenation, suboxic conditions dominate the remainder of our GoA record as evinced by generally higher DCA Axis 1 scores and lower BDO estimates (0.55 - 0.80 ml/L). Mo/Al and U/Al values in our record are also generally low (<80th upper quantile) during the Holocene, supporting oxygenation levels above the threshold accumulation for these metals. California margin slope Site ODP 1017, also increased in oxygenation after early Holocene dysoxia, while sites in the SBB, Baja California, and Sea of Japan remained as dysoxic as during the B/A (Cannariato et al., 1999; Cannariato and Kennett, 1999; Shibahara et al., 2007; Ohkushi et al., 2013; Tetard et al., 2017). Therefore, the GoA has a Holocene oxygenation history more similar to slope sites elsewhere in the North Pacific as compared to sites from more restricted basins, suggesting that local processes drive the maintenance of dysoxia at those sites. Previous work in the SBB and the California margin also suggests local changes in productivity become a more prominent control of oxygenation during the Holocene (Ivanochko and Pederson, 2004).

2.4.4.2. Dysoxia during the last glacial

Long sedimentary records extending to MIS 3 that permit high-resolution analyses are generally lacking in the higher latitudes of the eastern North Pacific unlike more southern sites. In our ~54 kyr-long GoA record, faunal DCA Axis 1 scores and our modified BDO estimates suggest better-oxygenated background conditions during the

glacial than during the Holocene. Similarly, on the California margin paleo-oxygen records based on foraminiferal proxies indicate better oxygenation in glacial times than in MIS 1 and 2 (Cannariato et al., 1999; Cannariato and Kennett, 1999; Ohkushi et al., 2013; Tetard et al., 2017). Thus, our paleo-oxygen reconstruction is overall consistent with lower-latitude foraminiferal records.

Despite the better-oxygenated background conditions of the glacial, we reconstruct three dysoxic events at 36.9 - 36.8 ka, 44 - 43.9 ka and 46.7 - 45.7 ka that have BDO estimates <0.5 ml/L in more than one sample and are corroborated by enriched redox sensitive metals. Co-registered faunal assemblages and redox-sensitive metal concentrations also support shorter duration dysoxic events registered in single samples (Figure 2.3). BDO estimates suggest these MIS 3 dysoxic events are as low-oxygen as those in the better-studied deglacial and early Holocene (Figure 2.5). A lower-resolution U1419 record of biomarkers for the anaerobic oxidation of ammonium has a glacial high at ~46 ka, which corresponds with our longest period of dysoxia in MIS 3, and a lesser peak at ~29 ka coincident with a single-sample dysoxic event we detect, suggesting that water column oxygenation was also lowest during these intervals (Zindorf et al., 2020). While potential uncertainties in age models make it difficult to directly align these events with those of other regions, similarly timed short-lived decreases in oxygenation occur in Baja California and the SBB where they appear to coincide with Daansgard-Oeschger (D-O) events and interstadials (Cannariato et al., 1999; Tetard et al., 2017). Thus, it is likely that these glacial-age low-oxygen events reported at lower latitudes occurred throughout the North Pacific Margin, including at subarctic latitudes. In addition, high-productivity

events are recorded in the Bering Sea during MIS 3 that are also similar in timing to D-O events (Schlung et al., 2013), thus these shorter-term glacial events in GoA may also be influenced by productivity as hypothesized for the B/A dysoxic event and suggested by the high relative abundances of phytodetritus-sensitive species prior to the low-oxygen events (Figure 2.2).

Given many of these glacial dysoxic events in GoA lasted no longer than ~100 - 400 years based upon the ages of adjacent samples in which faunas indicate suboxic to weakly hypoxic conditions and redox metals are not enriched, it is clear that high-resolution sampling is necessary to capture these environmental changes. Given that our sample spacing exceeds 100 years in ~60% of cases, it is likely that our reconstruction also omits some low oxygen events recognized elsewhere in the North Pacific and certainly omits events that are shorter in duration than 100 years. For example, SBB records capture 9 dysoxic events from ~22 to 45 ka (Cannariato and Kennett, 1999), however our GoA record captures 6 events over the same interval. In addition, short-lived low-oxygen events are susceptible to bioturbation, which could have obscured the low-oxygen signal in the faunal record, and to oxic burn down of redox sensitive metals, which would remove this chemical tracer of low-oxygen (Zheng et al., 2002).

2.4.5. Rates of faunal and oxygenation changes

While consecutive samples are typically similar to each other in their faunal composition given the high resolution of our sampling, changes in DCA Axis 1 scores exceeding 1 SD/100 years do occur between sequential adjacent samples, suggesting that changes in faunal composition can occur quite rapidly (Figure 2.5). Re-analysis

considering potential down-slope transport suggested by the modern analog comparisons yield similar rates, thus the occurrence of downslope transport cannot explain the rapid changes in oxygenation conditions. Further, independent evidence for sedimentary transport at this site for the last ~54 ka is unreported. Changes in grain size and faunal composition could instead reflect in situ changes in environmental changes expected with influx of ice-rafted debris during glacial melting or blockage of fjords as glaciers retreat (Davies et al., 2011; Penkrot et al., 2018).

Systematic biases in the BDO equation imply that calculations of the rate of change from well-oxygenated conditions to low-oxygen conditions will be underestimates. Despite this shortcoming, we find multiple rapid changes in BDO values exceeding 0.5 ml/L per 100 years, even after accounting for potential downslope transport. Uncertainty in the age model can also affect our calculations of rates, however any errors due to interpolation between the high-resolution radiocarbon data points should have an equal likelihood of decreasing rates as increasing them. Thus, it is likely that biologically significant changes in oxygenation can occur on decadal to centennial timescales in the upper OMZ of the GoA.

2.5. Conclusions

Cross-validated faunal and geochemical proxies reveal dysoxic and suboxic intervals during glacial, deglacial and interglacial times in GoA. Our quantitative paleo-oxygen reconstructions using total benthic foraminiferal assemblages, rather than index taxa, are robust to size fraction differences and suggest that the larger size fraction is sufficient for reconstructing paleo-oxygenation. Comparisons between modern and fossil

assemblages demonstrate that oxygenation in the upper OMZ in GoA was lower than anywhere in the modern GoA during the last deglacial and during three distinct intervals in MIS 3. Thus, an intense OMZ can develop in this subarctic region during both glacial and interglacial times, similar to lower latitudes and restricted basins elsewhere in the North Pacific. Similarities in the timing of events across the North Pacific suggests a common, basin-wide driver of oxygenation, perhaps related to warm climate events, enhanced productivity around the basin margins, or changing intermediate-depth ventilation. While many of the low-oxygen events in GoA are geologically brief, transitions between oxic and suboxic conditions, or between suboxic and dysoxic conditions, can occur in less than 100 years, rapidly enough to have ecological consequences. Quantitative estimates of oxygenation such as these from benthic foraminiferal assemblages are important for modeling of future changes in oxygen minimum zones and their ecosystem effects.

2.6. References

Addison, J. A., Finney, B. P., Dean, W. E., Davies, M. H., Mix, A. C., Stoner, J. S., & Jaeger, J. M. (2012). Productivity and sedimentary $\delta^{15}N$ variability for the last 17,000 years along the northern Gulf of Alaska continental slope. *Paleoceanography*, *27*(1), PA1206. https://doi.org/10.1029/2011PA002161

Alve, E. (2003). A common opportunistic foraminiferal species as an indicator of rapidly changing conditions in a range of environments. *Estuarine, Coastal and Shelf Science*, *57*(3), 501–514. doi.org/10.1016/S0272-7714(02)00383-9

Belanger, C. L., Du, J., Payne, C. R., & Mix, A. C. (2020). North Pacific deep-sea ecosystem responses reflect post-glacial switch to pulsed export productivity, deoxygenation, and destratification. *Deep Sea Research Part I: Oceanographic Research Papers*, 103341. doi.org/10.1016/j.dsr.2020.103341

Belanger, C. L., Orhun, O. G., & Schiller, C. M. (2016). Benthic foraminiferal faunas reveal transport dynamics and no-analog environments on a glaciated margin (Gulf of Alaska). *Palaeogeography, Palaeoclimatology, Palaeoecology*, *454*, 54–64. https://doi.org/10.1016/j.palaeo.2016.04.032

Belanger, C. L., & Villarosa Garcia, M. (2014). Differential drivers of benthic foraminiferal and molluscan community composition from a multivariate record of early Miocene environmental change. *Paleobiology*, *40*(3), 398–416. https://doi.org/10.1666/13019

Bergen, F. W., & O'Neil, P. (1979). Distribution of Holocene foraminifera in the Gulf of Alaska. *Journal of Paleontology*, *53*(6), 1267–1292.

Bernhard, J. M., Casciotti, K. L., McIlvin, M. R., Beaudoin, D. J., Visscher, P. T., & Edgcomb, V. P. (2012). Potential importance of physiologically diverse benthic foraminifera in sedimentary nitrate storage and respiration. *Journal of Geophysical Research: Biogeosciences*, *117*, G03002. https://doi.org/10.1029/2012JG001949

Bograd, S. J., Castro, C. G., Di Lorenzo, E., Palacios, D. M., Bailey, H., Gilly, W., & Chavez, F. P. (2008). Oxygen declines and the shoaling of the hypoxic boundary in the California Current. *Geophysical Research Letters*, *35*, L12607. https://doi.org/10.1029/2008GL034185

Bouchet, V. M. P., Alve, E., Rygg, B., & Telford, R. J. (2012). Benthic foraminifera provide a promising tool for ecological quality assessment of marine waters. *Ecological Indicators*, *23*, 66–75. https://doi.org/10.1016/j.ecolind.2012.03.011

Bubenshchikova, N., Nürnberg, D., & Tiedemann, R. (2015). Variations of Okhotsk Sea oxygen minimum zone: Comparison of foraminiferal and sedimentological records for latest MIS 12–11c and latest MIS 2–1. *Marine Micropaleontology*, *121*, 52–69. https://doi.org/10.1016/j.marmicro.2015.09.004

Bush, A. M., & Brame, R. I. (2010). Multiple paleoecological controls on the composition of marine fossil assemblages from the Frasnian (Late Devonian) of Virginia, with a comparison of ordination methods. *Paleobiology*, *36*(4), 573–591.

Buzas, M. (1990). Another look at confidence limits for species proportions. *Journal of Paleontology, 64*(5), 842-843. https://doi:10.1017/S002233600001903X

Calvert, S. E., & Pedersen, T. F. (1993). Geochemistry of recent oxic and anoxic marine sediments: implications for the geological record. *Marine Geology*, *113*(1–2), 67–3227.

Cannariato, K., & Kennett, J. (1999). Climatically related millennial-scale fluctuations in strength of California margin oxygen-minimum zone during the past 60 k.y. *Geology*, *27*, 975–978.

Cannariato, K. G., Kennett, J. P., & Behl, R. J. (1999). Biotic response to late Quaternary rapid climate switches in Santa Barbara Basin: Ecological and evolutionary implications. *Geology*, *27*(1), 63–66.

Carlson, P. R. (1989). Seismic reflection characteristics of glacial and glacimarine sediment in the Gulf of Alaska and adjacent fjords. *Marine Geology*, *85*(2–4), 391–416.

Cartapanis, O., Tachikawa, K., & Bard, E. (2011). Northeastern Pacific oxygen minimum zone variability over the past 70 kyr: Impact of biological production and oceanic ventilation. *Paleoceanography*, *26*(4), PA4208. https://doi.org/10.1029/2011PA002126

Cedhagen, T. (1991). Retention of chloroplasts and bathymetric distribution in the sublittoral foraminifera *Nonionellina labradorica*. *Ophelia*, *33*, 17–30. https://doi.org/10.1080/00785326.1991.10429739

Childers, A. R., Whitledge, T. E., & Stockwell, D. A. (2005). Seasonal and interannual variability in the distribution of nutrients and chlorophyll a across the Gulf of Alaska shelf: 1998–2000. *Deep Sea Research Part II: Topical Studies in Oceanography*, *52*(1), 193–216. https://doi.org/10.1016/j.dsr2.2004.09.018

Correa-Metrio, A., Bush, M. B., Cabrera, K. R., Sully, S., Brenner, M., Hodell, D. A., et al. (2012). Rapid climate change and no-analog vegetation in lowland Central America during the last 86,000 years. *Quaternary Science Reviews* 38: 63-75. https://doi.org/10.1016/j.quascirev.2012.01.025

Crusius, J., Calvert, S., Pedersen, T., & Sage, D. (1996). Rhenium and molybdenum enrichments in sediments as indicators of oxic, suboxic and sulfidic conditions of deposition. *Earth and Planetary Science Letters*, *145*, 65–78. https://doi.org/10.1016/S0012-821X(96)00204-X

Davies, M. H., Mix, A. C., Stoner, J. S., Addison, J. A., Jaeger, J., Finney, B., & Wiest, J. (2011). The deglacial transition on the southeastern Alaska Margin: Meltwater input, sea level rise, marine productivity, and sedimentary anoxia. *Paleoceanography and Paleoclimatology*, *26*, PA2223. https://doi.org/10.1029/2010PA002051

Deutsch, C., Brix, H., Ito, T., Frenzel, H., & Thompson, L. (2011). Climate-forced variability of ocean hypoxia. *Science*, *333*(6040), 336–339. https://doi.org/10.1126/science.1202422

Diaz, R. J., & Rosenberg, R. (2008). Spreading dead zones and consequences for marine ecosystems. *Science*, *321*(5891), 926–929. https://doi.org/10.1126/science.1156401

Dobson, M. R., O'Leary, D., & Veart, M. (1998). Sediment delivery to the Gulf of Alaska: source mechanisms along a glaciated transform margin. *Geological Society, London, Special Publications*, *129*(1), 43-66.

Du, J., Haley, B. A., Mix, A. C., Walczak, M. H., & Praetorius, S. K. (2018). Flushing of the deep Pacific Ocean and the deglacial rise of atmospheric CO_2 concentrations. *Nature Geoscience*, *11*(10), 749–755. https://doi.org/10.1038/s41561-018-0205-6

Echols, R. J., & Armentrout, J. M. (1980). Holocene foraminiferal distribution patterns on shelf and slope, Yakataga-Yakutat area, Northern Gulf of Alaska. *AAPG Bulletin*, *64*(3), 440–441.

Erdem, Z., & Schönfeld, J. (2017). Pleistocene to Holocene benthic foraminiferal assemblages from the Peruvian continental margin. *Palaeontologia Electronica*, *20.2.35A*, 1–32. https://doi.org/10.26879/764

Forcino, F. L., Leighton, L. R., Twerdy, P., & Cahill, J. F. (2015). Reexamining Sample Size Requirements for Multivariate, Abundance-Based Community Research: When Resources are Limited, the Research Does Not Have to Be. *PLOS ONE*, *10*(6), e0128379. https://doi.org/10.1371/journal.pone.0128379

Fürsich, F. T., & Aberhan, M. (1990). Significance of time-averaging for palaeocommunity analysis. *Lethaia*, *23*(2), 143–152. https://doi.org/10.1111/j.1502-3931.1990.tb01355.x

Gallo, N. D., & Levin, L. A. (2016). Fish ecology and evolution in the world's oxygen minimum zones and implications of ocean deoxygenation. *Advances in Marine Biology*, *74*, 117–198. https:// doi.org/10.1016/bs.amb.2016.04.001

Garcia, H. E., Boyer, T. P., Locarnini, R. A., Antonov, J. I., Mishonov, A. V, Baranova, O. K., et al. (2013). World ocean atlas 2013. Volume 3: Dissolved oxygen, apparent oxygen utilization, and oxygen saturation. In S. Levitus & A. Mishonov (Eds.), *NOAA Atlas NESDIS 75* (p. 27).

Gilly, W. F., Beman, J. M., Litvin, S. Y., & Robison, B. H. (2013). Oceanographic and biological effects of shoaling of the oxygen minimum zone. *Annual Review of Marine Science*, *5*, 393–420.

Glock, N., Roy, A.-S., Romero, D., Wein, T., Weissenbach, J., Revsbech, N. P., et al. (2019). Metabolic preference of nitrate over oxygen as an electron acceptor in foraminifera from the Peruvian oxygen minimum zone. *Proceedings of the National Academy of Sciences*, *116*(8), 2860–2865. https://doi.org/10.1073/pnas.1813887116

Gooday, A. J. (1993). Deep-sea benthic foraminiferal species which exploit phytodetritus: Characteristic features and controls on distribution. *Marine Micropaleontology*, *22*(3), 187–205. https://doi.org/10.1016/0377-8398(93)90043-W

Gooday, A. J., & Goineau, A. (2019). The contribution of fine sieve fractions (63–150 μm) to foraminiferal abundance and diversity in an area of the Eastern Pacific Ocean licensed for polymetallic nodule exploration. *Frontiers in Marine Science*, *6*, 114. https://doi.org/10.3389/fmars.2019.00114

Gooday, A. J., & Jorissen, F. J. (2012). Benthic Foraminiferal Biogeography: Controls on Global Distribution Patterns in Deep-Water Settings. *Annual Review of Marine Science*, *4*(1), 237–262. https://doi.org/10.1146/annurev-marine-120709-142737

Goslee, S. C., & Urban, D. L. (2007). The ecodist package for dissimilarity-based analysis of ecological data. *Journal of Statistical Software*, *22*(7), 1–19.

Gray, W. R., Rae, J. W. B., Wills, R. C. J., Shevenell, A. E., Taylor, B., Burke, A., et al. (2018). Deglacial upwelling, productivity and CO2 outgassing in the North Pacific Ocean. *Nature Geoscience*, *11*(5), 340–344. https://doi.org/10.1038/s41561-018-0108-6

Gulick, S. P. S., Jaeger, J. M., Mix, A. C., Asahi, H., Bahlburg, H., Belanger, C. L., et al. (2015). Mid-Pleistocene climate transition drives net mass loss from rapidly uplifting St. Elias Mountains, Alaska. *Proceedings of the National Academy of Sciences*, *112*(49), 15042 – 15047. https://doi.org/10.1073/pnas.1512549112

Helly, J. J., & Levin, L. A. (2004). Global distribution of naturally occurring marine hypoxia on continental margins. *Deep Sea Research Part I: Oceanographic Research Papers*, *51*(9), 1159–1168.

Ito, T., Minobe, S., Long, M.C. & Deutsch, C. (2017). Upper ocean O_2 trends: 1958–2015. *Geophysical Research Letters*, *44*(9), 4214–4223.

Ivanochko, T. S., & Pedersen, T. F. (2004). Determining the influences of Late Quaternary ventilation and productivity variations on Santa Barbara Basin sedimentary oxygenation: a multi-proxy approach. *Quaternary Science Reviews*, *23*(3), 467–480. https://doi.org/10.1016/j.quascirev.2003.06.006

Jochum, K. P., Weis, U., Schwager, B., Stoll, B., Wilson, S. A., Haug, G. H., et al. (2016). Reference Values Following ISO Guidelines for Frequently Requested Rock Reference Materials. *Geostandards and Geoanalytical Research*, *40*(3), 333–350. https://doi.org/10.1111/j.1751-908X.2015.00392.x

Jaccard, S. L., & Galbraith, E. D. (2013). Direct ventilation of the North Pacific did not reach the deep ocean during the last deglaciation. *Geophysical Research Letters*, *40*(1), 199–203. https://doi.org/10.1029/2012GL054118

Jaccard, S. L., & Galbraith, E. D. (2012). Large climate-driven changes of oceanic oxygen concentrations during the last deglaciation. *Nature Geoscience*, *5*(2), 151–156. https://doi.org/10.1038/ngeo1352

Jaeger, J. M., Gulick, S. P. S., LeVay, L. J., Asahi, H., Bahlburg, H., Belanger, C. L., et al. (2014). *Proceedings of the Integrated Ocean Drilling Program Vol. 341: Expedition reports Southern Alaska margin*. Integrated Ocean Drilling Program.

Jorissen, F. J., Fontanier, C., & Thomas, E. (2007). Paleoceanographical proxies based on deep-sea benthic foraminiferal assemblage characteristics. In C. Hillaire–Marcel & A. De Vernal (Eds.), *Proxies in Late Cenozoic Paleoceanography*, *1*, 263–325. https://doi.org/10.1016/S1572-5480(07)01012-3

Keeling, R. F., Körtzinger, A., & Gruber, N. (2010). Ocean deoxygenation in a warming world. *Annual Review of Marine Science*, *2*(1), 199–229. https://doi.org/10.1146/annurev.marine.010908.163855

Klinkhammer, G. P., & Palmer, M. R. (1991). Uranium in the oceans: Where it goes and why. *Geochimica et Cosmochimica Acta*, *55*(7), 1799–1806. https://doi.org/10.1016/0016-7037(91)90024-Y

Knudson, K. P., & Ravelo, A. C. (2015). North Pacific Intermediate Water circulation enhanced by the closure of the Bering Strait. *Paleoceanography*, *30*(10), 1287–1304. https://doi.org/10.1002/2015PA002840

Li, G., Rashid, H., Zhong, L., Xu, X., Yan, W., & Chen, Z. (2018). Changes in Deep Water Oxygenation of the South China Sea Since the Last Glacial Period. *Geophysical Research Letters*, *45*(17), 9058–9066. https://doi.org/10.1029/2018GL078568

Max, L., Lembke-Jene, L., Riethdorf, J. R., Tiedemann, R., Nürnberg, D., Kühn, H., & MacKensen, A. (2014). Pulses of enhanced north Pacific intermediate water ventilation from the Okhotsk Sea and Bering Sea during the last deglaciation. *Climate of the Past*, *10*(2), 591–605. https://doi.org/10.5194/cp-10-591-2014

McKay, J. L., Pedersen, T. F., & Southon, J. (2005). Intensification of the oxygen minimum zone in the northeast Pacific off Vancouver Island during the last deglaciation: Ventilation and/or export production? *Paleoceanography*, *20*, PA4002. https://doi.org/10.1029/2003PA000979

McCune, B., Grace, J. B. J. B., & Urban, D. L. (2002). Analysis of Ecological Communities. *MjM Software Design* (Vol. 28). Gleneden Beach, OR.

McManus, J., Berelson, W., Severmann, S., Poulson, R., Hammond, D., Klinkhammer, G., & Holm, C. (2006). Molybdenum and uranium geochemistry in continental margin sediments: Paleoproxy potential. *Geochimica et Cosmochimica Acta*, *70*, 4643–4662. https://doi.org/10.1016/j.gca.2006.06.1564

Mix, A. C., Lund, D. C., Pisias, N. G., Bodén, P., Bornmalm, L., Lyle, M., & Pike, J. (1999). Rapid climate oscillations in the northeast Pacific during the last deglaciation reflect Northern and Southern Hemisphere sources. *Geophysical Monograph-American Geophysical Union*, *112*, 127–148.

Moffitt, S. E., Hill, T. M., Ohkushi, K., Kennett, J. P., & Behl, R. J. (2014). Vertical oxygen minimum zone oscillations since 20 ka in Santa Barbara Basin: A benthic foraminiferal community perspective. *Paleoceanography*, *29*(1), 44–57. https://doi.org/10.1002/2013PA002483

Moffitt, S. E., Moffitt, R. A., Sauthoff, W., Davis, C. V, Hewett, K., & Hill, T. M. (2015). Paleoceanographic insights on recent oxygen minimum zone expansion: Lessons for modern oceanography. *PLOS ONE*, *10*(1), e0115246. https://doi.org/10.1371/journal.pone.0115246

Molnia, B. F. (1983). Subarctic Glacial-Marine Sedimentation: A Model. In B. F. Molnia (Ed*.) Glacial-Marine Sedimentation*. pp. 95–144. Boston, MA: Springer US. https://doi.org/10.1007/978-1-4613-3793-5_2

Muratli, J. M., McManus, J., Mix, A., & Chase, Z. (2012). Dissolution of fluoride complexes following microwave-assisted hydrofluoric acid digestion of marine sediments. *Talanta*, *89*, 195–200.

Muratli, J., Chase, Z., Mix, A., & McManus, J. (2010). Increased glacial-age ventilation of the Chilean margin by Antarctic Intermediate Water. *Nature Geoscience*, *3*: 23-26.

Murray, J. W. (2001). The niche of benthic foraminifera, critical thresholds and proxies. *Marine Micropaleontology*, *41*(1), 1–7. https://doi.org/10.1016/S0377-8398(00)00057-8

Ohkushi, K. I., Itaki, T., Nemoto, N. (2003). Last Glacial–Holocene change in intermediate-water ventilation in the Northwestern Pacific. Quaternary Science Reviews, 22, 1477-1484.

Ohkushi, K., Hara, N., Ikehara, M., Uchida, M., & Ahagon, N. (2016). Intensification of North Pacific intermediate water ventilation during the Younger Dryas. *Geo-Marine Letters*, *36:* 353–360. https://doi.org/10.1007/s00367-016-0450-x

Ohkushi, K., Kennett, J. P., Zeleski, C. M., Moffitt, S. E., Hill, T. M., Robert, C., et al. (2013). Quantified intermediate water oxygenation history of the NE Pacific: A new benthic foraminiferal record from Santa Barbara basin. *Paleoceanography*, *28*(3), 453–467. https://doi.org/10.1002/palo.20043

Oksanen, J., Blanchet, F. G., Friendly, M., Kindt, R., Legendre, P., McGlinn, D., et al. (2017). vegan: Community Ecology Package. cran.r-project.org/package=vegan

Paulmier, A., & Ruiz-Pino, D. (2009). Oxygen minimum zones (OMZs) in the modern ocean. *Progress in Oceanography*, *80*(3), 113–128. https://doi.org/10.1016/j.pocean.2008.08.001

Penkrot, M. L., Jaeger, J. M., Cowan, E. A., St-Onge, G., & Levay, L. (2018). Multivariate modeling of glacimarine lithostratigraphy combining scanning XRF, multisensory core properties, and CT imagery: IODP Site U1419. *Geosphere*,14(4), 1935–1960. https://doi.org/10.1130/GES01635.1

Pierce, S. D., Barth, J. A., Shearman, R. K., & Erofeev, A. Y. (2012). Declining oxygen in the Northeast Pacific. *Journal of Physical Oceanography*, *42*(3), 495–501.

Piña-Ochoa, E., Høgslund, S., Geslin, E., Cedhagen, T., Revsbech, N. P., Nielsen, L. P., et al. (2010). Widespread occurrence of nitrate storage and denitrification among Foraminifera and Gromiida; *Proceedings of the National Academy of Sciences*, *107*(3), 1148 LP – 1153. https://doi.org/10.1073/pnas.0908440107

Praetorius, S. K., Mix, A. C., Walczak, M. H., Wolhowe, M. D., Addison, J. A., & Prahl, F. G. (2015). North Pacific deglacial hypoxic events linked to abrupt ocean warming. *Nature*, *527*, 362–366. https://doi.org/10.1038/nature15753

R Core Team. (2016). R: A Language and Environment for Statistical Computing. Vienna, Austria. www.r-project.org/

Rella, S. F., Tada, R., Nagashima, K., Ikehara, M., Itaki, T., Ohkushi, K., et al. (2012). Abrupt changes of intermediate water properties on the northeastern slope of the

Bering Sea during the last glacial and deglacial period. *Paleoceanography*, *27*(3). https://doi.org/10.1029/2011PA002205

Saravanan, P., Gupta, A. K., Zheng, H., Rai, S. K., & Panigrahi, M. K. (2020). Changes in Deep-Sea Oxygenation in the Northeast Pacific Ocean During 32–10 ka. *Geophysical Research Letters*, *47*(11), e2019GL086613. https://doi.org/10.1029/2019GL086613

Scarponi, D., & Kowalewski, M. (2004). Stratigraphic paleoecology: Bathymetric signatures and sequence overprint of mollusk associations from upper Quaternary sequences of the Po Plain, Italy. *Geology*, *32*(11), 989–992.

Schlung, S. A., Ravelo, A. C., Aiello, I. W., Andreasen, D. H., Cook, M. S., Drake, M., et al. (2013). Millennial-scale climate change and intermediate water circulation in the Bering Sea from 90 ka: A high-resolution record from IODP Site U1340. *Paleoceanography*, *28*(1), 54–67. https://doi.org/10.1029/2012PA002365

Schmidtko, S., Stramma, L., & Visbeck, M. (2017). Decline in global oceanic oxygen content during the past five decades. *Nature*, *542*, 335–339. https://doi.org/10.1038/nature21399

Schmiedl, G., Mitschele, A., Beck, S., Emeis, K.-C., Hemleben, C., Schulz, H., et al. (2003). Benthic foraminiferal record of ecosystem variability in the eastern Mediterranean Sea during times of sapropel S5 and S6 deposition. *Palaeogeography, Palaeoclimatology, Palaeoecology*, *190*, 139–164. https://doi.org/10.1016/S0031-0182(02)00603-X

Schönfeld, J., Alve, E., Geslin, E., Jorissen, F., Korsun, S., & Spezzaferri, S. (2012). The FOBIMO (FOraminiferal BIo-MOnitoring) initiative—Towards a standardized protocol for soft-bottom benthic foraminiferal monitoring studies. *Marine Micropaleontology*, *94–95*, 1–13. https://doi.org/10.1016/j.marmicro.2012.06.001

Schroeder, C. J., Scott, D. B., & Medioli, F. S. (1987). Can smaller benthic foraminifera be ignored in paleoenvironmental analyses? *Journal of Foraminiferal Research*, *17*(2), 101–105. https://doi.org/10.2113/gsjfr.17.2.101

Sen Gupta, B. K., Shin, I. C., & Wendler, S. T. (1987). Relevance of specimen size in distribution studies of deep-sea benthic foraminifera. *PALAIOS*, *2*(4), 332–338. https://doi.org/10.2307/3514758.

Shibahara, A., Ohkushi, K., Kennett, J. P., & Ikehara, K. (2007). Late Quaternary changes in intermediate water oxygenation and oxygen minimum zone, northern Japan: A benthic foraminiferal perspective. *Paleoceanography*, *22*, PA3213. https://doi.org/10.1029/2005PA001234

Schlitzer, R. (2018). Ocean Data View, https://odv.awi.de.

Stabeno, P. J., Bond, N. A., Hermann, A. J., Kachel, N. B., Mordy, C. W., & Overland, J. E. (2004). Meteorology and oceanography of the Northern Gulf of Alaska. *Continental Shelf Research*, *24*(7–8), 859–897.

Sun, X., Corliss, B. H., Brown, C. W., & Showers, W. J. (2006). The effect of primary productivity and seasonality on the distribution of deep-sea benthic foraminifera in the North Atlantic. *Deep Sea Research Part I: Oceanographic Research Papers*, *53*(1), 28–47. https://doi.org/10.1016/j.dsr.2005.07.003

Takahashi, K., Ravelo, A. C., & Okazaki, Y. (2016). Introduction to Pliocene–Pleistocene paleoceanography of the Bering Sea. *Deep Sea Research Part II: Topical Studies in Oceanography*, *125–126*, 1–7. https://doi.org/10.1016/j.dsr2.2016.03.001

Taylor, M. A., Hendy, I. L., & Chappaz, A. (2017). Assessing oxygen depletion in the Northeastern Pacific Ocean during the last deglaciation using I/Ca ratios from multiple benthic foraminiferal species. *Paleoceanography*, *32*(8), 746–762. https://doi.org/10.1002/2016PA003062

Tetard, M., Licari, L., & Beaufort, L. (2017). Oxygen history off Baja California over the last 80 kyr: A new foraminiferal-based record. *Paleoceanography*, *32*. https://doi.org/10.1002/2016PA003034

Tribovillard, N., Algeo, T. J., Lyons, T., & Riboulleau, A. (2006). Trace metals as paleoredox and paleoproductivity proxies: An update. *Chemical Geology*, *232*(1), 12–32. https://doi.org/10.1016/j.chemgeo.2006.02.012

van Geen, A., Zheng, Y., Bernhard, J.M., Cannariato, K.G., Carriquiry, J., Dean, W.E., Eakins, B.W., Ortiz, J.D. and Pike, J. (2003). On the preservation of laminated sediments along the western margin of North America. *Paleoceanography*, *18*, 1098. https://doi:10.1029/2003PA000911.

Vaquer-Sunyer, R., & Duarte, C. M. (2008). Thresholds of hypoxia for marine biodiversity. *Proceedings of the National Academy of Sciences*, *105*(40), 15452–15457. https://doi.org/10.1073/pnas.0803833105

Walczak, M. H., Mix, A. C., Cowan, E. A., Fallon, S., Fifield, L. K., Du, J., Haley, B., Hobern, T., Padman, J, Praetorius, S. K., Schmittner, A., Stoner, J. S., Zellers, S. D.

(2020). Phasing of millennial-scale climate variability in the Pacific and Atlantic Oceans. *Science.* https://doi.org/10.1126/science.aba7096

Weinkauf, M., & Milker, Y. (2018). The effect of size fraction in analyses of benthic foraminiferal assemblages: A case study comparing assemblages from the >125 and >150 μm size fractions. *Frontiers in Earth Science*, *6*(37). https://doi.org/10.3389/feart.2018.00037

Whitney, F. A., Freeland, H. J., & Robert, M. (2007). Persistently declining oxygen levels in the interior waters of the eastern subarctic Pacific. *Progress in Oceanography*, *75*(2), 179–199. https://doi.org/10.1016/j.pocean.2007.08.007

Zheng, Y., Anderson, R. F., van Geen, A., & Fleisher, M. Q. (2002). Remobilization of authigenic uranium in marine sediments by bioturbation. *Geochimica et Cosmochimica Acta*, *66*(10), 1759–1772. https://doi.org/10.1016/S0016-7037(01)00886-9

Zheng, Y., Anderson, R. F., van Geen, A., & Kuwabara, J. (2000). Authigenic molybdenum formation in marine sediments: a link to pore water sulfide in the Santa Barbara Basin. *Geochimica et Cosmochimica Acta*, *64*(24), 4165–4178. https://doi.org/10.1016/S0016-7037(00)00495-6/10.1016/S0016-7037(00)00495-6

Zindorf, M., Rush, D., Jaeger, J., Mix, A., Penkrot, M. L., Schnetger, B., et al. (2020). Reconstructing oxygen deficiency in the glacial Gulf of Alaska: Combining biomarkers and trace metals as paleo-redox proxies. *Chemical Geology*, 119864. https://doi.org/https://doi.org/10.1016/j.chemgeo.2020.119864

Zou, J., Shi, X., Zhu, A., Kandasamy, S., Gong, X., Lembke-Jene, L., et al. (2020). Millennial-scale variations in sedimentary oxygenation in the western subtropical North Pacific and its links to North Atlantic climate. *Climate of the Past*, *16*(1), 387–407. https://doi.org/10.5194/cp-16-387-2020

2.7. Supplemental Figures and Tables

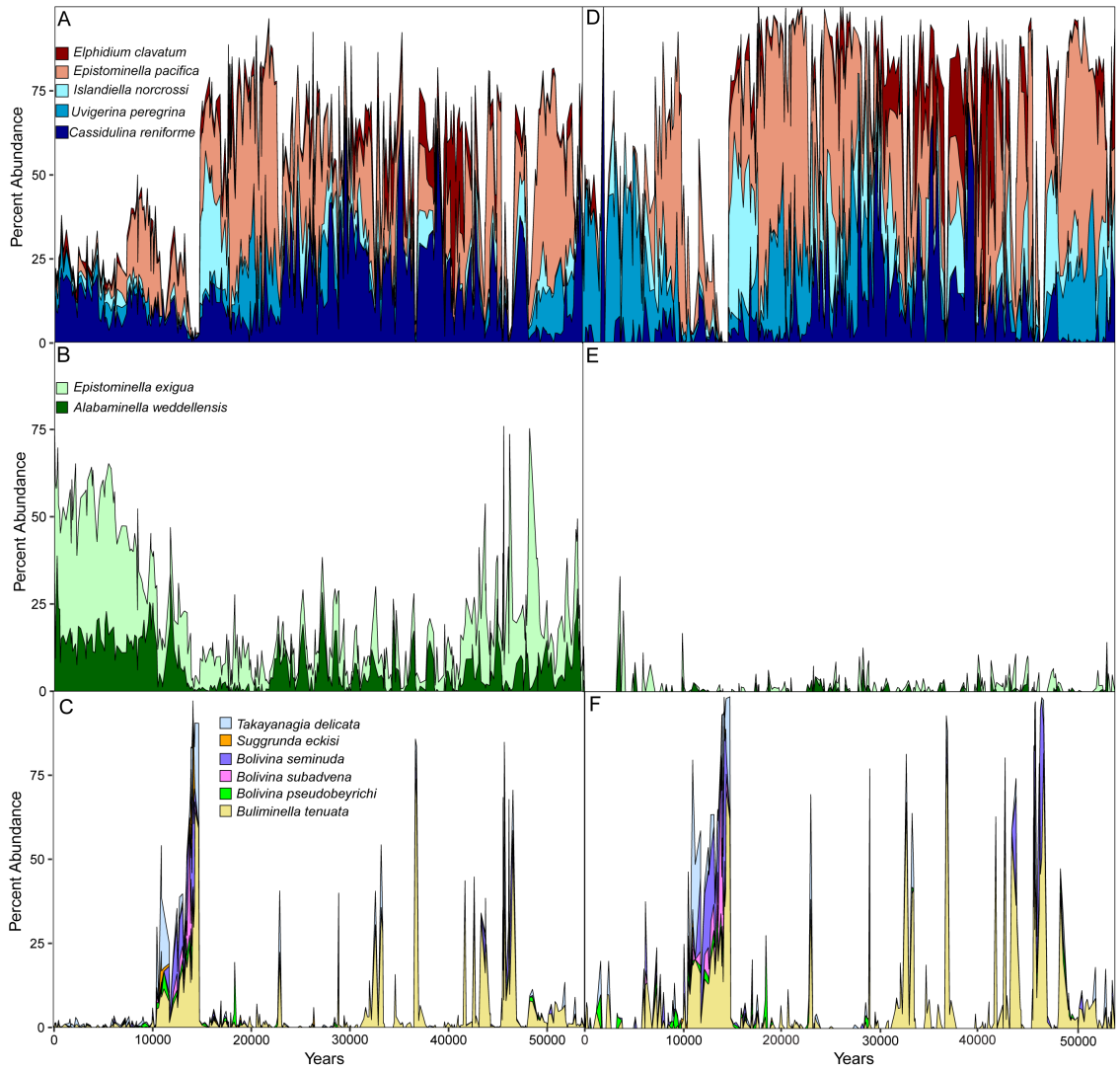

Figure 2.7 Relative abundance of numerically and ecological important species. A -- C, percent abundances for the >63 µm size fraction (duplicated from main text Figure 2.2) and D -- F, percent abundances for the >125 µm size fraction. (A) and (D), numerically important species. (B) and (E), opportunistic species. (C) and (F), six species with reported oxygen tolerances <0.1 ml/L.

Supplemental Table 2.1 Number of benthic foraminifera counted in the >63 µm size fraction by taxon and size fraction and redox sensitive metal concentrations for all Site U1419 fossil samples included in analyses. Samples with modern analogs are indicated by "1", samples with no analog with "0;" the environment (shelf or slope) of the nearest modern analog is indicated for each sample. Letters following species names indicate size fraction: A = >355 µm, B = 250-355 µm, C =125-250 µm, D = 63-125 µm.

Supplemental Table 2.2 Published oxygen tolerances for benthic foraminifera found in Site U1419 samples.

Supplemental Table 2.3 Benthic foraminiferal taxa from modern and fossil samples with oxygen category assignments used in modified Behl dissolved oxygen calculations. Taxa present in the fossil data set are assigned to an oxygenation category using DCA axis 1 species scores from analyses using the >63 µm size fraction. Taxa present only in the modern dataset are assigned to an oxygenation category using the sign of the Pearson correlation between the relative abundance of that taxon and the modern oxygen estimates for the sample location derived from World Ocean Atlas 2013.

Supplemental Table 2.4 Faunal analysis results including (a) detrended correspondence analysis sample scores for each three size-fraction categories examined, (b) dissolved oxygen from literature-based Behl calculations and calculations using the total fauna from the >63 µm and >125 µm size fractions and (c) rates of ecological and oxygenation with and without assemblages with shelf modern nearest neighbors for the >63 µm size fraction.

Supplemental Table 2.5 Detrended correspondence analysis species scores for the three size fraction categories examined.

Supplemental Table 2.6 Dissolved oxygen values calculated using benthic foraminiferal faunas for modern Gulf of Alaska samples with dissolved oxygen measurements derived from World Ocean Atlas 2013 (following Belanger et al., 2016).

Supplemental Table 2.7 Number of no-analog fossil assemblages and fossil assemblages with modern analogs from the slope and shelf of the Gulf of Alaska. Median sedimentary grain size given using the percent weight of grains >63 µm. Interquartile range in parentheses.

3. QUANTITATIVE COMPARISONS AMONG NORTH PACIFIC PALEO-OXYGENATION RECORDS USING MULTIVARIATE ANALYSES OF BENTHIC FORAMINIFERAL ASSEMBLAGES

3.1. Introduction

The North Pacific Ocean (NP) has one of the most extensive and intense oxygen minimum zones (OMZs) in the world oceans (Paulmier and Ruiz-Pino, 2009; Pierce et al., 2012; Tetard et al., 2017; Lembke-Jene et al., 2018). Over the last few decades, OMZs have expanded and intensified, which poses a threat to ecosystem health (Diaz and Rosenberg, 2008; Bograd et al., 2008; Keeling et al., 2010; Deutsch et al., 2011; Gilly et al, 2013.) The intensity and spatial extent of future hypoxic conditions will likely vary with changes in global climate ocean circulation, and nutrient availability (Helly and Levin, 2004; Rabalais et al., 2009). Further, climate modules predict that organic carbon export to the deep sea will increase in high latitudes with ongoing global climate change (Sweetman et al., 2017), which can also enhance OMZ intensity and extent.

Paleogeographic records provide the opportunity to investigate changes in OMZ conditions during past environmental changes. Pleistocene NP sedimentary records reveal fluctuations between oxic (>1.4 ml/L O_2), suboxic (0.5-1.4 ml/L) and dysoxic intervals (<0.5 ml/L) off the coast of Japan, California, Gulf of Alaska, China Sea; Bering and Okhotsk Sea across the eastern and the western NP (Mix et al., 1999; Cannariato and Kennett, 1999; Mckay et al., 2005; Ikehara et al., 2006; Shibahara et al., 2007; Jaccard and Galbraith, 2012; Ohkushi et al., 2013; Max et al., 2014; Bubenshchikova et al., 2015;

Moffitt et al., 2015; Taylor et al. 2017; Tetard et al., 2017; Li et al., 2018; Saravanan et al., 2020; Zou et al., 2020; Zindorf et al., 2020; Sharon et al., 2021; Sakai et al., 2021). These dysoxic events were hundreds to few thousands of years in duration with some regions remaining low oxygen after severe dysoxia associated with deglacial warming ~15 kyrs ago whereas others recovered to more oxic conditions.

Multiple hypotheses have been proposed for the occurrence of low-oxygen events during the late Pleistocene including increased water column stratification, decreased ventilation, melt-water pulses, increased surface productivity, regional setting, and increased sea surface temperatures (SST) leading to decrease in oxygen solubility (Davies et al., 2011; Jaccard and Galbraith, 2012; Ohkushi et al., 2013; Praetorius et al., 2015; Moffitt et al., 2015; Tetard et al., 2017; Li et al, 2020; Praetorius et al., 2020). Low-oxygen events across the North Pacific appear contemporaneous, particularly for dysoxic events associated with the Bølling-Allerod and early Holocene, suggesting global and basinwide drivers (Bograd et al., 2008; Ohkushi et al., 2013; Moffitt et al. 2015). Dysoxic events and OMZ intensity in the NP over the past 60,000 years have been linked to orbital and millennial scale climate changes related to Daansgard-Oshgard (D/O) and Heinrich events, further supporting an ultimate driver tied to global climate cycles (Behl and Kennett, 1996; Mix et al., 1999; Cannariato and Kennett, 1999; Shibahara et al., 2007; Davies et al., 2011; Cartapanis et al., 2014; Praetorius and Mix, 2014; Moffitt et al., 2015).

However, the relative severities of the dysoxic events across these records are largely unknown and may vary with regional differences in circulation, temperature, and nutrient sources (Davies et al., 2011; Ohkushi et al., 2013; Praetorius et al., 2015; Moffitt

et al., 2015; Tetard et al., 2017). For example, dysoxic events in the Santa Barbara Basin (SBB) maybe amplified by its restricted circulation and more restricted settings in the deeper SBB reach lower oxygen values than shallower sites (Bograd et al., 2002; Ohkushi et al., 2013; Moffitt et al., 2014). In Baja California Sur, the California Margin, and the Subarctic Pacific, low-oxygenation events may be amplified by increased export production and decreased ventilation (Mckay et al., 2005; Shibahara et al., 2007; Barron et al., 2009; Davies et al., 2011; Cartapanis et al., 2011; Tetard et al., 2017). Furthermore, expansion of the Eastern Tropical North Pacific OMZ maybe controlled by the relative influences of North Pacific Intermediate Water and Subarctic Water from the north and Equatorial Subsurface Waters from the south (Cartapanis et al., 2011). In the Gulf of Alaska (GoA), melt-water pluses and changes in sea-ice cover, which each affect surface productivity and water column stratification, have also been associated with dysoxic events (Barron et al., 2009; Davies et al., 2011; Addison et al., 2012; Praetorius et al., 2015; Praetorius et al., 2020). Understanding how these drivers may impact the relative severity of these oxygenation changes is important for identifying the ecosystems that will be most severely impacted by future changes in oxygenation.

The relative severity of paleo-oxygenation declines is difficult to compare among sites because the behavior of commonly used proxies, such as redox sensitive metals, faunal assemblages, and sedimentary laminations, can vary depending on local environmental factors and each proxy has different sensitivities to changing oxygenation (Jaccard and Galbraith, 2012; Moffitt et al., 2015). This limits our ability determine the conditions under which severe dysoxia develops and to forecast which oceanic regions are

most vulnerable to future deoxygenation. Here, we develop quantitative paleo-oxygenation estimates for sites in the northeastern Pacific that allow us to compare the relative severity of dysoxia on the same scale for sites in the Gulf of Alaska, California Margin, Santa Barbara Basin and Baja California Sur based using multivariate analyses of benthic foraminiferal faunas. These analyses reveal spatial heterogeneity in the severity of deoxygenation at intermediate water depths during established dysoxic events, which may be related to site-level characteristics. In addition, our alignment of all sites to a common oxygenation scale suggests that some previous oxygenation studies greatly overestimated the amplitude of oxygenation changes, which would alter their interpretations of paleoceanographic conditions. Furthermore, these methods demonstrate that intervals of dysoxia in the Gulf of Alaska that occurred during the last deglacial and during MIS 3 were as severe as dysoxia recorded in Eastern Subtropical North Pacific OMZ, suggesting that even high-latitude regions with open ocean circulation can experience severe declines in oxygen that can threaten local ecosystem function and economically important fisheries.

3.1.1. Paleoceanographic Proxies for Oxygenation

Sedimentary laminations, benthic foraminiferal assemblage compositions, $\delta^{15}N$, and the concentration of redox-sensitive metals like Mo, Re, U in sediments are commonly used to detect low-oxygen conditions in paleoceanographic records (Tribovillard et al., 2006; Murray, 2006; Jaccard and Galbraith, 2012; Moffitt et al., 2015). Laminations are good indicators of severe dysoxia as macrofauna cannot survive such low oxygen, which results in a lack of bioturbation, and laminations can also suggest higher export

productivity from the surface (van Geen et al., 2003; Moffitt et al., 2015). Increases in denitrification based on high ratios of $\delta^{15}N$ have been used to infer severe dysoxia (Emmer and Thunell, 2000). The concentrations of redox-sensitive metals are also often used in regional oxygenation studies and take advantage of the different solubilities of these metals at different oxygen concentrations, which determines their accumulation in the sedimentary record (Crusius et al., 1996; Zheng et al., 2000; McManus et al., 2006; Tribovillard et al., 2006; Moffitt et al., 2015). Each of these oxygenation proxies are only sensitive to changes at relatively low-oxygen concentrations and are best at detecting dysoxia and resolving the differences between suboxic and dysoxic conditions.

Multi-proxy studies that compare records of sedimentary, faunal, and geochemical proxies frequently find correspondence between these proxies when measured in a single sedimentary record (Davies et al., 2011; Praetorius et al., 2015; Tetard et al., 2017; Sharon et al., 2021). However, each of these proxies have their own range of oxygen sensitivities and, thus, studies using different proxies cannot be directly compared quantitatively (Jaccard and Galbraith, 2012; Moffitt et al., 2015). Further, the same proxy may not have the same sensitivity across disparate sites under varying oceanographic conditions. For example, local sedimentary environments may cause variations in the concentration of redox-sensitive metals due to differences in sediment accumulation rates, the supply of metals, and rates of remobilization (Jaccard and Galbraith, 2012). Remobilization is especially challenging as it can remove previously deposited redox-sensitive metals from the sedimentary record and, thus, fail to preserve the presence of a low-oxygen environment. Similarly, sedimentary laminations that are retained under low-oxygen

conditions can get disturbed by bioturbation when oxygenation returns if sufficient sedimentation has not occurred for the sedimentary interval to pass out of the taphonomically active zone (Fürsich and Aberhan, 1990).

Benthic foraminiferal faunal composition responds to rapidly changing environments and can be a reliable proxy for recording rapid changes in the oxygenation levels (Kaiho, 1994; Bernhard et al., 1997; Murray 2006; Gooday and Jorissen, 2012; Moffitt et al., 2015). Foraminiferal records are particularly useful because studies of modern species-level ecology reveal species-level oxygenation tolerances which can be used to quantify paleo-oxygenation. Furthermore, when faunal analyses use species in aggregate as whole assemblages, faunal composition can be used to construct oxygen levels as a continuous variable rather than as oxygenation categories bracketed by the threshold behavior of the proxies. These fossil records can also be affected by bioturbation when oxygen level permit active metazoans, however this will dampen the amplitude of the record of oxygenation changes rather than remove the signal of a low-oxygen environment as can occur with sedimentary laminations and redox-sensitive metals. Benthic foraminifera have been instrumental in reconstructing changes in paleo-oxygenation globally and are used extensively in paleo-oxygenation studies in the NP (Cannariato and Kennett, 1999; Karlsen et al., 2000; Ikehara et al., 2006; Shibahara et al., 2007; Nigam et al., 2007; Ohkushi et al., 2013; Grunert et al., 2015; Bubenshchikova et al., 2015; Tetard et al., 2017; Taylor et al., 2017; Psheneva and Gorbarenko, 2017; Palmer et al., 2020; Belanger et al., 2020; Sharon et al., 2021). Whereas some of these previous studies compare faunal assemblages between sites in a relatively geographically restricted

region (Cannariato and Kennett, 1999; Shibahara et al., 2007; Ohkushi et al., 2013; Moffitt et al., 2015), comparisons of these faunas on a common quantitative scale across larger regions are rarely attempted due differences in faunal composition among sites.

3.2. Study Area and Methods

In this study, we use benthic foraminifera assemblage analyses to quantitatively compare relative oxygenation over the past ~54,000 kyrs at four sites (Figure 3.1) in the eastern North Pacific: the Gulf of Alaska (IODP Site U1419; Sharon et al., 2021), Santa Barbara Basin (Site MD02-2503 and Site MD02-2504; Ohkushi et al., 2013), and in Baja California Sur in the eastern equatorial North Pacific OMZ (Site MD02-2508; Tetard et al., 2017). Paleo-oxygenation studies using benthic foraminiferal faunas frequently rely on the abundances a limited number of foraminiferal index species placed into dysoxic, suboxic and oxic categories based upon measured oxygen tolerances in modern individuals of those species (Cannariato and Kennett, 1999, Davies et al., 2011; Ohkushi et al., 2013; Praetorius et al., 2015; Tetard et al., 2017). However, analyses that include the whole fauna can better replicate core top dissolved oxygen (DO) values and can produce oxygenation records with fewer threshold effects (Sharon et al., 2021). Thus, in our quantitative analyses we only use datasets for which the counts of all benthic foraminiferal taxa are reported. However, we also include semi-quantitative comparisons to other contemporaneous records where partial faunal data is available including from the California Margin and SBB (ODP 1017 and ODP 893 respectively; Cannariato and Kennett, 1999) and on the Cascadia Margin (ODP Hole 890B; Saravanan et al., 2020) and qualitive comparisons to studies using other paleo-oxygenation proxies (Table 3.1). All

the study sites record dysoxia during warm periods like the B-A interval (Cannariato and Kennett, 1999; Ohkushi et al., 2013; Praetorius et al., 2015; Tetard et al., 2017; Sharon et al., 2021). Only four records (U1419, ODP 1017, ODP 893 and MD02-2508) extend beyond ~34 kyrs.

Sites were chosen to have similar water depths to attain benthic foraminiferal assemblages that are similar and that could be taxonomically standardized across the sites. Of the seven study sites in which we reanalyze the faunal assemblages, Site U1419 in GoA, ODP 1017 on the San Lucia Slope and MD02-2508 in Baja California Sur are located on the continental slope whereas the remaining sites are in the SBB (Figure 3.1). Amongst the slope sites, GoA is dominantly a downwelling zone while ODP 1017 is within a major upwelling system (Davies et al., 2011; Cannariato and Kennett, 1999). In addition, strong-wind driven upwelling is seen at MD02-2508 (Thomas et al., 2001; Cartapanis et al., 2011). U1419 and ODP 1017 are located in the modern northeastern Pacific OMZ while MD02-2508 is at the northern limit of the modern Eastern Tropical North Pacific OMZ (Cartapanis et al., 2011; 2014)

Table 3.1 Sites analyzed in this study and other sites in the North Pacific used to make BDO comparison

Sites ↓	Record Covered (age)	Location (water depth)	Latitude & Longitude	Modern OMZ depth	Number of samples analyzed (Size fraction)	Number of species included in analyses	Median (IQR) number of individuals per sample	Proxies used	Method used to study oxygenation by original authors	Type of Benthic foraminiferal data available	Author
U1419 and EW0408-85JC Continental Slope	~54 kyrs	Khitrov Bank, Gulf of Alaska (697 m and 682 m)	59.5553° N, 144.1535° W	~ 670 – 1060 m	355 (>125 μm)	46	81 (46-141)	Benthic foraminifera and Mo/Al and U/Al	DCA	Abundance counts	Sharon et al., 2021
MD02-2508 Continental Slope	~80 kyrs	Baja California Sur, Mexico (606 m)	23.4652° N, 111.596° W	~500 – 1000 m	188 (>150 μm)	57	312 (285-371)	Benthic foraminifera and Mo/Al and U/Al	PCA and CA	Abundance counts	Tetard et al., 2017
MD02-2503	~34 kyrs	SBB (Sill depth; 569 m)	34.2862°N; 120.0365°W	~500 – 1000 m	307 (>63 μm)	79	165 (59-340)	Benthic foraminifera	PCA	Abundance counts	Ohkushi et al., 2013
MD02-2504	~24 kyrs	SBB (Basin depth; 481 m)	34.2333°N; 119.868°W	~500 – 1000 m	191 (>63 μm)	64	183 (85-322)	Benthic foraminifera	PCA	Abundance counts	Ohkushi et al., 2013
ODP Hole 890B	32.19 - 10.58 kyrs	Vancouver Island, Cascadia margin (1326.3 m)	48.6625° N; 126.882° W	750 and 1330 m, OMZ most prominent at ~920 m	228 (125 μm +)	109	~300	Benthic & planktic foraminifera, Biofacies, O and C isotopes, grain and bulk denisty	Abundances	Dysoxic, suboxic & oxic species relative percentages	Saravana et al., 2020
ODP 1017E Santa Lucia Slope	~59 kyrs	California margin, 60 km westof Point Conception, (955 m)	34.535° N, 121.107° W	~525 – 1000 m	386 (>150 μm)	NA	~300	Benthic foraminifera	Index taxa	Dysoxic, suboxic & oxic species relative percentages	Cannariato and Kennett, 1999
ODP 893A	~60 kyrs	SBB (Sill depth; 576.5 m) at the upper edge of the OMZ at ~ 475 m	34.535° N, 121.107° W	500 – 1500 m	719 (>150 μm)	NA	~300	Benthic foraminifera & laminations	Index taxa	Dysoxic, suboxic & oxic species relative percentages	Cannariato et al., 1999

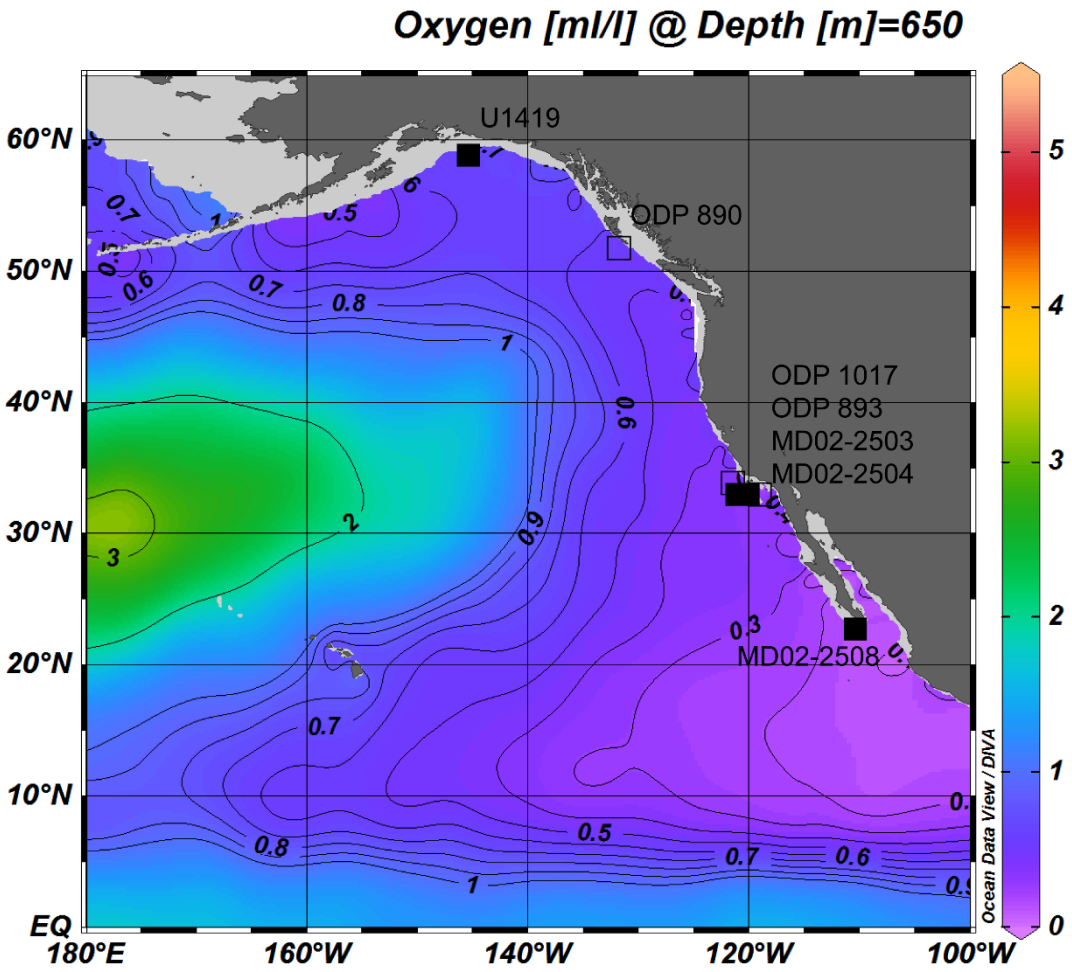

Figure 3.1 Location map of sites analyzed in this study. Filled symbols indicate sites included in multivariate analyses and for which we calculated a modified BDO. Open symbols we calculated a BDO based upon the ecological categorizations of the original authors. Background shading depicts oxygen concentrations at 650 m depth in ml/L. Figure created in Ocean Data View with World Ocean Atlas 2013 data (Garcia et al., 2013; Schlitzer et al., 2018).

3.2.1. Benthic Foraminiferal Records

3.2.1.1. Gulf of Alaska (U1419)

Site U1419 and jumbo piston core EW0840-85JC were cored on the continental slope at Khitrov Bank at 59.5553° N, 144.1535° W in GoA at a water depth of 697 m and 682 m (Jaeger et al., 2014). In the present, the OMZ in GoA is at ~ 670–1,060 m (Paulmier and Ruiz-Pino, 2009), placing this site in the upper OMZ where the modern oxygen concentration is ~0.59 ml/L (World Ocean Atlas, 2013). Site U1419 lies under North Pacific Intermediate Water (NPIW) and is influenced by Alaska Coastal current (Jaeger et al., 2014).

Changes in the production and ventilation of NPIW have been linked to the strength of OMZ and oscillations in oxic and dysoxic conditions during the Pleistocene (Keigwin, 1998; Hendy and Pederson, 2006). In the modern, NPIW is the densest water mass in the North Pacific and forms in the northwestern Pacific at the sea of Okhotsk due to extreme cooling in the winters (Yasuda, 1997; Mix et al., 1999; Shibahara et al., 2007; Ohkushi et al., 2016). In the past, both the Okhotsk and Bering Seas are proposed as sources of NPIW, especially during glacial times, whereas the Bering Sea was proposed as a source of NPIW during the LGM (Tanaka and Takahashi, 2005; Rella et al., 2012; Knudson and Ravelo, 2015; Ohkushi et al., 2016). Furthermore, there was a shift from the Bering Sea to the Okhotsk Sea as a NPIW source after the LGM (Tanaka and Takahashi, 2005). Increase in production and ventilation of NPIW have been linked to the colder and well-oxygenated periods in the North Pacific (Mix et al., 1999; Shibahara et al., 2007; Okazaki et al., 2010; Ohkushi et al. 2013; Knudson and Ravelo, 2015).

Changes in productivity have also been implicated in the development and maintenance of hypoxic events in GoA. The GoA is a high nutrient low chlorophyll

(HNLC) zone and productivity here is mostly limited due to sunlight (Stabeno et al., 2004; Davies et al., 2011). Adequate sunlight leads to an increase in seasonal productivity which may cause dysoxia due to increased consumption of oxygen (Davies et al., 2011; Praetorius et al., 2015). Dysoxic periods in the B-A and early Holocene intervals with high SST were linked to melt-water pulses due to glacial melting and flooding, sea-level rise, remobilization of iron which may have led to increased productivity (Davies et al., 2011; Praetorius et al., 2015). These were based on proxies like presence of laminations, alkenones, rise in $\delta^{15}N$, increase in both dysoxic benthic foraminifera and redox sensitive trace metals (Davies et al. 2011; Praetorius et al., 2015; Penkrot et al., 2018; Belanger et al., 2020; Sharon et al., 2021).

At site U1419, we include benthic foraminifera from the >125 μm size fraction from 355 samples in our analyses. Samples are 2-3 cm wide intervals with a median age resolution of 127 years and spans ~54,000 years (Sharon et al., 2021). The median number of specimens per sample is 81 (interquartile range, IQR= 46 – 141; Table 3.1). While the original publication provided benthic foraminiferal counts in the >63 μm size fraction, we use the >125 μm size fraction because opportunistic species in 63-125 um size fraction that are not present at the other sites dominate many of the U1419 samples. Excluding the 63-125um size fraction results in lower counts at U1419 than at the other sites, however, previous multivariate analyses of the >63 μm and >125 μm size fractions yielded similar paleo-oxygenation records, thus the lower number of individuals per sample should not affect our comparisons here (Sharon et al., 2021). A total of 67 benthic foraminifera species were observed in >125 μm size fraction at U1419 (Sharon et al., 2021).

3.2.1.2. Cascadia Margin (ODP Hole 890B)

ODP Hole 890B is located near the Vancouver Islands on the Cascadia margin at a water depth of 1326 m at 48°39.75′N;126°52.89′W, close to the lower depth boundary of the modern OMZ (Figure 3.1; Table 3.1; Saravanan et al., 2020). The OMZ in this region exists between 750 m and 1330 m and is most prominent at a depth of ~920 m with oxygen concentration ranging between 0.3 to 0.5 ml/L (Mckay et al., 2005). The core record extends from ~32 to ~10 ka. Open ocean upwelling can also be observed at this site (Saravanan et al., 2020).

While faunal abundances were available for this site, the taxonomic composition is quite dissimilar from the other sites, perhaps due to its deeper water depth. Thus, we use the author's original categorization of taxa into oxygen categories for semiquantitative comparisons. This data set contains 228 samples with benthic foraminifera in >125 μm size fraction (Table 3.1). A total of 109 benthic foraminifera species occurs at ODP Hole 890B (Saravanan et al., 2020).

3.2.1.3. San Lucia Slope (ODP Site 1017)

ODP Site 1017 is located on Santa Lucia slope at ~955 m water depth, 60 km west of Point Conception on the Californian margin at 34°32.10'N, 121°06.43'W) (Cannariato and Kennett, 1999; Table 3.1). The OMZ in this area exists between ~525 m and ~1000 m and this site is located near the base of the Eastern Tropical North Pacific (ETNP) OMZ at 955 m (Cannariato and Kennett, 1999, Hendy and Pederson, 2005). Strong, persistent, coastal upwelling enhances biological productivity in this region, which may contribute to the low-oxygen conditions (Hendy and Pedersen, 2005; Cannariato and Kennett, 1999).

Two bottom water sources bathe the site; the well-oxygenated NPIW from the north and poorly oxygenated waters carried by California Undercurrent from the ETNP in the south (Hendy and Pedersen, 2005).

The foraminiferal data reported for this site were summarized as the relative abundance of dysoxic, suboxic and oxic faunal indicators and thus we only included this site in our semi-quantitative analyses. These data have a sampling resolution of ~ 130 years over the past ~60 kyrs (Cannariato and Kennett, 1999).

3.2.1.4. Baja California Sur (MD02-2508)

The site MD02-2508 is a continental slope site located 90 km off the coast of Baja California (23°27.910N, 111°35.740W) in Mexico (Tetard et al., 2017). This site is located directly at the northern edge of the ETNP OMZ core (Cartapanis et al., 2011; Tetard et al., 2017).

In the modern, Subarctic Water (SW) is transported by the California Current (CC), which brings the highly oxygenated cold water from the north to Baja California Sur (Cartapanis et al., 2011). In addition, at water depths of ~ 1000 m, the NPIW travels from the northern latitudes to south (Cartapanis et al., 2011). The California Undercurrent transports low-oxygen Equatorial Subsurface Waters (ESsW) to the north. The OMZ near Baja California Sur is divided into ETNP from 0° to 25°N and Eastern Subtropical North Pacific (ESTNP; 25°N to 52°N) regions. In the modern, oxygenation at this site is impacted by the productivity and ventilation of both the ETNP and ESTNP, which are influenced and dominated by ESsW and NPIW, respectively (Cartapanis et al., 2011; Tetard et al., 2017). The OMZ fluctuations recorded over the past 80 kyrs are mainly

influenced by the oxygenated and productive water mass coming from the north and dysoxic waters coming from the south (Tetard et al., 2017). Based on benthic foraminifera, a semiquantitative record of oxygen reflected suboxic to weakly hypoxic changes in the ENP OMZ related to Heinrich stadials at MD02-2508 (Tetard et al., 2017).

We analyze 188 samples with benthic foraminiferal counts from this site in our multivariate analyses. The median number of individuals per sample was 312 (IQR = 285 - 371) (Table 3.1). This data set has a sampling resolution of one sample every 10 to 20 cm, which equates to an average time resolution of 450 years for the ~80 kyrs record (Table 3.1). A total of 96 benthic foraminiferal species were recorded in this record (Tetard et al., 2017).

3.2.1.5. Santa Barbara Basin (ODP 893, MD02-2503, MD02-2504)

SBB is a classic site to study dysoxia and is often used in comparative studies across sites in the North Pacific (Cannariato and Kennett, 1999; Mckay et al., 2005; Shibahara et al., 2007; Taylor et al., 2017; Tetard et al., 2017; Saravanan et al., 2020). It is a restricted basin bound by Channel Islands on the south, California coast on the north and has sills on the east (230 m) and west (475 m). These sills control the surface water flows into this basin making it a restricted basin (Bograd et al., 2002). The SBB is influenced by southward flowing CC and northward flowing Southern California Countercurrent or Davidson Current (Hendy et al., 2002; Hill et al., 2006).

As compared to other California margin sites, the dysoxia at SBB is basin enhanced (Moffitt et al., 2014). Due to restricted ventilation, the bottom waters at the sill are dysoxic (DO; <0.1 ml/L; Emmer and Thunell, 2000). However, a study of the modern

basin showed annual renewal of these bottom waters interspersed with relatively stagnant intervals over a 15 year-long study (Bograd et al., 2002). The basin does not get flushed each year and renewal events are not only restricted to winter-spring. The authors concluded that the renewal cycles likely also varied in the past and that interannual cycles of basin flushing by oxygenated waters with the possibility of extended periods occurred when the conditions were more or less favorable for bottom water renewal (Bograd et al., 2002). Factors like interannual variability in the strength, duration, timing of coastal upwelling and in regional circulation and hydrography, which are largely controlled by impact of El Nino events, regulates the flushing potential of the basin (Bograd, 2002). In the modern, low-oxygen waters (~0.5 ml/L on average) derived from the OMZ enter the basin at the western sill and become further depleted in oxygen by the remineralization of organic matter from highly productive surface waters (Behl and Kennett, 1996; Ohkushi et al., 2013). Oxygen levels in the basin decline to <0.1 ml/L at depths below 525 m, which is also seen in preservation of annual laminations (Emery and Hülsemann, 1961; Thunell et al., 1995, Cannariato et al., 1999; Ohkushi et al., 2013).

We use benthic foraminiferal counts from cores MD02-2503, which is located at basin depth (569 m water depth; 34.2862°N; 120.0365°W), and MD02-2504, which is at sill depth (481 m water depth; 34.2333°N, 119.868°W) in our multivariate analyses. We use 307 samples from MD02-2503 that span the past ~34 kyrs and 191 samples from MD02-2504 that span the last ~24 kyrs (Ohkushi et al., 2013). These records yield a sampling resolution of ~100-126 years for each site. The median number of individuals per sample is 165 (IQR= 59 - 340) at MD02-2503 and 183 (IQR = 85-322) at MD02-2504.

The original authors observed a total of 87 species at these two sites (Supplemental Table 3.1; Ohkushi et al., 2013).

As with ODP 1017, faunal data for ODP 893 is reported as the percent abundance of ecological groups (dysoxic, suboxic and oxic) by the original authors (Cannariato et al., 1999). ODP 893 is located adjacent to MD02-2503 in SBB at a water depth of 576.5 m and records the upper edge of the OMZ (Kennett and Ingram, 1995; Cannariato et al., 1999; Ohkushi et al., 2013). This dataset records the past ~60 kyrs and contains a total of 719 samples benthic foraminifera in the >150 μm size fraction at a resolution of one sample every 70 years for the Holocene, 50-70 years for MIS 3 portions of the record, and one sample every 300 years from 10-26 ka (Cannariato et al., 1999; Table 3.1).

3.2.2. Data preparation and analysis

We taxonomically standardized species identifications from Site U1419 in GoA (Sharon et al., 2021), MD02-2503 and MD02-2504 in SBB (Ohkushi et al., 2013) and site MD02-2508 near Baja California Sur, Mexico (Tetard et al., 2017) by comparing species plates and examining known synonymies prior to multivariate analysis. Congeneric species that were rare across the data sets and difficult to confidently taxonomically standardize at the species-level were pooled at the genus-level. These species count data were placed in a single data matrix for multivariate analyses that combine all four sites. Only those species and generic groups that occurred in more than one sample and comprised at least 2% of the samples in at least one sample were included in analyses following Sharon et al. (2021). Sites where published data were incompatible with this data matrix are analyzed separately and not included in the multivariate analysis.

3.2.2.1. Multivariate Analysis

Multivariate analyses of benthic foraminiferal assemblages are commonly used to reduce the dimensionality of faunal datasets and extract the dominant faunal patterns for temporal analysis (Scarponi and Kowalewski, 2004; Bush and Brame, 2010; Hannaa et al., 2013; Belanger and Villa Rosa Garcia, 2014; Belanger et al., 2016). These types of analyses have been previously used to reconstruct the oxygenation history of sites within in the NP (Ohkushi et al, 2013; Tetard et al., 2017; Belanger et al., 2020; Sharon et al., 2021), however each take a different analytical approach making it difficult to directly compare paleo-oxygenation among localities. In some of these oxygen studies, multivariate analyses such Principal Component Analysis (PCA) and Correspondence Analysis (CA) were used to translate the relative abundances of benthic foraminifera into an oxygenation record (Ohkushi et al, 2013; Tetard et al., 2017). However, PCA uses Euclidean distances to measure the dissimilarity between samples, which is inappropriate for relative abundance data in which many samples have only a subset of the total species in the data set (Legendre and Legendre, 2012). We also avoid using correspondence analysis (CA) here because data with long ecological gradients tend be compressed at the ends of the axes and overdispersed at the center of the ordination space, which can make interpretation of samples spacing along the gradient difficult. In another study, Principal Coordinates analysis (PCO) analyses was instead used to interpret the primary gradients in benthic foraminifera assemblages and indirectly related those gradients to environmental variables (Belanger et al. 2016).

We chose to use Detrended Correspondence Analyses (DCA) as our ordination method following Sharon et al. (2021), because this method extracts a strong gradient on its first axis that is readily relatable to the oxygen tolerances of species and to independently measured geochemical proxies for paleo-oxygenation; in contrast PCO analyses are less sensitive to the oxygen gradient and we do not see the relationship with oxygenation until the third axis (Belanger et al., 2016; Belanger et al., 2020; Supplemental Table 3.4). DCA is based on the chi-squared dissimilarity of faunal relative abundances among samples, like CA, but corrects for the arch effect common in CA (McCune and Grace, 2002; Tyler and Kowalewski, 2014). DCA has been criticized because it may introduce other distortions to the ordination (Bush and Brame, 2010) and often only the first and second axes are readily interpretable in terms of faunal and environmental gradients (Hannaa et al., 2013). However, DCA is commonly used in ecological studies to reliably identify the dominant faunal gradient (McCune and Grace, 2002; Bush and Brame, 2010; Scarponi and Kowalewski, 2004; Ortiz et al., 2011; Belanger and Villa Rosa Garcia, 2014; Hannaa et al., 2013). To avoid potential issues of distortion on later DCA axes, we only interpret DCA Axis 1 in terms of environmental gradients.

For DCA analyses, we used the function "decorana" in package vegan of R programming language (R core team, 2016; Oksanen et al., 2017). To extract the proportional variance summarized by each axis, we use the Pearson correlation between the Euclidean dissimilarity of the DCA sites cores and the Bray-Curtis dissimilarity of the faunal abundances for each site with function "*mantel*" in the package "*ecodist*" ("after the fact method" of McCune and Grace, 2002). To test if the DCA Axis scores produced

by our analysis combining all sites is similar to previously published patterns of paleo-oxygenation change for individual sites we perform a Spearman rank order correlation between our DCA Axis scores and the oxygenation metrics of the original authors (Ohkushi et al., 2013; Tetard et al., 2017; Sharon et al., 2021).

3.2.2.2. Quantitative Oxygen Estimates

Whereas ordination scores allow us to interpret the relative oxygen concentrations present at the time of deposition of a sample, it does not readily produce oxygenation values relatable to measured oxygen concentrations in the modern. Previous workers have sought to create transfer functions that translate faunal abundances into oxygenation values. For example, Ohkushi et al. (2013) used 19 index taxa to calculate estimated oxygen values using the Behl Dissolved Oxygen (BDO; Formula 1). Tetard et al., (2017), plotted assemblages on a ternary diagram based on their respective relative abundances of 4 dysoxic species and 4 suboxic species and categorized all remaining species in the assemblage as oxic; they then calculated oxygenation using the position of samples on the diagram. Including only a few species as opposed to the total assemblage in the oxygen calculations can severely affect the calculated oxygenation values and lead to less accurate paleoenvironmental interpretations (Sharon et al., 2021). Sharon et al. 2021 modified the BDO method to include all species in the data set by assigning oxygen preferences to species with unpublished tolerances based upon their DCA ordination positions with respect to species with published tolerances. This successfully replicated the modern measured oxygenation values using the core-top faunal assemblages and thus use the modified BDO here to transform DCA sample scores to quantitative oxygenation values.

Formula 1 from Ohkushi et al., 2013:

Behl dissolved oxygen (BDO) index formula = (Dysoxic% x 0.1 + Suboxic% x 0.5 + Weakly hypoxic-oxic% x 1.5)/100

We also calculated BDO using the original equation for sites ODP 890, ODP 893, and ODP 1017 and for which published percentages of total dysoxic, suboxic and oxic species were available (Cannariato et al., 1999; Cannariato and Kennett, 1999; Saravanan et al., 2020) for comparison. However, these calculations are not on the same scale as those derived from the multivariate analyses we perform.

3.3. Results

3.3.1. Faunal Characteristics Across Sites

Across the four datasets we combine in our multivariate analyses, Sites (U1419, MD02-2503, MD02-2504 and MD02-2508), there are a total of 193 species of benthic foraminifera after taxonomic standardization. Of these, we retain 122 species and congeneric groups after removing 71 species that comprised < 2% of the fauna in all samples in which it occurred (Supplemental Table 3.1). Only 14 of the 122 species occur at all four sites (Supplemental Table 3.1). The most frequently occurring and numerically abundant species across all the sites are *Buliminella tenuata* and *Uvigerina peregrina*; each species occurs in >70% of all samples and comprises >30% of individuals in >12% of the samples (Supplemental Table 3.1). *Bolivina argentea,* is present at all sites and occurs in ~48% of samples, however, this species occurs more frequently at MD02-2508

(99% of samples) than at MD02-2503 and MD02-2504 (~50% of samples) and is even less frequent at U1419 (11% of samples). Similarly, other species commonly used as indicators of dysoxic environments, including *Bolivina seminuda, Bolivina subadvena, B. argentea, B. tenuata, Takayangia delicata* (Supplemental Table 3.2) are present in >95% of samples from MD02-2508 but occur less frequently at the other three sites (Supplemental Table 3.1).

Some taxa are shared among a subset of the four sites. The three more southern sites (MD02-2503, MD02-2504 and MD02-2508) share 23 species that are not found at U1419 (Supplemental Table 3.1). Other frequently occurring taxa are shared between U1419, MD02-2503 and MD02-2504 to the exclusion of MD02-2508. For example, *Epistominella pacifica* occurs in 88% of samples from U1419 and in ~60% of samples at sites MD02-2503, MD02-2504, but is absent from MD02-2508. Similarly, *Nonionella labradorica* and *Cassidulina reniforme* only occur at U1419, MD02-2503 and MD02-2504; *C. reniforme* is particularly common at U1419 where it occurs in 81% of samples.

Other species occur frequently at only one site despite being numerically abundant at that site. For example, *Bolivina tumida,* which can thrive at <0.1 ml/L oxygen, was exclusive to SBB and is an extremophile associated with methane seeps and laminated sediments (Hill et al., 2003; Moffitt et al., 2014). At U1419, *Elphidium clavatum, Nonionella digitata*, and *Islandiella norcrossi* are common, but these species are rarely found at the other three sites (<2 individuals in 5 samples). Further, *Alabaminella weddellensis, Bolivina earlandi,* and *Bolivina decussata* occur only at U1419; these species have smaller test sizes and are most common in the 63-125 μm size fraction; thus

they may be excluded from MD02-2508 which used >150 μm size fraction whereas a few individuals were retained in >125 μm size fraction of GoA (Sharon et al., 2021).

ODP Hole 890B on the Cascadia margin, which we did not include in the multivariate analyses, shares only 25% of its species with the four sites we do include. Similar to other sites, *U. peregrina* and *B. tenuata* frequently occur and are seen in 82% and 50% of the samples, respectively. Like at U1419, *E. pacifica* occurs frequently (~72% of samples) at ODP Hole 890B, however *C. reniforme* occurs in only 9% of samples. *Elphidium* spp. was also more diverse with 3 species commonly recognized in samples for ODP Hole 890B. Species that are exclusive to and numerically abundant at ODP Hole 890B include *Bulimina coastata, Cassidulina laevigata*, and *Bolivina spathulata* (Supplemental Table 3.1; Saravanan et al., 2020).

3.3.2. Primary gradients in faunal composition

DCA Axis 1 summarizes 39% of the faunal variation whereas DCA Axis 2 and DCA Axis 3 summarize 13% and 16%, respectively. DCA Axis 4 only summarized 0.04% of the faunal variation and we will not discuss it further. Species with the most positive DCA Axis 1 scores include *B. tumida, Bolivina advena, Suggrunda eckisi, Chilostomella oolina, B. argentea,* and *Bolivina interjuncta* (Figure 3.2; Supplemental Table 3.3). These species are commonly found in dysoxic to suboxic settings (Supplemental Table 3.2; Sen Gupta and Castillo, 1993; Schmiedl et al., 2003; Gooday and Jorissen, 2012; Ohkushi et al., 2013; Schonfeld et al., 2013; Tetard et al., 2017; Erdem and Schonfeld, 2017). *B. argentea* is categorized as a suboxic indicator in some studies (Ohkushi et al., 2013; Tetard et al., 2017), however others suggest it may tolerate dysoxia (Palmer et al., 2020; Sharon

et al., 2021). Other species associated with dysoxic environments including *B. seminuda, Bolivina pseudobeyrichi, T. delicata, B. subadvena,* and *B. tenuata* also have DCA Axis 1 species scores > 0.8 (Figure 3.2; Supplemental Table 3.3). Species with strong negative DCA Axis 1 scores include *Triloculina trihedra, E. clavatum, Astrononion gallowayi, N. digitata, I. norcrossi* and *Stainforthia complanata* (Figure 3.2; Supplemental Table 3.3). Species associated with glacial conditions, including *E. clavatum*, *E. pacifica* and *C. reniforme* (Korsun and Hald, 2000; Ohkushi et al., 2003; Murray, 2006; Praetorius et al., 2015; Belanger et al., 2020) also have strong negative DCA Axis 1 scores.

Sites MD02-2503 and MD02-2504 from SBB have samples with the most positive DCA Axis scores of the four localities, but these sites also have samples with negative DCA Axis 1 scores (Figure 3.3). Site MD02-2508 has the narrowest range of DCA Axis 1 scores with only positive values (Figure 3.3). Most of the samples from U1419 have negative DCA Axis 1 scores, however ~13% of samples have positive DCA Axis 1 scores that overlap with samples from MD02-2503, MD02-2504, and MD02-2508 (Figure 3.3, Figure 3.2 (A)).

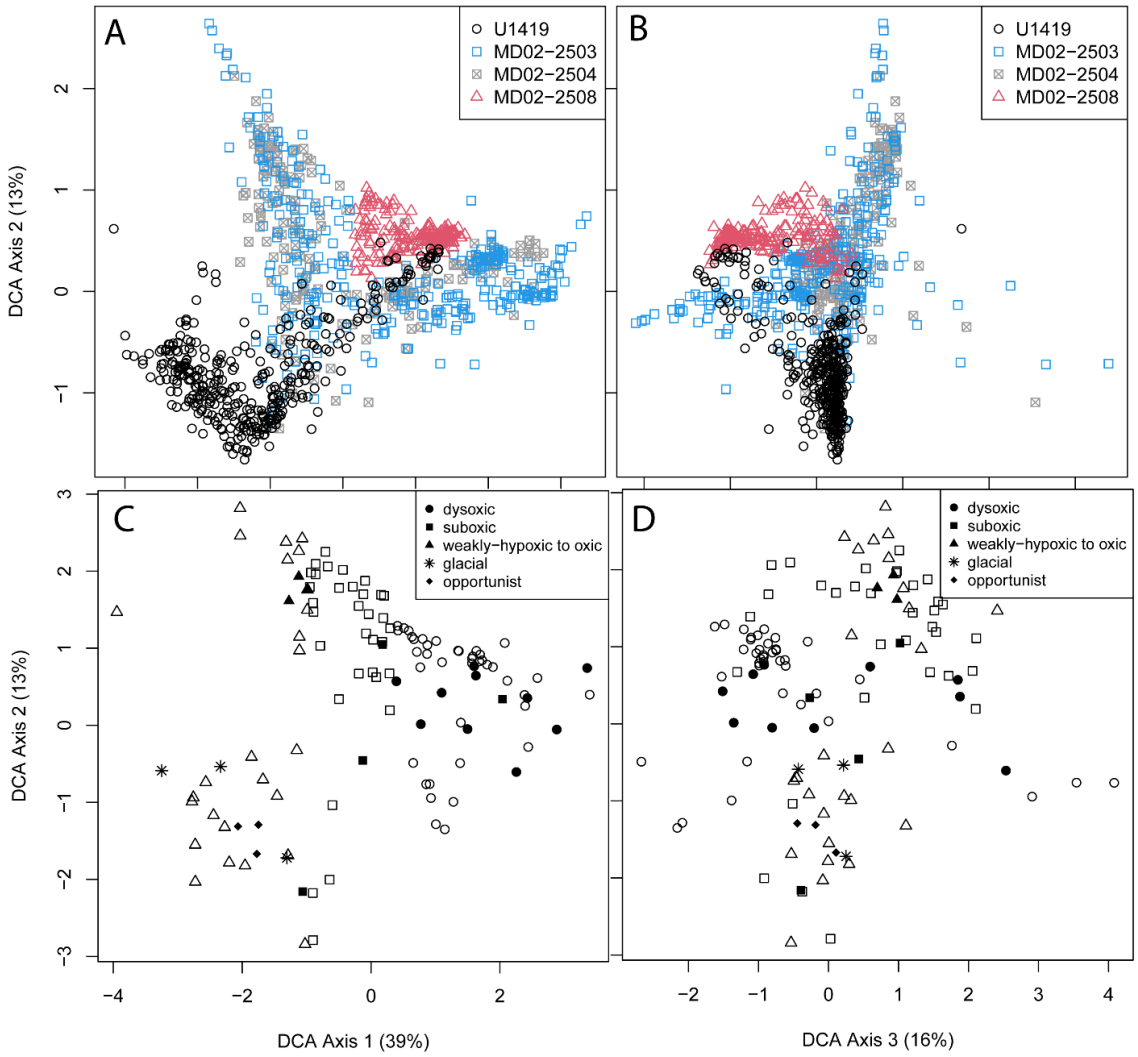

Figure 3.2 Detrended Correspondence Analysis (DCA). A and B depict sample scores, C and D depict species scores. Filled symbols in C and D are species whose ecological preferences were derived from the literature; open symbols are oxygenation tolerances inferred by the co-variance with species with known oxygenation tolerances.

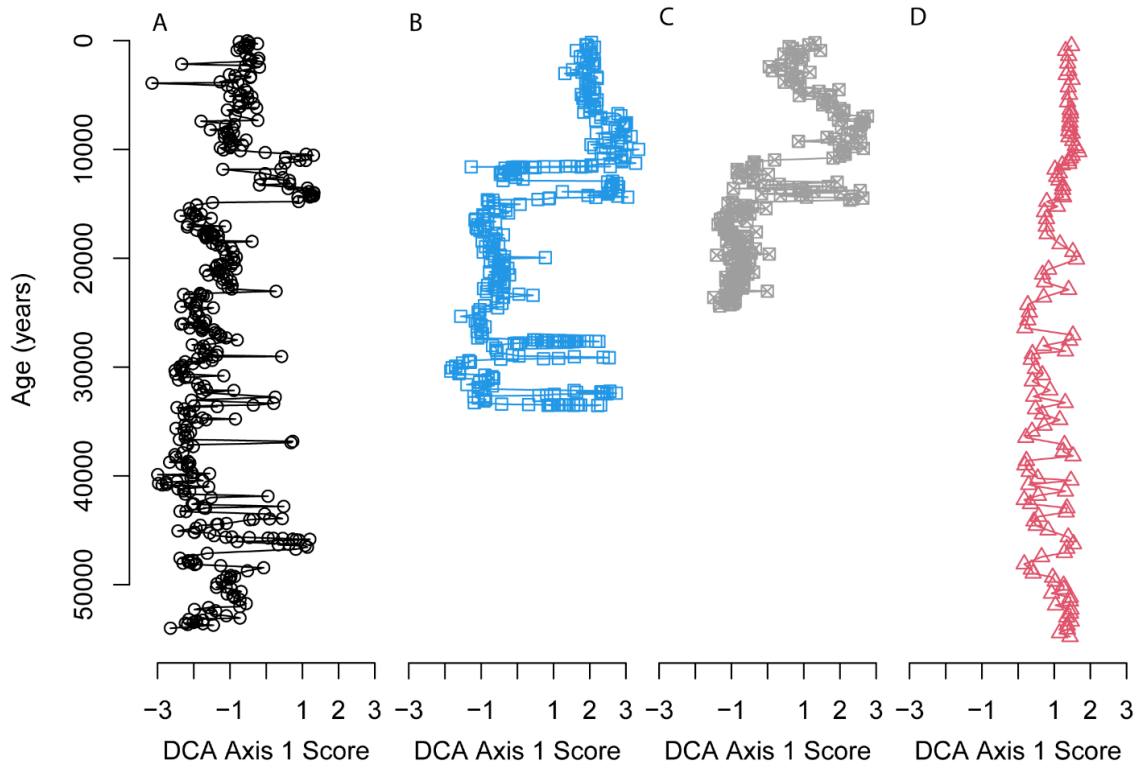

Figure 3.3 DCA sample scores through time for the four sites analyzed. (A) U1419; (B) MD02-2503; (C) MD02-2504; (D) MD02-2508.

Species with strong positive DCA Axis 2 scores include *Cibicides mckannai, Cibicides lobulatus, Cibicidoides* spp., *Cassidulina translucens,* and *Rutherfordoides*, which are commonly associated with hard substrates (Supplemental Table 3.3; Murray, 2006). These species rarely occur and most frequently occurred at MD02-2503 and MD02-2504. Species with strong negative DCA Axis 2 scores, including *Nonionella pulchella, B. decussata, B. earlandi, Chilostomella fimbriata,* and *Globobulimina affinis,* only occur at U1419. These species, along with other species with strong negative scores including *Trifarina angulosa, Stainforthia fusiformis* and *Bulimina mexicana* are associated with high primary productivity (Alve, 1994; Hayward et al., 2004; Murray,

2006). Furthermore, *E. pacifica,* which is numerically abundant at U1419, had a strong negative DCA Axis 2 score. While species that are tolerant of dysoxia are segregated on DCA Axis 1, they are not segregated along DCA Axis 2 (Figure 3.2 (C); Supplemental Table 3.3).

Species with a tolerance for dysoxia and suboxia have strong negative to strong positive DCA Axis 3 scores (Figure 3.2 (C); Supplemental Table 3.3). For example, *Globobulimina pacifica* and *C. oolina* have the highest positive DCA Axis 3 scores (>2.5). Other species associated with low-oxygen environments including *S. eckisi* and *Nonionella stella* also had positive scores of >1.8 whereas *T. delicata* and *B. tenuata* had negative DCA Axis 3 scores < -1.5.

3.3.3. Oxygenation calculations

We used the dysoxic species *N. stella* (Ohkushi et al., 2013) to mark the boundary between suboxic-dysoxic categories at a DCA Axis 1 score of 0.39 given all species known in the literature to tolerate dysoxic conditions had DCA Axis 1 scores between 0.39 and 3.4. All species with unpublished oxygen preferences in this range of DCA Axis 1 scores were, thus, categorized as dysoxia-tolerant. The weakly hypoxic to oxic taxon *Quinqueloculina* spp. was used to mark the suboxic-weakly hypoxic to oxic boundary at DCA score -0.98; all species known in the literature to be indicative of suboxic environments had DCA Axis 1 scores between -0.95 and 0.39. Thus, we categorized all species with DCA Axis 1 scores between -0.95 and 0.39 as indicative of suboxic conditions and all species with DCA Axis 1 scores < -0.95 as indicative of weakly hypoxic to oxic environments.

At U1419, our modified BDO (mBDO) provides a faunal-based oxygenation value of 0.65 ml/L for the core-top sample, which is similar to the DO of 0.59 ml/L interpolated from the World Ocean Atlas (Table 3.2). Similarity, the youngest sample from MD02-2508, which has the lowest modern DO value of our four sites (0.13 ml/L), had a mBDO value of 0.10 ml/L. The youngest samples from the two sites in SBB, MD02-2503 and MD02-2504 had calculated mBDO values of 0.11 ml/L and 0.23 ml/L, respectively, which are lower than the DO values interpolated from the World Ocean Atlas (Table 3.2). In the downcore records, mBDO values ranging from dysoxic to oxic occur at all the sites except MD02-2508 (Figure 3. 4 A - D).

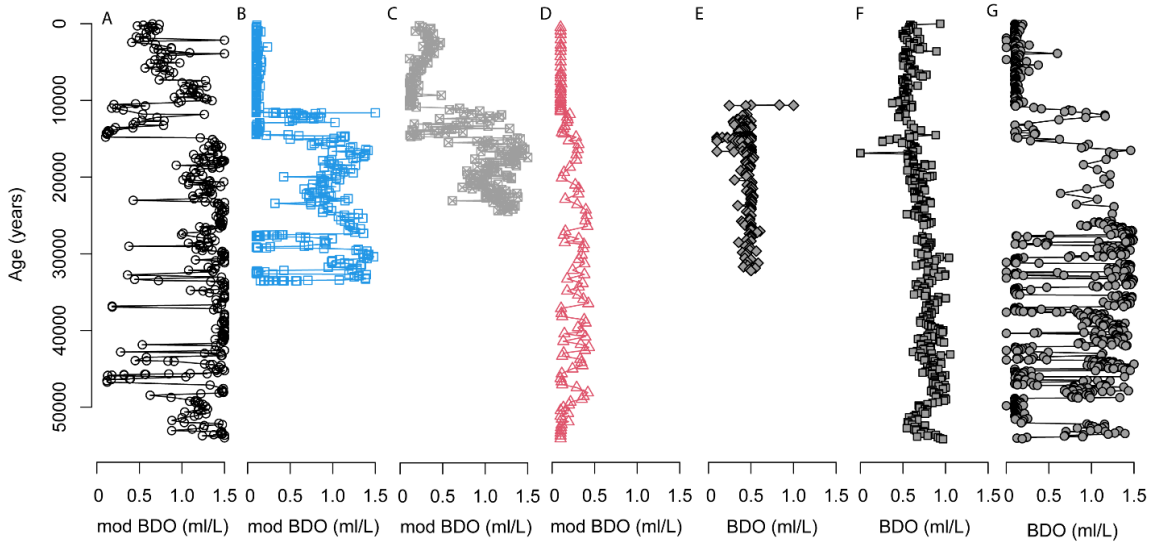

Figure 3.4 Dissolved oxygen calculation for each site. A-D are the modified BDO derived from the DCA analyses. E -- G calculate BDO from a restricted number of species and follow the oxygenation tolerances assigned by the original authors. (A) U1419; (B) MD02-2503; (C) MD02-2504; (D) MD02-2508; (E) ODP Hole 890B; (F) ODP 1017; (G) ODP 893.

Table 3.2 The calculated BDO values of site core tops and measured modern oxygen values for the sites under study.

Sites ↓	Modern measured oxygen level (ml/L)	Calculated core-top mBDO value (ml/L)
U1419/85JC (GoA)	0.59	0.65
MD02-2508 (Baja Sur California)	0.13	0.10
MD02-2503 (SBB)	0.36	0.11
MD02-2504 (SBB)	0.47	0.23
ODP 893 (SBB)	0.34	0.10
ODP 1017 (Point Conception, Californian Margin)	0.54	0.94

We use the oxygenation categories assigned to foraminiferal species by the original authors for the three sites we discuss but do not include in the multivariate analyses. The youngest sample from ODP 893 has a similar BDO value as that of the adjacent MD02-2503 using our mBDO (Table 3.2). At ODP Hole 890B, 50% of samples have BDO values <0.44 ml/L whereas other samples are near the suboxic-dysoxic boundary with BDO values ~0.50 ml/L. ODP 1017 has BDO values between 0.5-1 ml/L (Figure 3.4; Supplemental Table 3.4). Neither of the sites produced BDO values >1 ml/L. BDO values for the core top samples were 0.83 ml/L and 0.94 ml/L for ODP Hole 890B and ODP 1017, respectively (Figure 3.4; Supplemental Table 3.4).

3.3.3.1. Comparison between oxygenation estimates

The mBDO estimates we calculate here differ from the oxygenation values derived by the original authors, however the rank order correlation between the estimates is strong

(Figure 3.5). The Spearman correlations between the mBDO values herein with the >63 μm and >125 μm size fraction mBDO values from our previous paper (Sharon et al., 2021) are 0.80 (95% confidence interval (CI) = 0.75-0.84) and 0.84 (95% CI = 0.81-0.87), respectively. Our mBDO for MD02-2503 also has a Spearman correlation of 0.84 (95% Confidence Interval = 0.80 - 0.87) when compared to BDO calculations from the previous study (Ohkushi et al., 2013). Similarly, slightly a lower but a positive Spearman correlation of 0.74 (95% CI = 0.66 - 0.80) was also seen for MD02-2504 (Figure 3.5). For MD02-2508, the Spearman correlation between our BDO and oxygen calculations by Tetard et al. (2017) was 0.87 (95% CI = 0.82 - 0.91).

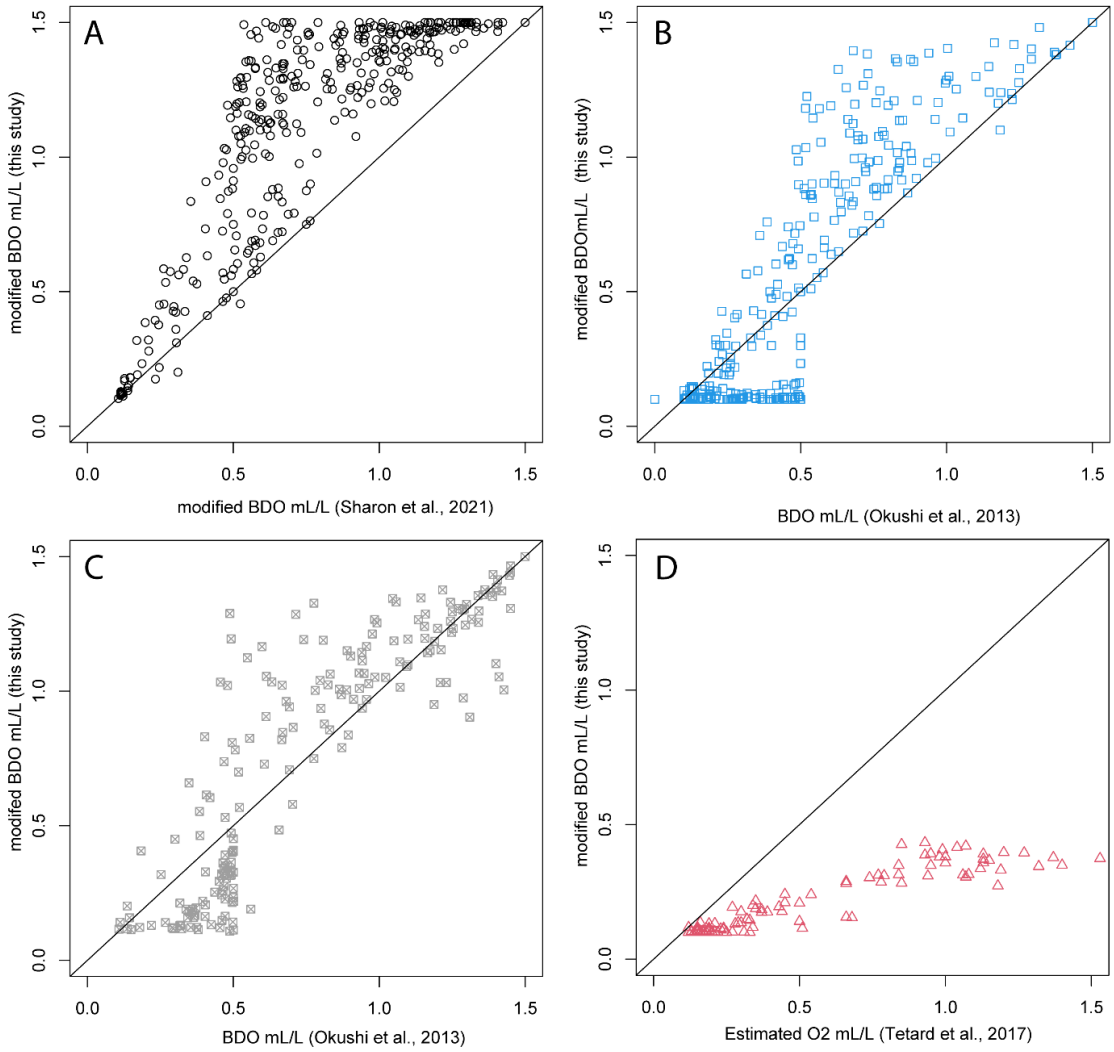

Figure 3.5 Comparison of oxygen concertation calculated using the modified BDO in this study and the dissolved oxygen concentrations estimated by the original authors. Black line is the 1:1 line.

Based on the mBDO calculated herein, Site U1419 is generally better oxygenated than the other sites we analyze given the majority of its mBDO values are >1 ml/L. However, Site U1419 also records low-oxygen conditions of equal magnitude to those observed at MD02-2503, ODP 893, and MD02-2508 during the B-A and for short

intervals (<200 yrs in duration) during MIS 3 (Figure 3.4). MD02-2508 remains low-oxygen throughout the ~60 kyr record with the maximum calculated mBDO value of 0.43 ml/L at ~ 42.2 ka. This southernmost site showed the narrowest range of mBDO values whereas the SBB sites had the greatest range in mBDO values (Figure 3.2 (A)). BDO values <0.15 ml/L occurred after the YD to the present at MD02-2503, MD02-2508 and ODP 893 whereas MD02-2504 had median mBDO of 0.22 ml/L and U1419 was better oxygenated (Figure 3.4; Supplemental Table 3.4).

We also calculated BDO values at ODP Hole 890B, ODP 893 and ODP 1017 using the original ecological categories (dysoxic, suboxic, oxic) of the original authors (Supplemental Table 3.4, Cannariato et al., 1999; Cannariato and Kennett, 1999; Saravanan et al., 2020), and thus are not directly comparable to the modified BDO. Overall, ODP 893 shows temporal correspondence to the mBDO of MD02-2503 and MD02-2504 all are from the SBB. Slope site ODP 1017 on the California mostly remains suboxic and has low variation in its oxygenation (Figure 3.4). ODP Hole 890B has a BDO value of ~0.50 ml/L or less in the majority of samples and is better oxygenated in only ~10% of samples (Figure 3.4).

3.3.3.2. MIS 3 events

At U1419, the median mBDO during MIS 3 (~29 - 54 ka) was 1.4 ml/L (IQR=1.2 - 1.5 ml/L), however, seven intervals with mBDO values <0.50 ml/L were recorded. The longest interval occurred from 46.7- 45.7 ka when median mBDO was 0.18 ml/L (IQR= 0.13 - 0.35 ml/L; Figure 3.4). In addition, mBDO values <0.50 ml/L were recorded single samples at ~ 43.9 ka, 42.8 ka, 33.3 ka, 32.7 ka and ~29 ka mBDO values <0.18 ml/L were

also recorded from 36.9-36.8 ka. In contrast, MD02-2508 in Baja California Sur has mBDO values < 0.43 ml/L throughout the ~54 ka record. In addition, several intervals with mBDO values of <0.15 ml/L occurred between ~54-14 ka with median mBDO of 0.17 ml/L (Figure 3.4; Supplemental Table 3.4). ODP 1017 on the San Lucia Slope is not calculated on the same scale as U1419 and MD02-2508 and should not be directly compared. ODP 1017 has BDO values between 0.5-1 ml/L throughout the MIS 3 with median BDO value of 0.80 ml/L (Figure 3.4).

The SBB sites we include in the mBDO calculations only extend to the youngest intervals of MIS 3. At MD02-2503, the median mBDO value from ~27.5 to 33.5 ka was 0.35 ml/L (IQR = 0.1 - 1) and the record spans values from 0.1 ml/L to >1 ml/L. The lowest BDO values (<0.15 ml/L) occurred at ~32.6-32.2 ka, ~27.7-27.5 ka, and ~29 ka (Figure 3.4). We could not calculate mBDO values for the longer SBB from site ODP 893 where BDO values <0.50 ml/L alternated with intermediate (0.5 - 1ml/L) to better-oxygenated (>1 ml/L) conditions throughout the MIS 3 with median BDO of 0.94 ml/L (IQR = 0.15 -1.24) (Figure 3.4). Despite the difference in scale, low BDO values during MIS3 at ODP 893 correspond to the low mBDO values at the U1419 and MD02-2503 (Figure 3.4).

3.3.3.3. MIS 2 Events (29-11.7 ka)

U1419 remained well-oxygenated between 29 ka and ~14.7 ka with a median mBDO value of 1.4 ml/L (IQR=1.2-1.4 ml/L); only one sample in this interval records an mBDO value of 0.43 ml/L at ~23 ka. At MD02-2508, median mBDO was 0.29 ml/L (IQR = 0.18 – 0.34) from 29 - ~14.7 ka. At MD02-2503, median mBDO values in MIS 2 are 1

ml/L (IQR = 0.9 - 1.2) with only two samples having mBDO values <0.50 ml/L; this is similar to the BDO at ODP 893 (Figure 3.1 (B)). The SBB site MD02-2504 which only extended to ~24 ka, also has higher mBDO values in MIS 2 with a median mBDO value of 1.2 ml/L (IQR = 1 - 1.3) from 29 - 14.7 ka than during MIS 3. ODP 1017 and ODP Hole 890B have median BDO values of and 0.66 (IQR = 0.62 - 0.73) and 0.47 ml/L (IQR = 0.41-50) for this interval, respectively.

During the pre-Bølling and Heinrich 1 (HS1) from 18-15 ka, Site U1419 had median BDO values of 1.4 ml/L. Similarly, median BDO values of 1.2 ml/L and 1.3 ml/L occurred at MD02-2503 and MD02-2504, respectively. Site ODP 893 also had better oxygenated conditions during this interval (Figure 3.4). Changes in oxygenation were not recorded at MD02-2508, ODP Hole 890B or ODP 1017; while MD02-2508 and ODP Hole 890B remained dysoxic with BDO of <0.50 ml/L, ODP 1017 remained suboxic with median BDO of 0.60 ml/L until 15.6 ka after which it declines to a median BDO of 0.38 ml/L from 15.6 - 15 ka.

3.3.3.3.1. Bølling-Allerød (14.7-12.9 ka)

During the Bølling-Allerød (B-A), 6 of the 7 sites, regardless of BDO scaling, have BDO values of <0.50 ml/L. At U1419, mBDO values shift from a high of 1.2 ml/L at 14.8 ka to the lowest possible mBDO value (0.10 ml/L) at 14.7 ka. Low mBDO values with a median of 0.14 ml/L (IQR = 0.12 - 0.27) persist at U1419 until the end of the B-A at 12.9 ka. Similarly, ODP Hole 890B transitioned from BDO values of ~0.4 ml/L to values as low as 0.1 ml/L from 15.3 to 12.8 ka. MD02-2503 also records low mBDO values with a median of 0.11 ml/L (IQR = 0.10 - 0.14) from 14.5 to 12.9 ka; the record at the ODP 893

is similar with a median BDO of 0.2 ml/L (IQR = 0.11 - 0.32). At MD02-2504, oxygenation varies between the Bølling (14.7 - 13.8 ka) and the Allerød (13.8 - 12.9 ka) intervals; the Allerød has a higher median mBDO value of 0.63 ml/L (IQR= 0.49 - 0.86) as compared to the median mBDO value of 0.22 ml/L (IQR=0.15 - 0.44) in the Bølling interval. At MD02-2508, already low mBDO values decline to a median of 0.13 ml/L (IQR = 0.13 - 0.15) and remain below 0.28 ml/L during the B-A; at this site lower values were present after the early Holocene and several times in MIS 3. ODP 1017 on the San Lucia Slope had no major change in BDO and values remained between 0.5 and 1 ml/L during the B-A.

3.3.3.3.2. YOUNGER DRYAS- (12.9–11.7 ka)

Following the B-A interval, mBDO values at U1419 increase to a median of 0.71 ml/L (IQR = 0.54 - 0.80) during the Younger-Dryas (12.7 - 11.7 ka) and are >0.60 ml/L at the SBB sites. At MD02-2503, mBDO changes abruptly from 0.14 to 1 ml/L at ~12.9 ka and maintains a median mBDO value of 0.66 ml/L (IQR = 0.60 - 0.81) until ~11.7 ka. At site MD02-2504, median mBDO values are 0.94 ml/L (IQR= 0.81 - 1.1) during the YD, which is also an increase from oxygen estimates for the preceding Allerød interval. Although not on the same scale as the other sites, BDO values at ODP 893 also increase during the YD (Figure 3.4).

In contrast to U1419 and the SBB sites, BDO estimates do not increase from the B-A to the YD at ODP Hole 890B, ODP 1017, and MD02-2508. At ODP 1017, median BDO values decrease from a median of 0.63 ml/L (IQR = 0.60 - 0.70) during the B-A to a median of 0.46 ml/L (IQR = 0.46 - 0.51) during the YD. At MD02-2508, mBDO also

increases slightly from a median of 0.14 ml/L (IQR= 0.13 - 0.15) in the B-A to a median of 0.18 ml/L (IQR = 0.18 - 0.19) during the YD. We do not observe a change in BDO between the B-A and YD at ODP Hole 890B.

3.3.3.4. Early Holocene (11.5-10.5 ka)

After the YD, early Holocene (11.5-10.5 ka) BDO values decline at all the sites except for ODP 1017 and ODP Hole 890B (Figure 3.4; Supplemental Table 3.4). At U1419, the median mBDO value for the early Holocene interval decreases to 0.23 ml/L (IQR = 0.20 - 0.31). At MD02-2503, the median mBDO value declines to 0.10 ml/L (IQR = 0.1 - 0.1) during the early Holocene whereas MD02-2504 declines to a median mBDO values of 0.64 ml/L (IQR=0.29-0.74). The development of lower mBDO values occurs at 10.5 ka at MD02-2503 but does not occur until 10.8 ka at MD02-2504. Similarly, ODP 893 has BDO values >0.7 ml/L from 11.5-11 ka and values do not decline to <0.50 ml/L until ~11 ka (Figure 3.4; Supplemental Table 3.4).

MD02-2508 declines to mBDO values <0.10 ml/L beginning at ~11.5 ka from values >0.18 ml/L during the YD. In contrast, ODP 1017 has low variability (values range from ~0.50 to 0.61 ml/L) between the YD and early Holocene. ODP Hole 890B does not have samples younger than 10.5 ka; the average BDO value of these post-YD samples is 0.60 ml/L (IQR = 0.44 - 0.83); ODP Hole 890B has the highest BDO value of ~1 ml/L in its record at ~10.6 ka (Figure 3.4; Supplemental Table 3.4).

3.3.3.5. Middle to Late Holocene

Modified BDO values increase at U1419 and ODP 1017 following the lower-oxygen early Holocene, however BDO values remain low at the other sites (Figure 3.4;

Supplemental Table 3.4). U1419 increases to a median mBDO value of 1.1 ml/L (IQR) from 10.2-7.4 ka followed by slight decrease to median mBDO value of 0.71 ml/L (IQR = 0.61 - 0.82) from 7.5 ka to the present. Occasional mBDO values <0.50 ml/L are record from ~2.4 ka to the present at U1419 (Figure 3.4). At ODP 1017 intermediate BDO values between 0.5-1 ml/L develop and continue throughout the Holocene.

In contrast, MD02-2503 and MD02-2504 in SBB continue to record low mBDO values throughout the Holocene; the basin core site (MD02-2503) is lower oxygen with median mBDO of 0.10 ml/L (IQR=0.1-0.1) than the sill depth core site (MD02-2504; Figure 3.4). At site MD02-2504, median BDO values of 0.13 ml/L (IQR = 0.12 - 0.15) continued from 10.6-6.9 ka after which values increased to a median of 0.32 ml/L (IQR = 0.22 - 0.35) from 6.8 ka to 0.2 ka. Although not on the same scale BDO values <0.10 ml/L continued throughout the Holocene at ODP 893, similar to MD02-2503 and MD02-2508 (Figure 3.4; Supplemental Table 3.4).

3.4. Discussion

DCA analyses of total foraminiferal faunas across the four sites we reanalyze reveal a primary gradient accounting for 39% of the faunal variation representing a gradient in oxygenation where species with the most positive DCA Axis 1 scores are known to tolerate <0.1 ml/L O_2 (Supplemental Table 3.2; Figure 3.2 (C)). Our previous study, which used similar methods but focused only on U1419, summarized 51% of the faunal variation on DCA Axis 1 (Sharon et al., 2021); this difference reflects the greater amount of faunal variation that is apportioned to later DCA axes due to site-to-site differences in faunal composition when all four sites were combined. Similarly, PCA

analyses performed on data from MD02-2508 at Baja California Sur summarized more variation on the first axis (52%; Tetard et al., 2017). In contrast, PCA analyses of MD02-2503 and MD02-2304 summarized just 22% of the faunal variation on the first axis in the original ordination analyses, which was also interpreted as an oxygen gradient (Ohkushi et al., 2013).

Most studies that use benthic foraminifera faunas focus their interpretations on subset of index taxa for which there is prior evidence for oxygen tolerances, even if multivariate analyses are performed on the entire assemblages (but see Sharon et al., 2021). However, many species covary with these index taxa and can significantly change counts within oxygenation categories. For example, our DCA analysis finds that sites MD02-2503 and MD02-2504 have 27 and 22 dysoxic species, respectively, in contrast to the 7 dysoxic species used to quantify oxygenation in the original publication (Okhushi et al., 2013). Similarly, MD02-2508 has 36 species we categorize as dysoxic based upon their DCA Axis 1 scores as compared to the 4 dysoxic species they use. Site U1419 from the Gulf of Alaska had only 9 dysoxic species in both the original and revised analyses. The abundance of dysoxic species could reflect a latitudinal gradient in the diversity of dysoxic species and simply reflect additional species present at the more southern localities. However, if this were the case, we would expect that sites would be arrayed along DCA Axis 1 by latitude, but samples from the southernmost site at Baja California Sur have intermediate values that are frequently surpassed by samples from the SBB. Further, while samples from U1419 generally have the lowest DCA Axis 1 scores, some

samples have values as high as those from the southern sites and thus the axis scores are not controlled by site.

We find that most inter-site variation unrelated to oxygenation is summarized on DCA Axis 2 and 3. Species with strong negative DCA Axis 2 scores were more common or were only found at U1419; these species are also associated with glacial environments and high seasonal productivity (Figure 3.2; Ohkushi et al., 2003). Species with strong positive DCA Axis 2 scores were rare and occurred almost exclusively at the SBB sites (Supplemental Table 3.1 and Supplemental Table 3.3). Species known to occur in dysoxic environments have DCA Axis 2 scores near zero and had no bias toward extreme DCA Axis 2 scores, indicating little influence of dysoxic species on site scores along DCA Axis 2. Dysoxic species have either strong negative or strong positive scores on DCA Axis 3 and do not reflect a clear environmental gradient, thus DCA Axis 3 likely also reflect site-to-site variation unrelated to oxygenation (Figure 3.2; Supplemental Table 3.3).

3.4.1. Placing North Pacific Oxygenation Events on a Common Scale

Given the strong association between DCA Axis 1 and species tolerant of low-oxygen conditions across sites and the lack of an association with later DCA axes, we are confident in using DCA Axis 1 scores as a basis for assigning species to oxygenation categories and for comparing relative oxygenation among the four sites. Further, temporal patterns in our DCA Axis 1 scores within sites correspond well with the published paleo-oxygenation histories of the study sites in terms of the rank order or reconstruction oxygenation values (Figure 3.2 (C) and 3.3; Supplemental Table 3.4; Ohkushi et al., 2013; Tetard et al., 2017; Sharon et al., 2021). Our previous work focused on U1419 found that

samples with DCA Axis 1 scores we inferred as indicating dysoxic conditions also had high concentrations of redox sensitive metals (Mo/Al and U/Al), which further supported our interpretations (Sharon et al., 2021).

Using DCA Axis 1 species scores to place species into oxygenation categories allows us to consider the full faunal assemblage in the mBDO calculation and ensures that all calculations are on the same oxygenation scale and thus comparable among sites. The mBDO results from the uppermost samples in each core are congruent with oxygenation values for the sites (Table 3.2). For instance, our mBDO calculations infer that U1419 is suboxic and that sites MD02-2503, MD02-2504, and MD02-2508 are dysoxic in the modern and the relative oxygenation among sites is similar whether calculated by our mBDO or retrieved from the WOA (Table 3.2). However, the mBDO values we calculate are ~0.25 ml/L lower for both SBB sites than the modern observed oxygenation values. This slight mismatch may reflect the interannual flushing of SBB with well-oxygenated waters (Bograd et al., 2002), which would increase the annual average oxygenation values calculated in the WOA. U1419 and MD02-2508 core tops replicate modern values within 0.06 ml/L O_2. In contrast, our calculation of BDO using the oxygen categories of the original authors for ODP 1017 is 0.4 ml/L O_2 lower than the modern WOA value whereas the values we calculate of ODP 893 are nearly identical to the co-located MD02-2503; this may be because the original BDO equation was developed for SBB samples (Ohkhusi et al, 2013). Thus, our mBDO reliably reconstructs oxygenation values, but BDO calculated without the full fauna may not yield as precise an oxygenation history.

On average, U1419 has the most oxic record with the majority of samples from MIS3 having mBDO values >1.0 ml/L, and frequently 1.5 ml/L, punctuated by values as low as 0.1 ml/L demonstrating brief development of dysoxia in an otherwise better oxygenated environment. This is consistent with our earlier reconstruction (Sharon et al., 2021), however placing the faunal variation at U1419 in the context of the other three sites generally increases our estimated oxygen levels above our previous estimates (Figure 3.5 (A)). This shift to higher values implies that some samples we previously interpreted as suboxic are weakly hypoxic to oxic on this scale. As with previous oxygen reconstructions (Davies et al., 2011; Praetorius et al., 2015; Sharon et al., 2021), we reconstruct an abrupt shift to dysoxic conditions at the B-A, an increase in oxygenation to primarily suboxic conditions during the YD, and a second dysxoic event of nearly equal severity in the Early Holocene. Whereas weakly hypoxic to oxic conditions return at ~10 ka, oxygen continues to gradually decline to the present suboxic value of ~0.6 ml/L O_2. This suggests that the modern suboxic condition of the OMZ in the GoA is a relatively recent development and was not as intense, or stable, prior to the mid-Holocene. The dominance of small opportunistic taxa in the 63 - 125 μm size fraction, excluded from mBDO calculations here, suggests highly pulsed export productivity events developed after ~ 8 kyrs in the GoA (Belanger et al., 2020), which may have driven the intensification of the OMZ at this site during the Holocene.

Assemblages from SBB (MD02-2503 and MD02-2504) do not reconstruct mBDO values of < 1.5 ml/L with only one exception and generally indicate less well-oxygenated conditions than GoA. BDO values calculated herein are generally lower than those

calculated by the Ohkushi et al. (2013) using a subset of the fauna when the original authors found values <0.5 ml/L (Figure 3.5 (B) and 3.5 (C)). This implies that for the lowest oxygen assemblages, our modification finds that they represent more severe dysoxic events than the original authors. Conversely, our calculations find that samples for which the original authors found values greater than ~0.5 ml/L were generally better oxygenated (Figure 3.5 (B) and 3.5 (C)). Assemblages from MD02-2503 reconstruct dysoxic events of longer duration than U1419 during MIS 3, beginning at ~32 ka, the oldest portion of the MD02-2503 record. Dysoxia develops gradually into the B-A when mBDO values reach a minimum of 0.1 ml/L and remain 0.1 m/L for the remainder of the record with the exception of a brief amelioration to suboxia during the YD.

In our analysis, MD02-2508 in Baja California Sur only produced mBDO values <0.43 ml/L in the 54 ka record we reanalyzed. BDO values <0.15 ml/L occur occasionally during MIS 3, during the B-A but are persistent after ~11 ka. This contrasts with the original study which estimated DO values from 0.1-2 ml/L (Tetard et al., 2017; Figure 3.5 (D)). The disagreement, however, is only in the amplitude of the changes and both records produce similar temporal patterns (Figure 3.6). The dissimilarity in oxygenation levels may be driven by the inclusion of fewer species in the original study than we use here. In addition, species we infer as tolerant as suboxic (including *U. peregrina*, *B. spissa*) have the most dissimilar PCA Axis 1 loadings from species we infer as tolerating dysoxia (including *B. seminuda*, *T. delicata*, *B. tenuata*, and *B. subadvena*) in the original analyses, indicating that the environmental gradient reconstructed using MD02-2508 alone does not include weakly hypoxic to oxic environments. Despite that truncated gradient, all species

not categorized as dysoxic or suboxic were considered indicative of oxic environments in Tetard et al., 2017, which would have overestimated oxygenation at the site. This is a significant difference because our estimates suggest that the ETNP OMZ has been persistently dysoxic since MIS 3 whereas the original conclusions postulate suboxic to weakly hypoxic conditions associated with Heinrich stadials (Tetard et al., 2017). Given this site is surrounded by highly dysoxic water masses merging from the north and the south in the modern, it is reasonable to find that MD02-2508 has been persistently dysoxic. Our results support that the ETNP OMZ has been stable over the last 54 ka.

Sites ODP 1017 and ODP 893 did not have sufficient faunal data to reanalyze and place these sites on the common scale. However, our BDO calculations for ODP 893 correspond well in both temporal pattern and mBDO values for co-located Site MD02-2503. ODP 1017 on the San Lucia Slope primarily produces BDO values consistent with suboxia. Dysoxic values were observed only just before the B-A interval at ~15.5 ka whereas the B-A itself reconstructed suboxic values. This is similar to the interpretations of the original authors, which find high abundances of dysoxic species (*B. argentea, B. tenuata, Chilostomella ovoidea)* and suboxic 1 (*U. peregrina* and *B. spissa*) species during the B-A and interstadials. During MIS 3, the Cannariato and Kennett (1999) found higher abundances of their suboxic 2 and oxic categories, consistent with the higher BDO values we reconstruct in the older portion of the record.

Site ODP Hole 890B on the Cascadia Margin had sufficient faunal data for analysis, however its faunas were quite distinct from the other sites, likely due to its deeper water depth, thus we calculated BDO using species and species categorizations of the

original authors. Here, our reconstruction was also similar to that of the original authors and we both concluded that conditions at the site were near the suboxic-dysoxic boundary (Saravanan et al., 2020).

3.4.2. Relative Severity and Duration of Low-Oxygen events in the North Pacific

3.4.2.1. MIS3

At all sites except ODP 1017 and ODP Hole 890B, we recorded dysoxic events during the MIS 3. Our mBDO suggests that the dysoxic events at U1419 were as severe as those in SBB with values <0.15 ml/L in both regions. The timing of the events was also similar; dysoxic events at MD02-2503 at ~33.5 ka (IS6), ~32.6-32.1 ka (IS5), ~29 ka (IS4) and ~ 27.7-27.5 ka (IS3) appear to correspond with dysoxic events at U1419 at ~32.7 ka, ~29 ka and suboxia at ~33.5 ka, ~27.5 ka, although they are shorter in duration in U1419 (Figure 3.4). Examining the record at ODP 893 allows us to extend the comparison between U1419 and SBB further into MIS 3 where we find also similar timing of events although they were shorter at U1419. Excursions to lower mBDO values indicating suboxic-dysoxic conditions occur at both U1419 and ODP 893 at ~41.7 ka, 42.8 ka, ~43.5 ka, 45.7-46.7 ka, ~48 ka, ~51 ka, ~53 ka. Some of the dysoxic events are as low-oxygen as the lowest-oxygen conditions recorded at MD02-2508, suggesting they were comparable to strong OMZ of the ETNP. Changes in oxygenation during MIS 3 have been previously related to millennial scale climatic oscillations, including and D/O events, and corresponding changes in ocean circulation, surface productivity, and export production (Cannariato et al., 1999; Cannariato and Kennett, 1999; Tetard et al., 2017).

3.4.2.2. B-A and Holocene

Dysoxic conditions with mBDO values <0.15 ml/L also occurred during the B-A at U1419, MD02-2503, and MD02-2508, suggesting that deoxygenation was equally severe among those sites. In contrast, similarly low-oxygen conditions at Site MD02-2504 occurred only during the Bølling with median mBDO of 0.22 ml/L that increases to 0.63 ml/L during Allerød (Supplemental Table 3.4). Previous oxygenation studies of the foraminiferal faunal data at MD02-2504, however, did not find this distinction (Ohkushi et al., 2013). Our reconstruction is supported by lamination indices at MD02-2504, which also suggested less severe low-oxygen conditions during the Allerød as compared to the Bølling (Moffitt et al., 2014). In addition, during B-A the sediments at MD02-2503 were more well laminated with a higher percent abundance of dysoxic species than at MD02-2504 (Figure 3.5 of Ohkushi et al., 2013). Similarly, our finding that MD02-2503 was, on average, more severely dysoxic than MD02-2504 during the B-A is supported by its lower species diversity (Ohkushi et al., 2013).

Although not on the same oxygenation scale, we reconstruct dysoxia throughout the B-A at ODP 893, consistent with previous studies (Cannariato et al., 1999). While there is little variation in the oxygenation history that we derive from ODP Hole 890B, the lowest BDO values (0.1 ml/L) in that record also occur at 15.3 ka, 15.1 ka and 14.8 ka, before and during the B-A. Previous work on the Cascadia Margin at site JT96-09 (920 m water depth) recorded a more intense low-oxygen event during the Allerød interval from ~13.5 to 12.6 ka based upon the dominance of *B. tenuata* (McKay et al., 2005). However, our reanalysis ODP Hole 890B at the deeper Cascadia Margin site (1326 m) is consistent with previous work on the same dataset (Saravanan et al., 2020), and thus is not due to

differences in methodology; instead, it may be related to the difference in water depth. The only exception to a severely dysoxic B-A in our analyses is at ODP 1017 where BDO calculations using the authors original species categories does not have values <0.50 ml/L, but we do observe a decrease in BDO with a median of 0.34 ml/L before the onset of B-A from 15.5-14.9 ka (Figure 3.4).

Oxygenation varied across the study sites during the early Holocene. Dysoxia was recorded from ~11.3 to 10.4 kyrs during early Holocene at U1419. Dysoxia based on >125 μm size fraction in the previous U1419 study was of similar severity to the reanalysis herein with mBDO <0.30 ml/L (Sharon et al., 2021). In addition, the onset of extremely low BDO values of <0.15 ml/L and <0.10 ml/L at the already dysoxic sites MD02-2503 and MD02-2508 were recorded at the beginning at ~10.5 ka. This dysoxia was as severe as during the B-A event and extended throughout the Holocene at the MD02-2503 and MD02-2508. In contrast, dysoxia at MD02-2504 did not occur until ~10.7 ka, before which we record suboxic conditions from ~11.5-10.9 ka of the early Holocene (Supplemental Table 3.4). ODP 1017 straddled the dysoxic-suboxic boundary from ~11.5-11 ka but returned to suboxic conditions (BDO >0.5 ml/L) from ~11-10.5 ka, suggesting that even this low-variability site had lower oxygen in the earliest Holocene. ODP Hole 890B has the highest BDO value in its record (1 ml/L) at ~10.7 ka, however this value is anomalous compared to the other early Holocene values that alternate between dysoxic to suboxic conditions. Another site near Vancouver Island also records dysoxia from ~10 to 11 ka, which the authors link to a decrease in ventilation and increase in productivity (Mckay et al., 2005).

In the middle to late Holocene, sites significantly diverge in their oxygenation histories and while some record suboxic conditions that are better oxygenated than the B-A and early Holocene, others remain dysoxic. U1419 is as well-oxygenated as the majority of MIS 3 from ~7.4 - 10 ka in the middle Holocene, then gradually declines in oxygen, but does not decline beyond suboxia through to the present. In SBB, the sill depth site (MD02-2504) recorded suboxic conditions from ~10.9-11.5 ka and although dysoxic it was slightly better oxygenated than the basin sites (MD02-2503 and ODP 893), which maintained extreme dysoxia from the early Holocene to present. These Holocene differences in oxygenation are further supported by differences in their lamination records (Ohkushi et al., 2013; Moffitt et al., 2014). Similarly, MD02-2508 does not produce BDO values >0.10 ml/L from ~11.5 ka to present.

Dysoxia was also observed in the northwestern Pacific Ocean during the B-A. Dysoxic species like *B. tenuata, B. tumida and B. pacifica* and laminations indicated lowest oxygen during the B-A off the coast of Japan (Ikehara et al., 2006; Shibahara et al., 2007). In the northern Japan, apart from the B-A lowest oxygen was also seen from 11.6-10 ka while suboxic species dominated most of the Holocene (Ikehara et al., 2006; Shibahara et al., 2007). These dysoxic events in Japan have been linked to increased primary productivity and decreased in intermediate water ventilation in the northwestern Pacific (Shibahara et al., 2007). In Okhotsk Sea, OMZ intensifications were also seen during B-A and early Holocene based on benthic foraminiferal abundances (Bubenshchikova et al., 2015).

In the northwestern Pacific, studies in NE Japan also reveal better-oxygenated (suboxic) conditions from the middle to late Holocene indicating a weaking of the OMZ, in contrast to the dysoxic conditions that developed during the B-A and preboreal (~11.3 - 10 ka; Shibahara et al., 2007). The NE Japan sites are from a similar water depth as ODP 1017, which also records suboxic conditions during the Holocene. The change to suboxia in NE Japan, in contrast to the maintenance of dysoxia into the Holocene as seen in the SBB, was attributed to a shallower OMZ in SBB, which is driven by high productivity caused by coastal upwelling that is not present in NE Japan (Shibahara et al., 2007). Hence, at sites with coastal upwelling, increased productivity may have caused a shallower and more intense OMZ in the eastern Pacific than in NE Japan and the difference in the depth of the OMZ resulted in different Holocene oxygenation histories (Shibahara et al., 2007). The sedimentary oxygenation changes in the subarctic Pacific during the Holocene and LGM was widely controlled by both the NPIW and export production of organic matter (Zou et al., 2020).

3.4.3. Spatial and temporal patterns in better-oxygenation conditions

Better-oxygenated conditions reaching the maximum BDO value of 1.5 ml/L occurred during MIS 3, the YD, and HS1 in GoA (U1419) and SBB (MD02-2503, MD02-2504, and ODP 893) with longer intervals of better oxygenated conditions at U1419 than in SBB. This is consistent to previous studies that also record better-oxygenated conditions related to colder intervals in the YD, LGM and the stadials (Cannariato et al., 1999; Davies et al., 2011; Ohkushi et al., 2013; Praetorius et al., 2015; Du et al., 2018; Belanger et al., 2020; Sharon et al., 2021). Previous studies in SBB attributed the higher oxygenated

intervals to a weaker OMZ that was positioned below the SBB site depths (Ohkushi et al., 2013).

In the continental slope records other than U1419, that we reanalyze, we do not reconstruct better-oxygenated conditions during MIS 3, Heinrich stadials and the YD as the original authors did, with the exception of U1419. Well-oxygenated conditions at MD02-2508 were inferred during the Heinrich stadials and YD by previous authors (Tetard et al., 2017), although when placed on the same oxygenation scale as the other sites, this site in the ETNP was consistently dysoxic. Similarly, others inferred that the OMZ contracted above the ODP 1017 water depth during the stadials (Cannariato and Kennett, 1999), however, in our analyses, ODP 1017 was suboxic throughout the MIS 3 and HS1 and samples from the YD were dysoxic. At ODP Hole 890B dysoxia also persisted through the YD and BDO values straddle at the dysoxic-suboxic boundary during the HS1 in our analyses. These are each sites of coastal upwelling, which may be driving low-oxygen conditions throughout the records whereas sites that are not strongly upwelling are able to increase in oxygenation, similar to the contrast we see in the Holocene portions of the records described above.

In the northwestern Pacific, faunal records from NE Japan are dominated by suboxic taxa during the last glacial and YD intervals indicating better oxygen conditions in contrast to high abundances of dysoxic taxa during warmer B-A (Shibahara et al., 2007). In the Okinawa Trough, enhanced sedimentary oxygen was also observed during LGM, HS1 and 2 while lower oxygen was seen during B-A and preboreal (Zou et al., 2020).

While warmer conditions in the NP during the B-A are associated with decrease in the formation of NPIW in the Okhotsk Sea, the colder HS1 and YD are associated with increase in formation of NPIW at the higher latitudes (Ikehara et al., 2006; Ohkushi et al., 2013; Max et al., 2014). During the colder intervals, enhanced ventilation is supported by the elimination of the vertical oxygen gradient at intermediate depths (~500-1000 m) at sites ODP 1017, ODP 893, MD02-2503 and MD02-2504 as inferred from benthic foraminiferal faunas (Ohkushi et al., 2013; Cannariato and Kennett, 1999). The colder HS1 and YD intervals also correspond with the most extensive sea-ice cover across the NP corresponding to lower SST and low marine productivity (Meheust et al, 2018; Praetorius et al., 2020). Furthermore, the colder intervals like YD and HS1 have been linked to the weakening of the OMZ related to declines in productivity, and thus organic carbon export (Jaccard et al.; 2005). Others hypothesize that colder intervals, such as the LGM, had a weakened California Undercurrent which resulted in less northward flow of low-oxygen waters (Hendy and Kennett 2003; Hendy and Pederson, 2006). This is consistent with our results that show no change in oxygenation in the ETNP, less-well oxygenated conditions on the California and Cascadia Margins, and the greatest oxygenation in GoA where the CU has the least impact.

3.4.4. Toward an improved understanding of North Pacific oxygenation and its drivers

The mechanism underlying dysoxic events in the North Pacific have been debated and understanding the patterns in relative oxygenation at disparate sites can illuminate the most likely drivers. Common to all sites, lower oxygen conditions, even when the decrease

in oxygenation is slight, occur during warmer times. Thus, North Pacific dysoxia is commonly interpreted as a result of other environmental changes in the region including freshwater-induced stratification, reduced sea-ice cover, enhanced productivity due to meltwater pulses or upwelling conditions, reduced ventilation or production of intermediate waters, and transport of low-oxygen waters from depth or tropical OMZs (Cannariato and Kennett, 1999; Mckay et al., 2005; Bubenshchikova et al., 2008; Davies et al., 2011; Jaccard et al., 2013; Max et al., 2014; Praetorius et al., 2015; Tetard et al., 2017; Meheust et al., 2016; Praetorius et al., 2020). In GoA, previous authors have also proposed that increase in productivity was rather driven by preceding dysoxia than vice versa (Praetorius et al., 2015; Gray et al., 2018).

Of the sites we were able to place on the same oxygenation scale, the most stable dysoxic conditions occur in the ETNP at MD02-2508 and the most persistently well-oxygenated conditions occur in GoA. We are hesitant to interpret too strictly the low variation on ODP Hole 890B and ODP 1017 given the taxonomic and methodological inconsistency, although constant suboxic conditions at ODP 1017 are consistent with its position in the lower OMZ. This suggests that conditions driving dysoxia are less frequent and shorter in duration at U1419 whereas they are common and persistent at lower latitudes.

High latitude OMZ expansion during the deglacial has also been linked to changes in ventilation or production of intermediate waters and changes in deep water circulation which also led to an increase in the atmospheric CO_2 rise (Cannariato and Kennett, 1999; Zheng et al., 2000; Cartapanis et al., 2011; Jaccard and Galbraith, 2012; Moffitt et al.,

2015; Du et al., 2018). This mechanism would result in concurrent changes in oxygenation, as we observe, but should not result in events of such disparate duration and cannot explain the persistent dysoxia at MD02-2508, MD02-2503 and MD02-2504 during the middle to late Holocene that is not reflected at U1419.

Given the link between low-oxygen conditions and D/O events, other authors have proposed regional stratification caused by factors like meltwater pulses and the impacts on sea-ice formation and ocean circulation as a driver of dysoxia (Davies et al., 2011; Praetorius et al., 2020). Very high stratification in the NP and tropical Pacific are known for their depleted oxygen (Li et al., 2020). Eighty percent of the observed oxygen decline in the world's oceans oxygen is related to enhanced stratification which as a result causes a decrease in deep-water ventilation and decrease in nutrient supply and further leads to biological depletion (Li et al., 2020).

Regional factors, like local oceanography and basin geometry, likely contributed to the oxygenation history of some of the sites. For example, SBB has the lowest oxygen conditions in our analyses due to its restricted setting, which limits ventilation to the basin (Bograd et al., 2002; Ohkushi et al., 2013). The site in Baja California Sur is located where low-oxygen water currents from the north (NPIW) and the south (ESsW) converge which may lead to complex ventilation patterns causing perpetual dysoxia at this site (Tetard et al., 2017). In addition, it being the southernmost located in the ETNP does make it more likely to be dysoxic. In contrast, since SBB apparently does not get flushed every year (Bograd et al., 2002), the wide range of oxygenation seen at the SBB sites may solely be due to the variation in periods and intensity of basin flushing with periods of dysoxia

corresponding to extended periods of no basin flushing alternating with intense flushing leading to better oxygenated condition.

The relative strength of CU moving northward and the NPIW moving southward, and the relative oxygenation of NPIW and ESsW masses, could explain the pattern of persistent dysoxia in our southernmost site (MD08-2508) which is closest to the ESsW and the generally better oxygenated conditions at our northernmost (U1419), which is closest to the site of NPIW formation. As the NPIW moves from the higher latitudes, it provides oxygenated waters to GoA and diminishes in its impact southward. On the other hand, the northward flowing CU transports low-oxygen water from the ETNP north; the proximity of MD02-2508 to the ETNP OMZ may explain this location being dysoxic for the entire record. The CU is known to travel to the Vancouver coast, but can extend to Alaska as well (Thomson and Krassovski, 2010). The percentage of Pacific Equatorial Waters off the Alaskan region is very low as compared to the upwelling regions towards the south, however the local productivity may be influenced by these water masses along the Alaskan continental margin in the absence of strong downwelling-favorable winds in the summers (Thomson and Krassovski, 2010). Changes in the relative balance of these two currents may explain the longer duration, well-oxygenated conditions, in GoA as compared to the persistent dysoxia of the ETNP OMZ. During the colder intervals when the NPIW ventilation and formation increased, a decline in the northward movement of CU from the ETNP has also been hypothesized as a driver of better oxygenation conditions (Kienast et al., 2002; Hendy and Kennett, 2003). During warmer intervals when NPIW formation decreased, there may have been a counteracting increase in the flow of this

dysoxic waters from the ETNP OMZ via CU that was able to reach GoA for short intervals during MIS3 and for a ~5 ka interval during the deglacial and early Holocene.

Both regional and global factors may influence the regional oxygenation conditions and no one driver need explain oxygenation at all sites. The variation in oxygenation levels and oxygenations histories we see across the study sites suggests different influences. Since, the deeper SBB core site MD02-2503 and MD02-2508 in Baja California Sur showed the most severe dysoxia amongst all the sites, we may deduce that the regional factors certainly enhance the effects of dysoxia caused by global or basinwide changes. Whereas the balance of southward flowing and northward flowing currents in the Holocene may give the expectation of well-oxygenated conditions at U1419 during the middle to late Holocene, the increase in pulsed productivity in Holocene may have driven the area suboxic (Belanger et al. 2020). This is in contrast to MIS 3 during which opportunist foraminifers were much less common (Sharon et al. 2021), suggesting that pulsed productivity was less persistent in the older parts of this record than in the Holocene.

3.5. Conclusions

To deconvolve the drivers of dysoxic events in the North Pacific, we must be able to quantitatively compare the relative severity and duration of the events across the region. Multivariate analyses of entire benthic foraminiferal faunas across sites allowed us to put those sites on a common oxygenation scale and thus directly compare their oxygenation histories in a way not possible with geochemical, sedimentological, or index taxon approaches. We found that it is important for these comparisons to be among sites at a

similar water depth such that species-level differences due to bathymetric gradients have a limited influence; geographic distance imposed less faunal dissimilarity. Extending this method to the other sites requires taxonomically-standardized whole faunal analyses and we encourage the creation of these data sets that permit geographically broad assessments of oxygenation change on a common quantitative scale.

3.6. References

Addison, J. A., Finney, B. P., Dean, W. E., Davies, M. H., Mix, A. C., Stoner, J. S., & Jaeger, J. M. (2012). Productivity and sedimentary $\delta^{15}N$ variability for the last 17,000 years along the northern Gulf of Alaska continental slope. *Paleoceanography*, *27*(1), PA1206. https://doi.org/10.1029/2011PA002161

Alve, E. (1994). Opportunistic features of the foraminifer Stainforthia fusiformis (Williamson): evidence from Frierfjord, Norway. *Journal of Micropalaeontology*, *13*(1), 24. https://doi.org/10.1144/jm.13.1.24

Ayoub-Hannaa, W., Huntley, J. W., & Fürsich, F. T. (2013). Significance of Detrended correspondence analysis (DCA) in palaeoecology and biostratigraphy: A case study from the Upper Cretaceous of Egypt. *Journal of African Earth Sciences*, 80, 48–59. https://doi.org/10.1016/j.jafrearsci.2012.11.012

Balestra, B., Krupinski, N. B. Q., Erohina, T., Fessenden-Rahn, J., Rahn, T., & Paytan, A. (2018). Bottom-water oxygenation and environmental change in Santa Monica Basin, Southern California during the last 23 kyr. Palaeogeography, Palaeoclimatology, Palaeoecology, 490, 17-37.

Barron, J. A., Bukry, D., Dean, W. E., Addison, J. A., & Finney, B. (2009). Paleoceanography of the Gulf of Alaska during the past 15,000 years: results from diatoms, silicoflagellates, and geochemistry. *Marine Micropaleontology*, *72*(3–4), 176–195.

Behl, R., & Kennett, J. (1996). Brief interstadial events in the Santa Barbara Basin, NE Pacific, during the past 60 kyr. *Nature*, *379*, 243–246. https://doi.org/10.1038/379243a0

Belanger, C. L., & Villarosa Garcia, M. (2014). Differential drivers of benthic foraminiferal and molluscan community composition from a multivariate record of early Miocene environmental change. *Paleobiology*, *40*(3), 398–416. https://doi.org/10.1666/13019

Belanger, C. L., Du, J., Payne, C. R., & Mix, A. C. (2020). North Pacific deep-sea ecosystem responses reflect post-glacial switch to pulsed export productivity, deoxygenation, and destratification. *Deep Sea Research Part I: Oceanographic Research Papers*, 103341. doi.org/10.1016/j.dsr.2020.103341

Belanger, C. L., Orhun, O. G., & Schiller, C. M. (2016). Benthic foraminiferal faunas reveal transport dynamics and no-analog environments on a glaciated margin (Gulf of Alaska). *Palaeogeography, Palaeoclimatology, Palaeoecology*, *454*, 54–64. https://doi.org/10.1016/j.palaeo.2016.04.032

Berger, W. H., Lange, C. B., & Weinheimer, A. (1997). Silica depletion of the thermocline in the eastern North Pacific during glacial conditions: Clues from Ocean

Drilling Program Site 893, Santa Barbara basin, California. *Geology*, *25*(7), 619. https://doi.org/10.1130/0091-7613(1997)025<0619:SDOTTI>2.3.CO2

Bernhard, J. M., Sen Gupta, B. K., & Borne, P. F. (1997). Benthic foraminiferal proxy to estimate dysoxic bottom-water oxygen concentrations; Santa Barbara Basin, U.S. Pacific continental margin. *Journal of Foraminiferal Research*, *27*(4), 301–310. Retrieved from http://dx.doi.org/10.2113/gsjfr.27.4.301

Bograd, S. J., Castro, C. G., Di Lorenzo, E., Palacios, D. M., Bailey, H., Gilly, W., & Chavez, F. P. (2008). Oxygen declines and the shoaling of the hypoxic boundary in the California Current. *Geophysical Research Letters*, *35*, L12607. https://doi.org/10.1029/2008GL034185

Bograd, S. J., Schwing, F. B., Castro, C. G., & Timothy, D. A. (2002). Bottom water renewal in the Santa Barbara Basin. *Journal of Geophysical Research: Oceans*, *107*(C12), 9. https://doi.org/10.1029/2001JC001291

Bubenshchikova, N., Nürnberg, D., & Tiedemann, R. (2015). Variations of Okhotsk Sea oxygen minimum zone: Comparison of foraminiferal and sedimentological records for latest MIS 12–11c and latest MIS 2–1. *Marine Micropaleontology*, *121*, 52–69. https://doi.org/10.1016/j.marmicro.2015.09.004

Bush, A. M., & Brame, R. I. (2010). Multiple paleoecological controls on the composition of marine fossil assemblages from the Frasnian (Late Devonian) of Virginia, with a comparison of ordination methods. *Paleobiology*, *36*(4), 573–591.

Cannariato, K. G., Kennett, J. P., & Behl, R. J. (1999). Biotic response to late Quaternary rapid climate switches in Santa Barbara Basin: Ecological and evolutionary implications. *Geology*, *27*(1), 63–66.

Cannariato, K., & Kennett, J. (1999). Climatically related millennial-scale fluctuations in strength of California margin oxygen-minimum zone during the past 60 k.y. *Geology*, *27*, 975–978.

Cartapanis, O., Tachikawa, K., & Bard, E. (2011). Northeastern Pacific oxygen minimum zone variability over the past 70 kyr: Impact of biological production and oceanic ventilation. *Paleoceanography*, *26*(4), PA4208. https://doi.org/10.1029/2011PA002126

Cartapanis, O., Tachikawa, K., Romero, O., & Bard, E. (2014). Persistent millennial-scale link between Greenland climate and northern Pacific Oxygen Minimum Zone under interglacial conditions. *Climate of the Past*, *10*, 405–418. https://doi.org/10.5194/cp-10-405-2014

Crusius, J., Calvert, S., Pedersen, T., & Sage, D. (1996). Rhenium and molybdenum enrichments in sediments as indicators of oxic, suboxic and sulfidic conditions of deposition. *Earth and Planetary Science Letters*, *145*, 65–78. https://doi.org/10.1016/S0012-821X(96)00204-X

Davies, M. H., Mix, A. C., Stoner, J. S., Addison, J. A., Jaeger, J., Finney, B., & Wiest, J. (2011). The deglacial transition on the southeastern Alaska Margin: Meltwater input, sea level rise, marine productivity, and sedimentary anoxia. *Paleoceanography and Paleoclimatology*, *26*, PA2223. https://doi.org/10.1029/2010PA002051

Diaz, R. J., & Rosenberg, R. (2008). Spreading dead zones and consequences for marine ecosystems. *Science*, *321*(5891), 926–929. https://doi.org/10.1126/science.1156401

Du, J., Haley, B. A., Mix, A. C., Walczak, M. H., & Praetorius, S. K. (2018). Flushing of the deep Pacific Ocean and the deglacial rise of atmospheric CO_2 concentrations. *Nature Geoscience*, *11*(10), 749–755. https://doi.org/10.1038/s41561-018-0205-6

Emery, K. O., & Hülsemann, J. (1961). The relationships of sediments, life and water in a marine basin. *Deep Sea Research (1953)*, *8*(3), 165-IN2. https://doi.org/10.1016/0146-6313(61)90019-3

Emmer, E., & Thunell, R. C. (2000). Nitrogen isotope variations in Santa Barbara Basin sediments: Implications for denitrification in the eastern tropical North Pacific during the last 50,000 years. *Paleoceanography*, *15*(4), 377–387. https://doi.org/10.1029/1999PA000417

Erdem, Z., & Schönfeld, J. (2017). Pleistocene to Holocene benthic foraminiferal assemblages from the Peruvian continental margin. *Palaeontologia Electronica*, *20.2.35A*, 1–32. https://doi.org/10.26879/764

Fürsich, F. T., & Aberhan, M. (1990). Significance of time-averaging for palaeocommunity analysis. *Lethaia*, *23*(2), 143–152. https://doi.org/10.1111/j.1502-3931.1990.tb01355.x

Garcia, H. E., Boyer, T. P., Locarnini, R. A., Antonov, J. I., Mishonov, A. V, Baranova, O. K., et al. (2013). World ocean atlas 2013. Volume 3: Dissolved oxygen, apparent oxygen utilization, and oxygen saturation. In S. Levitus & A. Mishonov (Eds.), *NOAA Atlas NESDIS 75* (p. 27).

Gilly, W. F., Beman, J. M., Litvin, S. Y., & Robison, B. H. (2013). Oceanographic and biological effects of shoaling of the oxygen minimum zone. *Annual Review of Marine Science*, *5*, 393–420.

Glock, N., Schönfeld, J., Eisenhauer, A., Hensen, C., Mallon, J., & Sommer, S. (2013). The role of benthic foraminifera in the benthic nitrogen cycle of the Peruvian oxygen minimum zone. *Biogeosciences*, *10*(7), 4767–4783. https://doi.org/10.5194/bg-10-4767-2013

Gooday, A. J., & Jorissen, F. J. (2012). Benthic Foraminiferal Biogeography: Controls on Global Distribution Patterns in Deep-Water Settings. *Annual Review of Marine Science*, *4*(1), 237–262. https://doi.org/10.1146/annurev-marine-120709-142737

Gray, W. R., Rae, J. W. B., Wills, R. C. J., Shevenell, A. E., Taylor, B., Burke, A., et al. (2018). Deglacial upwelling, productivity and CO2 outgassing in the North Pacific Ocean. *Nature Geoscience*, *11*(5), 340–344. https://doi.org/10.1038/s41561-018-0108-6

Grunert, P., Skinner, L., Hodell, D. A., & Piller, W. E. (2015). A micropalaeontological perspective on export productivity, oxygenation and temperature in NE Atlantic deep-waters across Terminations I and II. *Global and Planetary Change*, *131*, 174–191. https://doi.org/10.1016/j.gloplacha.2015.06.002

Hayward, B. W., Grenfell, H. R., Carter, R., & Hayward, J. J. (2004). Benthic foraminiferal proxy evidence for the Neogene palaeoceanographic history of the Southwest Pacific, east of New Zealand. *Marine Geology*, *205*(1), 147–184. https://doi.org/10.1016/S0025-3227(04)00022-2

Helly, J. J., & Levin, L. A. (2004). Global distribution of naturally occurring marine hypoxia on continental margins. *Deep Sea Research Part I: Oceanographic Research Papers*, *51*(9), 1159–1168.

Hendy, I. L., & Kennett, J. P. (2003). Tropical forcing of North Pacific intermediate water distribution during Late Quaternary rapid climate change? *Quaternary Science Reviews*, *22*(5), 673–689. https://doi.org/10.1016/S0277-3791(02)00186-5

Hendy, I. L., & Pedersen, T. F. (2005). Is pore water oxygen content decoupled from productivity on the California Margin? Trace element results from Ocean Drilling Program Hole 1017E, San Lucia slope, California. *Paleoceanography*, *20*(4). https://doi.org/10.1029/2004PA001123

Hendy, I. L., & Pedersen, T. F. (2006). Oxygen minimum zone expansion in the eastern tropical North Pacific during deglaciation. *Geophysical Research Letters*, *33*(20). https://doi.org/10.1029/2006GL025975

Hendy, I. L., Kennett, J. P., Roark, E. B., & Ingram, B. L. (2002). Apparent synchroneity of submillennial scale climate events between Greenland and Santa Barbara Basin, California from 30–10ka. *Quaternary Science Reviews*, *21*(10), 1167–1184. https://doi.org/10.1016/S0277-3791(01)00138-X

Hill, T. M., Kennett, J. P., & Spero, H. J. (2003). Foraminifera as indicators of methane-rich environments: A study of modern methane seeps in Santa Barbara Channel, California. *Marine Micropaleontology*, *49*(1), 123–138. https://doi.org/10.1016/S0377-8398(03)00032-X

Hill, T. M., Kennett, J. P., Pak, D. K., Behl, R. J., Robert, C., & Beaufort, L. (2006). Pre-Bølling warming in Santa Barbara Basin, California: surface and intermediate water records of early deglacial warmth. *Quaternary Science Reviews*, *25*(21–22), 2835–2845. https://doi.org/10.1016/j.quascirev.2006.03.012

Ikehara, K., Ohkushi, K., Shibahara, A., & Hoshiba, M. (2006). Change of bottom water conditions at intermediate depths of the Oyashio region, NW Pacific over the past 20,000 yrs. *Global and Planetary Change*, *53*(1), 78–91. https://doi.org/10.1016/j.gloplacha.2006.01.011

Jaccard, S. L., Haug, G. H., Sigman, D. M., Pedersen, T. F., Thierstein, H. R., & Röhl, U. (2005). Glacial/Interglacial Changes in Subarctic North Pacific Stratification. *Science*, *308*(5724), 1003–1006. https://doi.org/10.1126/science.1108696

Jaccard, S. L., & Galbraith, E. D. (2012). Large climate-driven changes of oceanic oxygen concentrations during the last deglaciation. *Nature Geoscience*, *5*(2), 151–156. https://doi.org/10.1038/ngeo1352

Jaccard, S. L., & Galbraith, E. D. (2013). Direct ventilation of the North Pacific did not reach the deep ocean during the last deglaciation. *Geophysical Research Letters*, *40*(1), 199–203. https://doi.org/10.1029/2012GL054118

Jaeger, J. M., Gulick, S. P. S., LeVay, L. J., Asahi, H., Bahlburg, H., Belanger, C. L., et al. (2014). *Proceedings of the Integrated Ocean Drilling Program Vol. 341: Expedition reports Southern Alaska margin*. Integrated Ocean Drilling Program.

Kaiho, K. (1994). Benthic foraminiferal dissolved-oxygen index and dissolved-oxygen levels in the modern ocean. *Geology*, *22*, 719–722. https://doi.org/10.1130/0091-7613(1994)022<0719:BFDOIA>2.3.CO;2

Karlsen, A. W., Cronin, T. M., Ishman, S. E., Willard, D. A., Kerhin, R., Holmes, C. W., & Marot, M. (2000). Historical trends in Chesapeake Bay dissolved oxygen based on benthic foraminifera from sediment cores. *Estuaries*, *23*(4), 488–508. https://doi.org/10.2307/1353141

Keeling, R. F., Körtzinger, A., & Gruber, N. (2010). Ocean deoxygenation in a warming world. *Annual Review of Marine Science*, *2*(1), 199–229. https://doi.org/10.1146/annurev.marine.010908.163855

Keigwin, L. D. (1998). Glacial-age hydrography of the far northwest Pacific Ocean. *Paleoceanography*, *13*(4), 323–339. https://doi.org/10.1029/98PA00874

Kennett, J. P., & Ingram, B. (1995). Paleoclimatic Evolution of Santa Barbara Basin during the Last 20 k.y.: Marine Evidence from Hole 893A, *146*, 309–325. https://doi.org/10.2973/odp.proc.sr.146-2.296.1995

Kennett, J. P., & Ingram, B. L. (1995). A 20,000-year record of ocean circulation and climate change from the Santa Barbara basin. *Nature*, *377*(6549), 510–514. https://doi.org/10.1038/377510a0

Kienast, S. S., Calvert, S. E., & Pedersen, T. F. (2002). Nitrogen isotope and productivity variations along the northeast Pacific margin over the last 120 kyr: Surface and subsurface paleoceanography. *Paleoceanography*, *17*(4), 7–17. https://doi.org/10.1029/2001PA000650

Knudson, K. P., & Ravelo, A. C. (2015). North Pacific Intermediate Water circulation enhanced by the closure of the Bering Strait. *Paleoceanography*, *30*(10), 1287–1304. https://doi.org/10.1002/2015PA002840

Korsun, S., & Hald, M. (2000). Seasonal dynamics of benthic foraminifera in a glacially fed fjord of Svalbard, European Arctic. *Journal of Foraminiferal Research*, *30*(4), 251–271. https://doi.org/10.2113/0300251

Legendre, P., & Legendre, L. (2012). *Numerical Ecology*. Elsevier Science. Retrieved from https://books.google.com/books?id=6ZBOA-iDviQC

Li, G., Cheng, L., Zhu, J., Trenberth, K. E., Mann, M. E., & Abraham, J. P. (2020). Increasing ocean stratification over the past half-century. *Nature Climate Change*. https://doi.org/10.1038/s41558-020-00918-2

Li, G., Rashid, H., Zhong, L., Xu, X., Yan, W., & Chen, Z. (2018). Changes in Deep Water Oxygenation of the South China Sea Since the Last Glacial Period. *Geophysical Research Letters*, *45*(17), 9058–9066. https://doi.org/10.1029/2018GL078568

Max, L., Lembke-Jene, L., Riethdorf, J. R., Tiedemann, R., Nürnberg, D., Kühn, H., & MacKensen, A. (2014). Pulses of enhanced north Pacific intermediate water ventilation from the Okhotsk Sea and Bering Sea during the last deglaciation. *Climate of the Past*, *10*(2), 591–605. https://doi.org/10.5194/cp-10-591-2014

McCune, B., Grace, J. B. J. B., & Urban, D. L. (2002). Analysis of Ecological Communities. *MjM Software Design* (Vol. 28). Gleneden Beach, OR.

McKay, J. L., Pedersen, T. F., & Southon, J. (2005). Intensification of the oxygen minimum zone in the northeast Pacific off Vancouver Island during the last deglaciation: Ventilation and/or export production? *Paleoceanography*, *20*, PA4002. https://doi.org/10.1029/2003PA000979

McManus, J., Berelson, W., Severmann, S., Poulson, R., Hammond, D., Klinkhammer, G., & Holm, C. (2006). Molybdenum and uranium geochemistry in continental margin sediments: Paleoproxy potential. *Geochimica et Cosmochimica Acta*, *70*, 4643–4662. https://doi.org/10.1016/j.gca.2006.06.1564

Méheust, M., Stein, R., Fahl, K., & Gersonde, R. (2018). Sea-ice variability in the subarctic North Pacific and adjacent Bering Sea during the past 25 ka: new insights from IP25 and Uk237 proxy records. *Arktos*, *4*, 1–19.

Méheust, M., Stein, R., Fahl, K., Max, L., & Riethdorf, J. R. (2016). High-resolution IP25-based reconstruction of sea-ice variability in the western North Pacific and Bering Sea during the past 18,000 years. *Geo-Marine Letters*, *36*. https://doi.org/10.1007/s00367-015-0432-4

Mix, A. C., Lund, D. C., Pisias, N. G., Bodén, P., Bornmalm, L., Lyle, M., & Pike, J. (1999). Rapid climate oscillations in the northeast Pacific during the last deglaciation reflect Northern and Southern Hemisphere sources. *Geophysical Monograph-American Geophysical Union*, *112*, 127–148.

Moffitt, S. E., Hill, T. M., Ohkushi, K., Kennett, J. P., & Behl, R. J. (2014). Vertical oxygen minimum zone oscillations since 20 ka in Santa Barbara Basin: A benthic

foraminiferal community perspective. *Paleoceanography*, *29*(1), 44–57. https://doi.org/10.1002/2013PA002483

Moffitt, S. E., Moffitt, R. A., Sauthoff, W., Davis, C. V, Hewett, K., & Hill, T. M. (2015). Paleoceanographic insights on recent oxygen minimum zone expansion: Lessons for modern oceanography. *PLOS ONE*, *10*(1), e0115246. https://doi.org/10.1371/journal.pone.0115246

Murray, J. W. (2006). *Ecology and applications of benthic foraminifera*. Cambridge University Press.

Nigam, R., Mazumder, A., Henriques, P., & Saraswat, R. (2007). Benthic foraminifera as proxy for oxygen-depleted conditions off the central west coast of India. *Journal of the Geological Society of India*, *70*, 1047–1054.

Ohkushi, K. I., Itaki, T., Nemoto, N. (2003). Last Glacial–Holocene change in intermediate-water ventilation in the Northwestern Pacific. Quaternary Science Reviews, 22, 1477-1484.

Ohkushi, K., Hara, N., Ikehara, M., Uchida, M., & Ahagon, N. (2016). Intensification of North Pacific intermediate water ventilation during the Younger Dryas. *Geo-Marine Letters*, *36:* 353–360. https://doi.org/10.1007/s00367-016-0450-x

Ohkushi, K., Itaki, T., & Nemoto, N. (2003). Last Glacial–Holocene change in intermediate-water ventilation in the Northwestern Pacific. *Quaternary Science Reviews*, *22*(14), 1477–1484. https://doi.org/10.1016/S0277-3791(03)00082-9

Ohkushi, K., Kennett, J. P., Zeleski, C. M., Moffitt, S. E., Hill, T. M., Robert, C., et al. (2013). Quantified intermediate water oxygenation history of the NE Pacific: A new

benthic foraminiferal record from Santa Barbara basin. *Paleoceanography*, *28*(3), 453–467. https://doi.org/10.1002/palo.20043

Okazaki, Y., Timmermann, A., Menviel, L., Harada, N., Abe-Ouchi, A., Chikamoto, M. O., et al. (2010). Deepwater formation in the North Pacific during the Last Glacial Termination. *Science*, *329*(5988), 200–204. https://doi.org/10.1126/science.1190612

Oksanen, J., Blanchet, F. G., Friendly, M., Kindt, R., Legendre, P., McGlinn, D., et al. (2017). vegan: Community Ecology Package. cran.r-project.org/package=vegan

Ortiz, S., Alegret, L., Payros, A., Orue-Etxebarria, X., Apellaniz, E., & Molina, E. (2011). Distribution patterns of benthic foraminifera across the Ypresian–Lutetian Gorrondatxe section, Northern Spain: response to sedimentary disturbance. *Marine Micropaleontology*, *78*(1–2), 1–13.

Palmer, H. M., Hill, T. M., Roopnarine, P. D., Myhre, S. E., Reyes, K. R., & Donnenfield, J. T. (2020). Southern California margin benthic foraminiferal assemblages record recent centennial-scale changes in oxygen minimum zone. *Biogeosciences*, *17*(11), 2923–2937. https://doi.org/10.5194/bg-17-2923-2020

Paulmier, A., & Ruiz-Pino, D. (2009). Oxygen minimum zones (OMZs) in the modern ocean. *Progress in Oceanography*, *80*(3), 113–128. https://doi.org/10.1016/j.pocean.2008.08.001

Penkrot, M. L., Jaeger, J. M., Cowan, E. A., St-Onge, G., & Levay, L. (2018). Multivariate modeling of glacimarine lithostratigraphy combining scanning XRF, multisensory core properties, and CT imagery: IODP Site U1419. *Geosphere*,14(4), 1935–1960. https://doi.org/10.1130/GES01635.1

Pierce, S. D., Barth, J. A., Shearman, R. K., & Erofeev, A. Y. (2012). Declining oxygen in the Northeast Pacific. *Journal of Physical Oceanography*, *42*(3), 495–501.

Praetorius, S. K., & Mix, A. C. (2014). Synchronization of North Pacific and Greenland climates preceded abrupt deglacial warming. *Science*, *345*(6195), 444–448. https://doi.org/10.1126/science.1252000

Praetorius, S. K., Condron, A., Mix, A. C., Walczak, M. H., McKay, J. L., & Du, J. (2020). The role of Northeast Pacific meltwater events in deglacial climate change. *Science Advances*, *6*(9). https://doi.org/10.1126/sciadv.aay2915

Praetorius, S. K., Mix, A. C., Walczak, M. H., Wolhowe, M. D., Addison, J. A., & Prahl, F. G. (2015). North Pacific deglacial hypoxic events linked to abrupt ocean warming. *Nature*, *527*, 362–366. https://doi.org/10.1038/nature15753

Psheneva, O. Y., & Gorbarenko, S. (2017). The responses of benthic foraminifera to paleoceanographic changes during the last glacial maximum, deglaciation, and the Holocene in the northwestern Pacific. *Russian Journal of Marine Biology*, *43*, 65–75. https://doi.org/10.1134/S1063074017010102

R Core Team. (2016). R: A Language and Environment for Statistical Computing. Vienna, Austria. www.r-project.org/

Rella, S. F., Tada, R., Nagashima, K., Ikehara, M., Itaki, T., Ohkushi, K., et al. (2012). Abrupt changes of intermediate water properties on the northeastern slope of the Bering Sea during the last glacial and deglacial period. *Paleoceanography*, *27*(3). https://doi.org/10.1029/2011PA002205

Sakai, K., Ohkushi, K., & Shibahara, A. (2021). Biotic response of benthic foraminifera to OMZ variations in the northwestern Pacific since the last deglaciation. *Geo-Marine Letters*, *41*. https://doi.org/10.1007/s00367-020-00671-7

Saravanan, P., Gupta, A. K., Zheng, H., Rai, S. K., & Panigrahi, M. K. (2020). Changes in Deep-Sea Oxygenation in the Northeast Pacific Ocean During 32–10 ka. *Geophysical Research Letters*, *47*(11), e2019GL086613. https://doi.org/10.1029/2019GL086613

Scarponi, D., & Kowalewski, M. (2004). Stratigraphic paleoecology: Bathymetric signatures and sequence overprint of mollusk associations from upper Quaternary sequences of the Po Plain, Italy. *Geology*, *32*(11), 989–992.

Schlitzer, R. (2018). Ocean Data View, https://odv.awi.de.

Schmiedl, G., Mitschele, A., Beck, S., Emeis, K.-C., Hemleben, C., Schulz, H., et al. (2003). Benthic foraminiferal record of ecosystem variability in the eastern Mediterranean Sea during times of sapropel S5 and S6 deposition. *Palaeogeography, Palaeoclimatology, Palaeoecology*, *190*, 139–164. https://doi.org/10.1016/S0031-0182(02)00603-X

Sen Gupta, B. K., & Machain-Castillo, M. L. (1993). Benthic foraminifera in oxygen-poor habitats. *Marine Micropaleontology*, *20*(3), 183–201. https://doi.org/10.1016/0377-8398(93)90032-S

Sharon, Belanger, C., Du, J., & Mix, A. (2021). Reconstructing paleo-oxygenation for the last 54,000 years in the Gulf of Alaska using cross-validated benthic

foraminiferal and geochemical records. *Paleoceanography and Paleoclimatology*, 36, e2020PA003986. https://doi.org/10.1029/2020PA003986

Shibahara, A., Ohkushi, K., Kennett, J. P., & Ikehara, K. (2007). Late Quaternary changes in intermediate water oxygenation and oxygen minimum zone, northern Japan: A benthic foraminiferal perspective. *Paleoceanography*, *22*, PA3213. https://doi.org/10.1029/2005PA001234

Stabeno, P. J., Bond, N. A., Hermann, A. J., Kachel, N. B., Mordy, C. W., & Overland, J. E. (2004). Meteorology and oceanography of the Northern Gulf of Alaska. *Continental Shelf Research*, *24*(7–8), 859–897.

Sweetman, A. K., Thurber, A. R., Smith, C. R., Levin, L. A., Mora, C., Wei, C.-L., et al. (2017). Major impacts of climate change on deep-sea benthic ecosystems. *Elementa: Science of the Anthropocene*, *5*. https://doi.org/10.1525/elementa.203

Tanaka, S., & Takahashi, K. (2005). Late Quaternary paleoceanographic changes in the Bering Sea and the western subarctic Pacific based on radiolarian assemblage. *Deep Sea Research Part II: Topical Studies in Oceanography*, *52*, 2131–2149. https://doi.org/10.1016/j.dsr2.2005.07.002

Taylor, M. A., Hendy, I. L., & Chappaz, A. (2017). Assessing oxygen depletion in the Northeastern Pacific Ocean during the last deglaciation using I/Ca ratios from multiple benthic foraminiferal species. *Paleoceanography*, *32*(8), 746–762. https://doi.org/10.1002/2016PA003062

Tetard, M., Licari, L., & Beaufort, L. (2017). Oxygen history off Baja California over the last 80 kyr: A new foraminiferal-based record. *Paleoceanography*, *32*. https://doi.org/10.1002/2016PA003034

Thomas, A. C., Carr, M.-E., & Strub, P. T. (2001). Chlorophyll variability in eastern boundary currents. *Geophysical Research Letters*, *28*(18), 3421–3424. https://doi.org/10.1029/2001GL013368

Thomson, R. E., and Krassovski, M. V. (2010), Poleward reach of the California Undercurrent extension, *J. Geophys. Res.*, 115, C09027, doi:10.1029/2010JC006280.

Thunell, R. C., Tappa, E., & Anderson, D. M. (1995). Sediment fluxes and varve formation in Santa Barbara Basin, offshore California. Oceanographic Literature Review, 43(6), 563–564.

Tribovillard, N., Algeo, T. J., Lyons, T., & Riboulleau, A. (2006). Trace metals as paleoredox and paleoproductivity proxies: An update. *Chemical Geology*, *232*(1), 12–32. https://doi.org/10.1016/j.chemgeo.2006.02.012

Tyler, C. L., & Kowalewski, M. (2014). Utility of marine benthic associations as a multivariate proxy of paleobathymetry: A direct test from recent coastal ecosystems of North Carolina. *PLOS ONE*, *9*(4), 1–15. https://doi.org/10.1371/journal.pone.0095711

van Geen, A., Zheng, Y., Bernhard, J.M., Cannariato, K.G., Carriquiry, J., Dean, W.E., Eakins, B.W., Ortiz, J.D. and Pike, J. (2003). On the preservation of laminated sediments along the western margin of North America. *Paleoceanography*, *18*, 1098. https://doi:10.1029/2003PA000911.

Yasuda, I. (1997). The origin of the North Pacific Intermediate Water. *Journal of Geophysical Research: Oceans*, *102*(C1), 893–909. https://doi.org/10.1029/96JC02938

Zheng, Y., Anderson, R. F., van Geen, A., & Kuwabara, J. (2000). Authigenic molybdenum formation in marine sediments: a link to pore water sulfide in the Santa Barbara Basin. *Geochimica et Cosmochimica Acta*, *64*(24), 4165–4178. https://doi.org/10.1016/S0016-7037(00)00495-6/10.1016/S0016-7037(00)00495-6

Zindorf, M., Rush, D., Jaeger, J., Mix, A., Penkrot, M. L., Schnetger, B., et al. (2020). Reconstructing oxygen deficiency in the glacial Gulf of Alaska: Combining biomarkers and trace metals as paleo-redox proxies. *Chemical Geology*, 119864. https://doi.org/https://doi.org/10.1016/j.chemgeo.2020.119864

Zou, J., Shi, X., Zhu, A., Kandasamy, S., Gong, X., Lembke-Jene, L., et al. (2020). Millennial-scale variations in sedimentary oxygenation in the western subtropical North Pacific and its links to North Atlantic climate. *Climate of the Past*, *16*(1), 387–407. https://doi.org/10.5194/cp-16-387-2020

3.7. Supplemental Figures and Tables

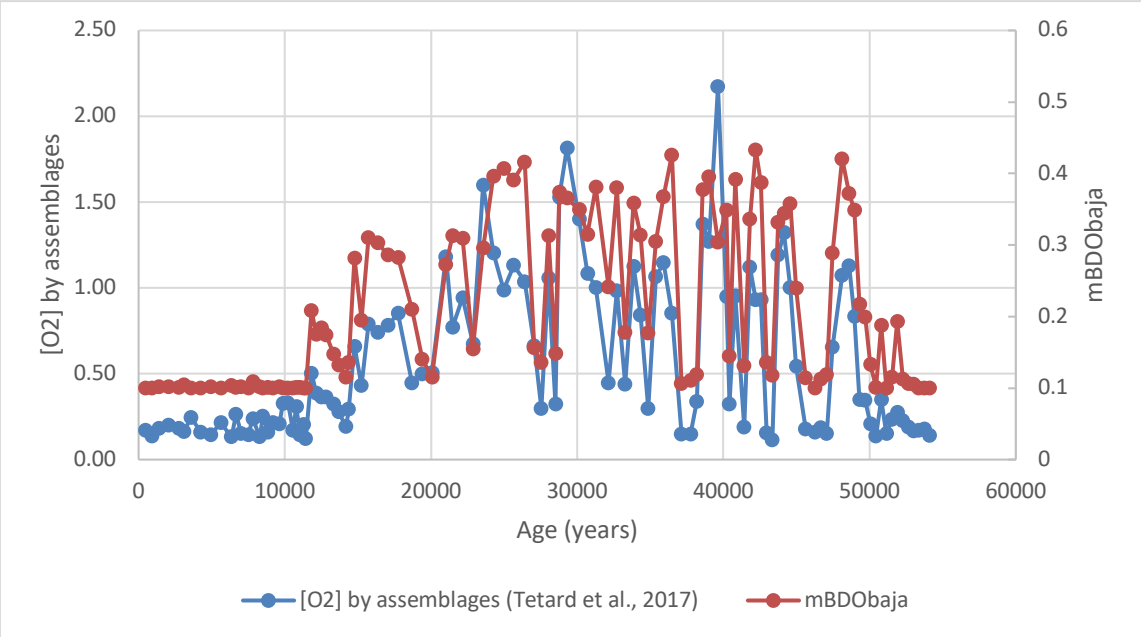

Figure 3.6 Modified Behl Dissolved Oxygen for MD02-2508 in Baja California Sur and oxygen estimations from Tetard et al., 2017 against age in a thousand years.

4. DRIVERS OF DYSOXIA IN THE GULF OF ALASKA

4.1. Introduction

Several drivers of dysoxia in the North Pacific (NP) have been proposed, which include surface productivity, increased water column stratification, melt-water pulses, increase in sea-surface temperature (SST), decreased ventilation, ocean circulation, global events related to D/O (Daansgard-Oeschger) cycles (Davies et al., 2011; Jaccard and Galbraith, 2012; Ohkushi et al., 2013; Praetorius et al., 2015; Moffitt et al., 2015; Praetorius et al., 2020). In the previous chapter, we worked on understanding which drivers in particular caused dysoxia at different sites in the NP based on different studies. We concluded that no single factor was responsible for the development of dysoxia and that there can be several influences at different sites. I inferred that not only can regional factors lead to dysoxia at geographically disparate sites, but that global events may have equally contributed to impact the regional drivers to cause basinwide dysoxic events around similar intervals like Bølling-Allerød (B-A) and early Holocene dysoxic events. It was also seen that dysoxic events in MIS 3 occurred during similar intervals in the Gulf of Alaska (GoA) and Santa Barbara Basin (SBB), suggesting common basin-wide or global drivers.

In GoA, some of the dysoxic events in the glacial were as severe as the deglacial dysoxic events (Sharon et al., 2021). In this chapter, I will test the hypotheses that dysoxic events during the deglacial and the glacial were caused by similar drivers. Alternatively, the causes of dysoxia maybe be dominated by different processes during glacial and the

deglacial periods. Previous studies in GoA focused on the deglacial and Holocene intervals have proposed various drivers of dysoxia, but no particular causes of dysoxia were concluded (Davies et al., 2011; Praetorius et al., 2015). In this study, I use multivariate statistical methods to test the relationships between proxies for oxygenation (Mo/Al, U/Al, Behl Dissolved Oxygen (BDO), the relative abundance of dysoxia-tolerant benthic foraminifera) and other environmental proxies ($\delta^{13}C$, $\delta^{18}O$, SST derived from alkenones, and the relative abundances of opportunistic benthic foraminifera) at Site U1419 in GoA to determine if the relationships among proxies, and thus the drivers of dysoxia, varied between climate states. Dysoxic events of similar severities occurred in the glacial and deglacial (Sharon et al., 2021), which may suggest a similar driver, however due to large global climatic differences we cannot assume that the driver of dysoxia was the same during these time intervals.

4.2. Methods

4.2.1. Study Site

Study sites U1419 and jumbo piston core EW0408-85JC in the Gulf of Alaska (GoA) are located on Khitrov Bank at 697 m and 682 water depth on the continental slope, respectively (Figure 4.1; Jaeger et al., 2014). Site U1419 lies within North Pacific Intermediate Water (NPIW) and is influenced by Alaska Coastal current. The Oxygen Minimum Zone (OMZ) in the region lies at ~670-1060 m in the present (Paulmier and Ruiz-Pino, 2009; Jaeger et al., 2014). The central GoA is a high nutrient low chlorophyll zone (HNLC) and productivity here is limited due to availability of nutrients like iron which is generally supplied by the fluvial systems (Stabeno et al., 2004). Primary

productivity blooms in early spring and summer due to abundant sunlight and nutrients from subsurface mixed layers brought up by upwelling in a dominantly downwelling system (Stabeno et al., 2004; Childers et al., 2005). Site U1419 chronology was based on Bayesian age model using 250 ^{14}C from separately analyzed planktonic and benthic foraminifera which were calibrated using Marine13 calibration curve (Walczak et al., 2020). High sedimentation rates supported exceptional preservation of foraminiferal data (Gulick et al., 2015).

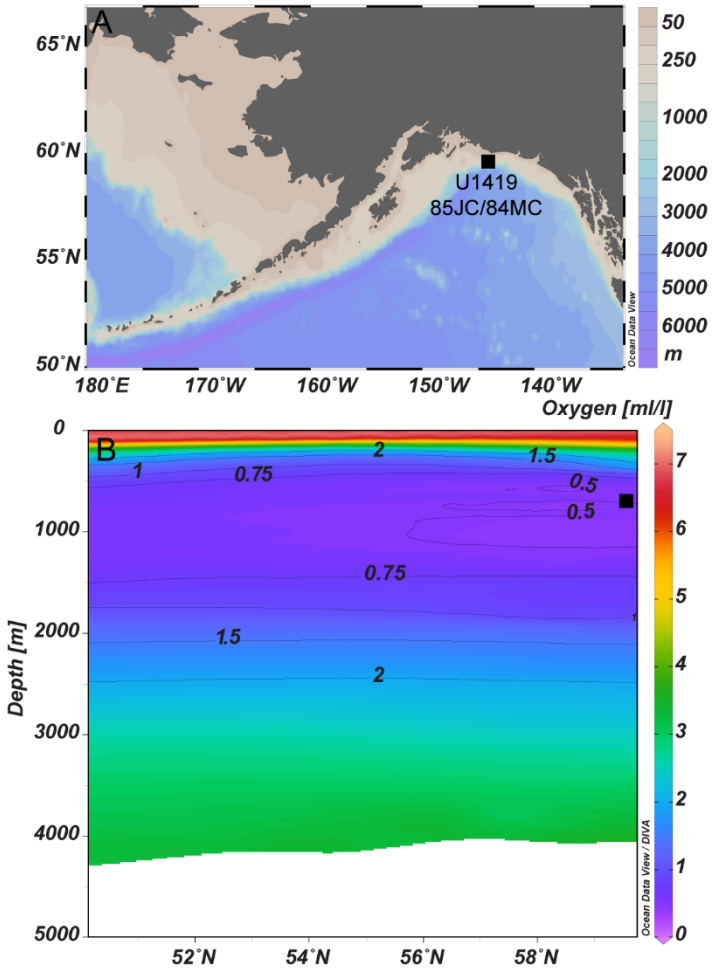

Figure 4.1 Study site locations. (A) Map showing the location of sites EW0408-85JC, EW0408-84MC and Site U1419 in the Gulf of Alaska. (B) Meridional cross section

(144^{O} W) of the oxygen concentration in the modern Eastern Pacific Ocean, showing location of site with respect to the oxygen minimum zone. Oxygenation data are from the World Ocean Atlas 2013 (Garcia et al., 2013) and both panels were constructed in Ocean Data View (Schlitzer, 2018).

4.2.2. Benthic foraminiferal and sedimentary data

Samples were disaggregated and wet-sieved at 63 μm, dried and then weighed. From these sieve fractions, we calculated the percentage of sediment >63 μm (hereafter "coarse fraction") as a function of the total sample weight. We used the weight percent of coarse fraction as a predictor variable to test if the faunal changes occurred as a response to changes in the sediment.

Benthic foraminiferal counts were collected for 355 samples in the >63 μm size fraction for a record that extends to 54,000 years (Sharon et al. 2021). The median number of foraminiferal individuals per sample was 268 (IQR = 159–404). In total, out of 74 taxa only 48 species and generic groups which comprised >2% in more than 1 sample were used in the analysis (Sharon et al. 2021). The samples were collected at 2-3 cm wide intervals (5-40 cc) and their median age resolution was 127 years (interquartile range [IQR]= 73-201 years) based on age model from Walczak et al. (2020). These benthic foraminiferal assemblages were previously used to reconstruct the oxygenation history for the past 54 kyrs in the GoA (Sharon et al., 2021).

To calculate the proportional abundance of species that can tolerate dysoxic conditions <0.1 ml/L O_2 (%dysoxic), we used six species including *Bolivina seminuda, Takayanagia delicata, Bolivina subadvena, Suggrunda eckisi, Bolivina pseudobeyrichi and Buliminella tenuata* that are known to be found in dysoxic settings in the literature

(Ohkushi et al., 2013; Tetard et al., 2017); this is a conservative number because we find that other species in this record covary with known dysoxia-tolerant species and, thus, are likely also tolerant of dysoxic conditions (Sharon et al., 2021). To calculate the relative abundance of opportunistic taxa (%opportunists) that respond pulsed fluxes of phytodetritus, we summed two phytodetritus-sensitive species (*Alabaminella weddellensis* and *Epistominella exigua*), which together have been used as a proxy for high organic carbon fluxes and productivity (Gooday 1993; Sun et al., 2006; Gooday and Jorissen, 2012; Belanger et al., 2020).

4.2.3. Paleoenvironmental Proxies

We analyze faunal responses with respect to three proxies for paleo-oxygenation: a faunal-based transfer function, Mo/Al, U/Al values and the Behl dissolved oxygen index (BDO). In Sharon et al. (2021), we quantitatively estimated oxygen by converting DCA Axis 1 site scores into BDO following Ohkushi et al., 2013 but instead of using only 19 species we used all the 48 species to calculate a modified BDO (mBDO). The dysoxic, suboxic and oxic groups required to calculate mBDO were categorized on the basis DCA Axis 1 species scores (see Sharon et al., 2021). Mo/Al and U/Al concentrations for this record were also previously published in Sharon et al. (2021). Accumulation of authigenic Mo and U occurs under dysoxic (<0.5 ml/L O_2) and suboxic (<1.4 ml/L O_2) conditions, respectively and have been used as a proxy for oxygen in our analyses (Crusius et al., 1996; Zheng et al., 2000; McManus et al., 2006; Tribovillard et al., 2006).

We also examine faunal responses with respect to paleoclimate proxies sensitive to glacial-interglacial conditions and sea surface temperature (SST). The $\delta^{13}C$ and $\delta^{18}O$

data were measured on planktonic foraminifera *Neogloboquadrina pachyderma* (sinistral) in the > 125 μm size fraction and the benthic foraminifera *Uvigerina peregrina* at Oregon State University College of Earth Ocean and Atmospheric Sciences Stable isotope Mass Spectrometer Facility using a Kiel-III carbonate preparation device connected to a Thermo-Finnigan MAT-252 mass spectrometer. The values are corrected to the PDB scale using both an in-house standard and the US National Institute of Standards and Technology RM8522 (NBS-19) standard. The $\delta^{13}C$ and $\delta^{18}O$ external precision on standards are 0.02 and 0.03 permil (+/- 1 standard deviation), respectively. Isotopic data from the youngest ~22 kyrs were previously published in Belanger et al., 2020; data from ~22 ka to ~54 ka are new to this study.

The SST values used herein are based upon alkenone data previously published by Praetorius et al. (2015). The original SST dataset, which extended from 17.6 to ~1.2 ka, was collected at a median age resolution of 112 years (IQR= 53-203 years). We estimate SST values for our samples using a linear interpolation and assuming constant sedimentation rates between samples. After interpolation, the median age resolution of SST data was 62 years (IQR= 22-115 years).

4.2.4. Multivariate analyses

For multivariate analyses, we divided our dataset into two subsets (~54-14.8 ka and ~14.7-0 ka) to determine if the primary drivers of faunal variation and factors associated with dysoxia differed during these time periods. The division at 14.7 ka corresponds with a sharp change in mBDO from of ~1 ml/L at 15 ka to 0.2 ml/L at 14.7 ka at the start of Bølling-Allerød (B-A) (Sharon et al., 2021). Thus, the younger subset

includes the B-A and early Holocene dysoxic events which have previously been associated with warmer periods and may be linked to high organic carbon export (Praetorius et al., 2015; Belanger et al., 2020; Payne and Belanger, 2021). Oxygenation in the younger subset was generally lower than in the older subset, suggesting the potential for different drivers of dysoxia (Sharon et al., 2021). In addition, the dysoxic events in the older subset were comparatively shorter in duration and have previously been linked to D/O cycles during MIS 2 and MIS 3, thus suggesting the potential for a different driver (Cannariato and Kennett, 1999; Sharon et al., 2021). Geochemical proxy data, including $\delta^{13}C$, $\delta^{18}O$, Mo/Al, and U/Al are available for both younger and older time intervals. However, SST data is only available for the 14.7-0 ka subset of the record.

4.2.4.1. Examining Faunal Gradients

In the previous chapters, we used Detrended Correspondence Analysis (DCA) on the >63 μm size fraction, in which DCA Axis 1 summarized the majority of the faunal variance (55%) and indicated that the dominant faunal gradient reflected an oxygenation gradient (Sharon et al., 2021). Here, we instead use Principal Coordinates Analysis (PCO), which is less controlled by the dominant faunal gradient than DCA, so that we can examine other faunal gradients that may reflect different environmental gradients, such as productivity or temperature. DCA uses the chi-square dissimilarity in faunal composition among samples (McCune et al., 2002) and other ecologically relevant dissimilarity metrics can reveal different gradients in faunal composition given the same data (Legendre & Legendre, 2012). For the PCO analyses herein, we use the Bray-Curtis dissimilarity, which is preferred as a distance measure in ecological studies (Legendre & Legendre, 2012;

Beals, 1984). To understand which environmental gradients controlled the faunal composition, we examined which species have similar PCO species scores and correspond to similar positive or negative PCO axes site scores. PCO is implemented in R programming language using the *"cmdscale"* function from the vegan package (Oksanen et al., 2017). The input for the *"cmdscale"* function is a distance matrix calculated using the function *"vegdist"* using the dissimilarity method "bray". The species scores are also calculated by the method of weighted averaging using the function *"wascores"*. We interpret environmental gradients using the known ecological preferences of the species with particular attention to species preferences for dysoxic, suboxic, oxic or high productivity environments as in Sharon et al. (2021).

4.2.4.2. Relationships among faunal gradients and environmental proxy timeseries

To understand how faunal and environmental proxy data covaried in our dataset, we used the Pearson's product moment correlation to calculate the correlation between the different proxies that representing oxygenation including Mo/Al, U/Al, mBDO, % dysoxic and the proxies indicating environmental variables like $\delta^{13}C$, $\delta^{18}O$ of *N. pachyderma* ($\delta^{13}C_{N.pachy}$, $\delta^{18}O_{N.pachy}$) and *U. peregrina* ($\delta^{13}C_{Uvi}$, $\delta^{18}O_{Uvi}$), % opportunistic taxa, percent weight of coarse sediment (% coarse), and SST. To account for changes that are related to glacial-interglacial conditions, partial correlations were calculated controlling for $\delta^{18}O_{Uvi}$. We base our primary interpretations on these partial correlations in the results, rather than the simple correlations, to focus our analysis on environmental changes not attributable simply to glacial-interglacial change. Associations between PCO axis scores and $\delta^{13}C$ isotope data from *N. pachyderma* and *U. peregrina* and % opportunistic taxa may reflect

relationships between surface productivity and organic export with faunal composition. Mo/Al and U/Al, which increase with decreasing oxygenation, will have positive relationships with $\delta^{13}C_{N.pachy}$ and % opportunistic species and negative relationships with $\delta^{13}C_{Uvi}$ if productivity and carbon export is playing a role in the development of dysoxia. Similarly, mBDO, which increases with increasing oxygenation will have a negative relationship with $\delta^{13}C_{N.pachy}$ and % opportunistic species and a positive relationship with $\delta^{13}C_{Uvi}$ if productivity and organic carbon export drive dysoxia. The $\delta^{18}O_{N.pachy}$ data can help trace the relationship between meltwater pulses and/or temperature to dysoxic conditions (Davies et al., 2011; Praetorius et al., 2015). Furthermore, we use SST data for 14.7-0 ka part of the record if temperature covaries with the development of dysoxic to suboxic conditions.

To avoid type 1 error resulting from multiple correlations, we apply a Bonferroni correction on the significance level (α=0.05) before interpretation. We calculated Pearson correlations in R using the "*cor*" function from the package *"stats"* (R Core Team, 2020). The correlation coefficients are displayed as a correlogram using the *"corrplot"* function from the package *"corrplot"* (Wei & Simko, 2017). Partial correlations are implemented using the *"ppcor.test"* function from the *"ppcor"* package in R (Kim, 2015).

4.2.4.3. Finding the best supported models for the drivers of faunal change

We also used multiple regression analysis to determine which environmental proxy variables ($\delta^{13}C$, $\delta^{18}O$, Mo/Al, U/Al, SST, %coarse, %opportunistic species) are the best predictors of faunal gradients (PCO axis scores). In addition, we test which environmental proxy variables ($\delta^{13}C$, $\delta^{18}O$, %opportunistic, %coarse, SST) are the best predictors of

proxies for low-oxygen conditions (Mo/Al, U/Al, mBDO). We also used %opportunists as a response and used Mo, U, SST, %coarse and all four isotopes as predictors to understand which environmental variables predict the relative abundance of opportunist taxa. All the predictor variables are z-score transformation to place the data on a common scale.

We use Akaike Information Criteria (AIC) backward selection method to find the best supported linear model that shows which predictor variables significantly control our response variables (Anderson et al., 2000). All predictors are z-score transformed to place them on a common scale before performing the AIC backward selection. AIC backward selection method is implemented in R using the *"stepAIC"* function from the package *"MASS"* (Venables and Ripley, 2002). We also perform a test of collinearity of the predictors using the variance inflation factor (VIF) (Bowerman and O'Connell. 1990). Predictors with VIF equal or greater than 5 are trimmed to ensure that collinearity is not influencing our models. VIF for linear models are calculated in R using the *"vif"* function from the *"car"* package (Fox and Weisberg, 2019).

4.3. Results

4.3.1. Gradients in faunal composition

4.3.1.1. Full record (~54 ka to present)

For the whole dataset, the proportion of variance summarized by PCO Axis 1 was 26% and PCO Axis 2 was 20%. Lower proportion of variances were summarized across PCO Axis 3 and 4 which was ~16% and 6%, respectively (Table 4.1).

Species with strongly negative PCO Axis 1 scores include *B. seminuda, T. delicata, B. subadvena, S. eckisi, B. pseudobeyrichi and B. tenuata* that are found in dysoxic settings (Figure 4.2; Supplemental Table 4.2; Supplemental Table 4.4; Ohkushi et al., 2013; Tetard et al., 2017). Opportunistic and phytodetritus sensitive species like *Trifarina angulosa, E. exigua, A. weddellensis, Buliminella elegantissima* also have negative scores (Murray, 2006; Sun et al., 2006; Gooday, 1993; Gooday & Jorissen, 2012). In addition, suboxic species like *Bolivina argentea* and *Bolivina spissa* also have negative PCO Axis 1 species scores (Supplemental Table 4.2; Supplemental Table 4.4; Tetard et al., 2017). Species like *Cassidulina reniforme, Elphidium clavatum, Epistominella pacifica, Islandiella norcrossi, Quinqueloculina* spp. have positive scores. Strongest negative PCO Axis 1 were seen ~ 8 times from ~48 ka to ~28 ka. PCO Axis 1 scores are mostly negative from 14.7 ka to present but are mostly positive in the older portions of the record (Figure 4.2).

All six species with published tolerances for dysoxia have strong, positive, PCO Axis 2 scores. Species known to tolerate suboxia, such as *B. argentea* and *B. spissa* (Tetard et al., 2017), also have positive PCO Axis 2 species scores. Species like *C. reniforme, Quinqueloculina* spp., *E. clavatum* and *I. norcrossi*, *Nonionella labradorica, T. angulosa* and *A. weddellensis* have negative PCO 2 Axis scores. Similar to PCO Axis 2 species scores, all the dysoxic species have similar negative PCO Axis 3 species scores. In contrast, species like *T. angulosa, E. exigua, A. weddellensis* have strong positive PCO Axis 3 scores. PCO Axis 2 scores have no clear temporal trend for most of the record but from ~8.4 ka to present the scores remained negative. In addition, PCO Axis 3 scores do

not show temporal trends as clear as PCO Axis 1 for most of the record but has strong negative scores during at ~45.8 ka, ~36.8 ka, B-A and early Holocene (Figure 4.2). In addition, most positive PCO Axis 3 scores were seen during the Holocene.

Table 4.1 Percent variance summarized by PCO Axes for the full record (0 - 54 ka), older (~54 - 14.8 ka) and younger data subsets (14.7 - 0 ka).

Data Analyzed ↓	PCO Axis 1	PCO Axis 2	PCO Axis 3	PCO Axis 4
Full Record	26	20	16	6
Younger subset	52	16	7	5
Older subset	30	20	10	8

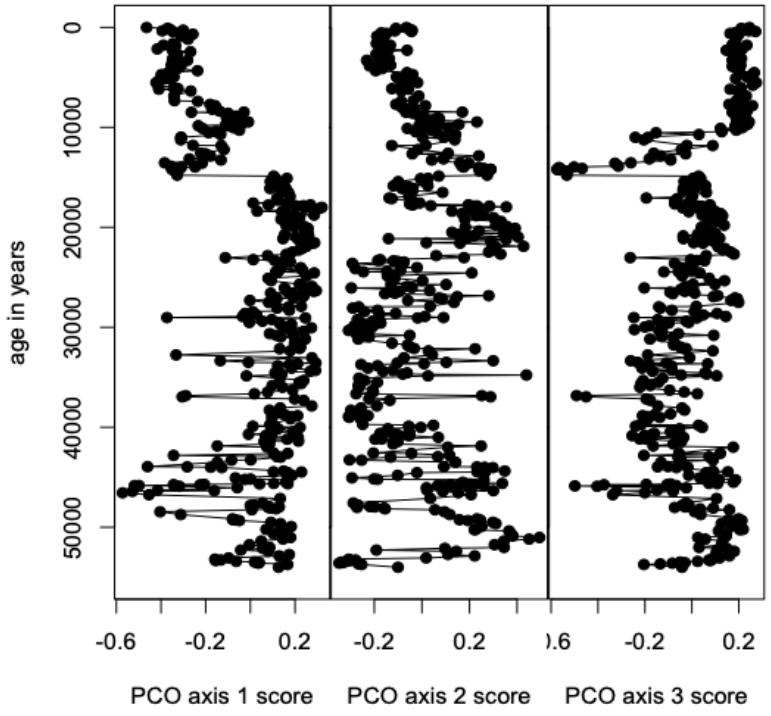
age in years
0
10000
20000
30000
40000
50000
-0.6
-0.2
0.2
-0.2
0.2
-0.2
0.2
PCO axis 1 score
PCO axis 2 score
PCO axis 3 score

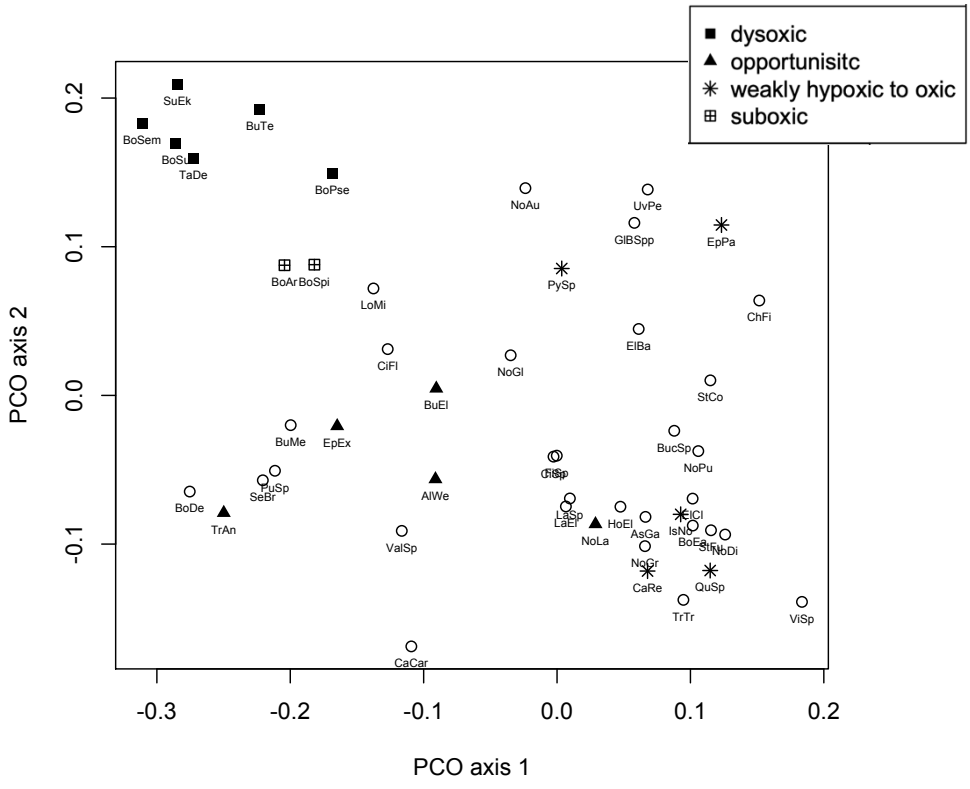
dysoxic
opportunisitc
weakly hypoxic to oxic
suboxic
PCO axis 2
PCO axis 1
0.2
0.1
0.0
-0.1
-0.3
-0.2
-0.1
0.0
0.1
0.2
SuEk
BuTe
BoSem
BoSu
TaDe
BoPse
NoAu
UvPe
GlBSpp
EpPa
BoAr
BoSpi
PySp
LoMi
ChFi
ElBa
CiFl
NoGl
StCo
BuEl
BuMe
EpEx
BucSp
NoPu
PuSp
SeBr
BoDe
AlWe
TrAn
LaSp
LaEl
HoEl
NoLa
AsGa
ValSp
NoCr
CaRe
QuSp
TrTr
ViSp
CaCar

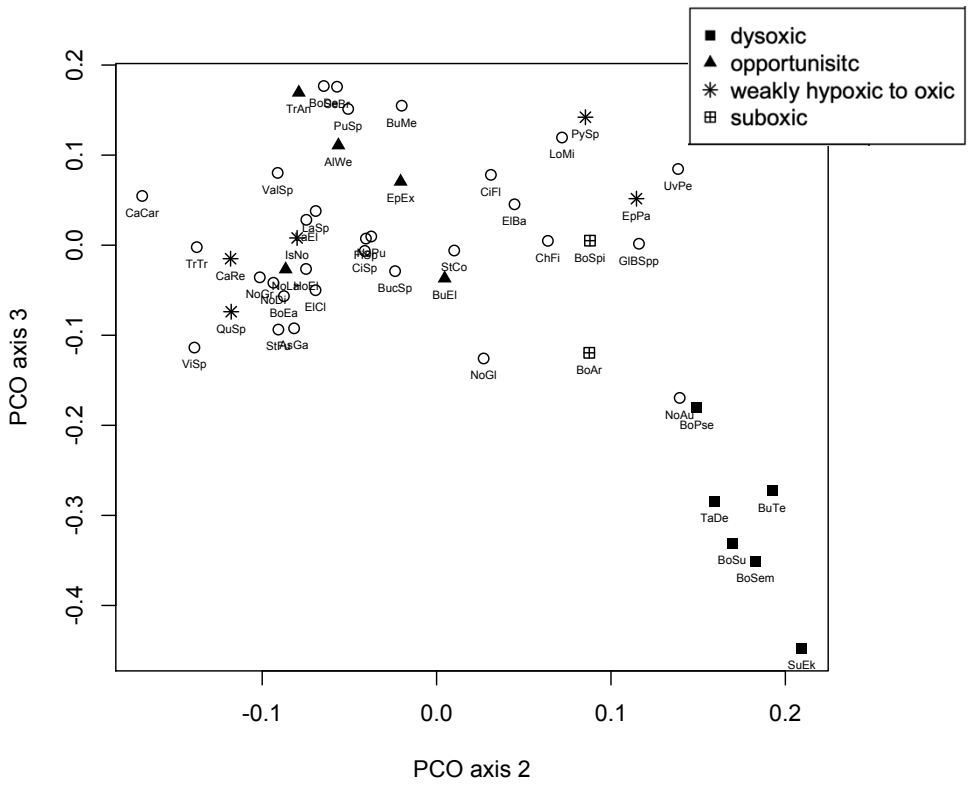

Figure 4.2 Top: PCO Axis 1, 2 and 3 samples scores against age for the analyses of the full record (0-54 ka). Middle: PCO Axis 1 and PCO Axis 2 species scores. Bottom: PCO Axis 2 and PCO Axis 3 species scores. Abbreviations as in Supplemental Table 4.2.

4.3.1.2. Before deglacial dysoxic event: ~54 - 14.8 ka (Older Subset)

For the 54-14.8 ka subset, PCO axes 1 and 2 summarize 30% and 20% of the total faunal variation, respectively. PCO Axis 3 and 4 summarize lower proportions (10% and 8% respectively; Table 4.1). Species which are associated with dysoxic settings, including *B. seminuda*, *T. delicata, B. tenuata B. pseudobeyrichi,* and *B. subadvena* have positive PCO Axis 1 scores (Figure 4.3; Supplemental Table 4.2; Supplemental Table 4.4). In addition, *E. exigua* and *T. angulosa* have similar positive PCO Axis 1 scores (Figure 4.3).

Species typically associated with well-oxygenated to weakly hypoxic environments, like *E. pacifica*, *Quinqueloculina* spp. and *Pyrgo* spp., have extreme positive and extreme negative PCO Axis 1 scores but are rare in this data set (Ohkushi et al., 2003; Ohkushi et al., 2013). While *Quinqueloculina* spp. comprises >2% in 13% of the total samples and >5% in only 3% of the total samples, *Pyrgo* spp. comprises >2% in only one sample. Species like *C. reniforme, E. clavatum, I. norcrossi* are associated with glacial and oxic conditions have negative PCO Axis 1 scores (Korsun and Hald, 2000; Ohkushi et al., 2003; Murray, 2006; Sakai et al., 2021). PCO Axis 1 scores show no temporal trends from ~54-14.8 ka (Figure 4.3).

On PCO Axis 2, four dysoxic species including *B. seminuda*, *T. delicata, B. tenuata* and *B. pseudobeyrichi* have extreme negative scores while the other two dysoxic species, *B. subadvena* and *S. eckisi,* have positive scores (Figure 4.3; Supplemental Table 4.2; Supplemental Table 4.4). In addition, the species generally known as productivity indicators, such as *E. exigua, B. elegantissima, T. angulosa, Nonionella labradorica,* also have negative scores (Murray, 2006; Sun et al., 2006). *Quinqueloculina* spp., *Pyrgo* spp., *C. reniforme, E. clavatum, I. norcrossi* and *E. pacifica* all have positive scores. PCO Axis 2 sample scores mostly remain positive but have strong negative scores ~ 8 times in the record (Figure 4.3).

Species like *E. exigua*, *A. weddellensis, T. angulosa, I. norcrossi* and *N. labradorica* have negative PCO Axis 3 scores. *I. norcrossi* has also been linked to productivity (Usami et al., 2013). The suboxic species *B. argentea* and *B. spissa* also have similar negative PCO Axis 3 scores. In addition, the dysoxic species had less positive PCO

Axis 3 scores. Most positive PCO Axis 3 were recorded at ~40 ka and no major trends or other extreme changes in the scores occurred for most of record (Figure 4.3).

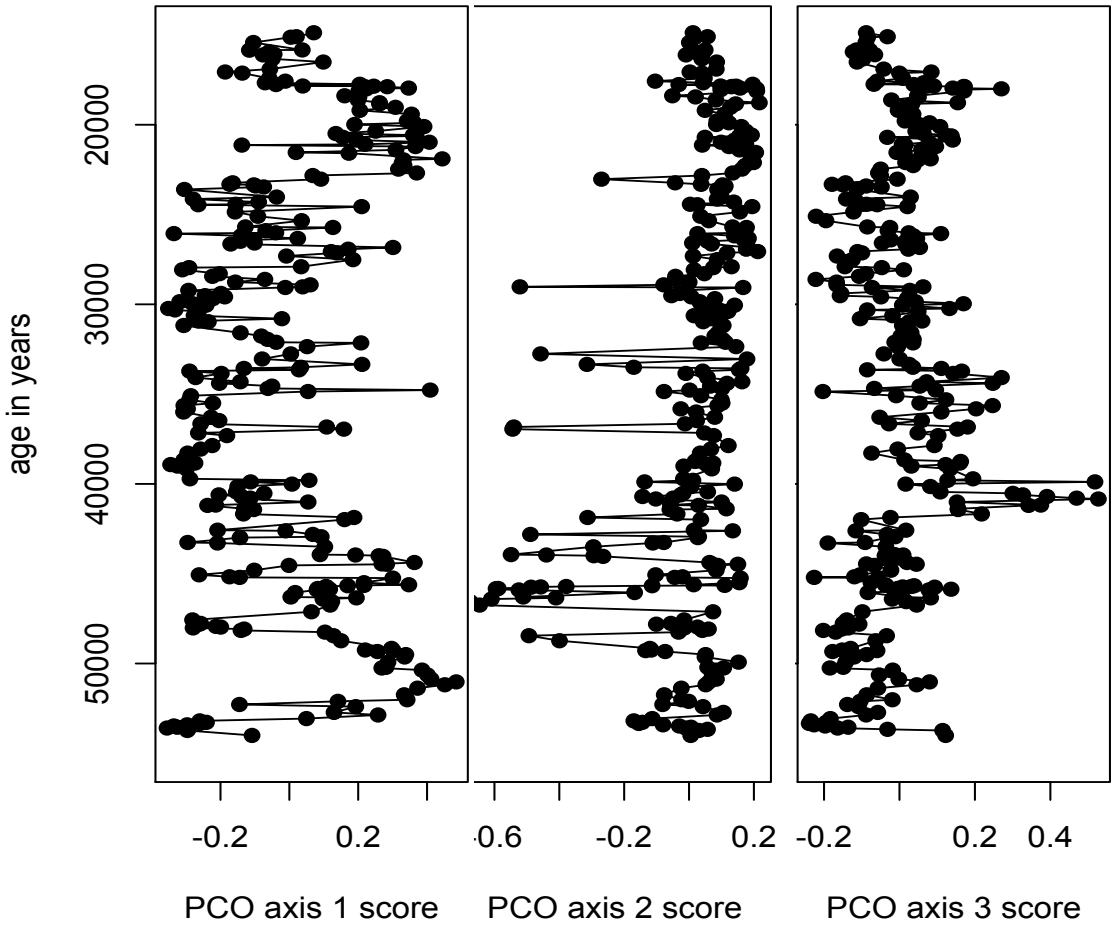

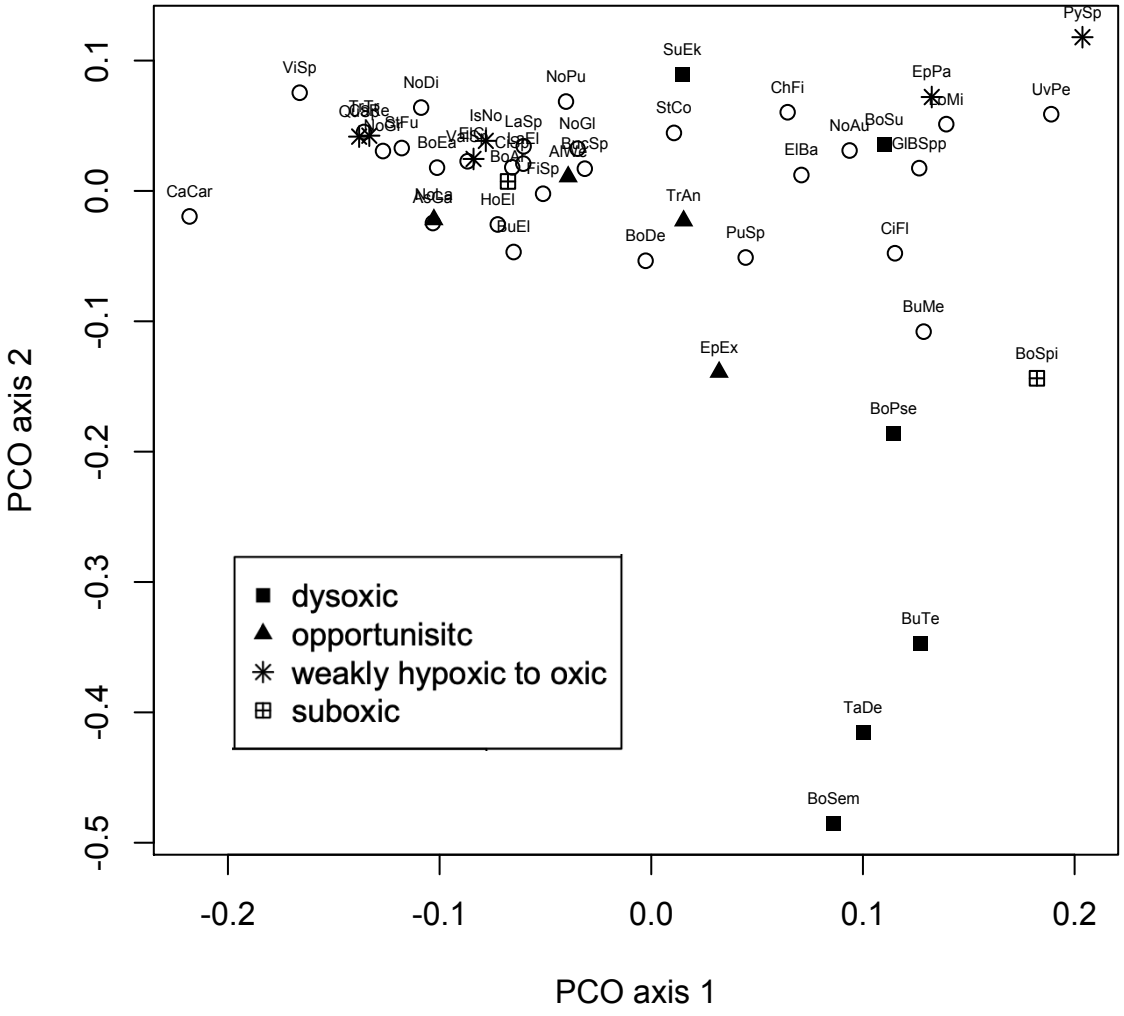
PySp
SuEk
ViSp
NoDi
NoPu
ChFi
EpPa
UvPe
StCo
NoAu
BoSu
ElBa
GlBSpp
CaCar
TrAn
BoDe
PuSp
CiFl
BuMe
EpEx
BoSpi
BoPse
BuTe
TaDe
BoSem
dysoxic
opportunisitc
weakly hypoxic to oxic
suboxic
PCO axis 2
PCO axis 1
0.1
0.0
-0.1
-0.2
-0.3
-0.4
-0.5
-0.2
-0.1
0.0
0.1
0.2

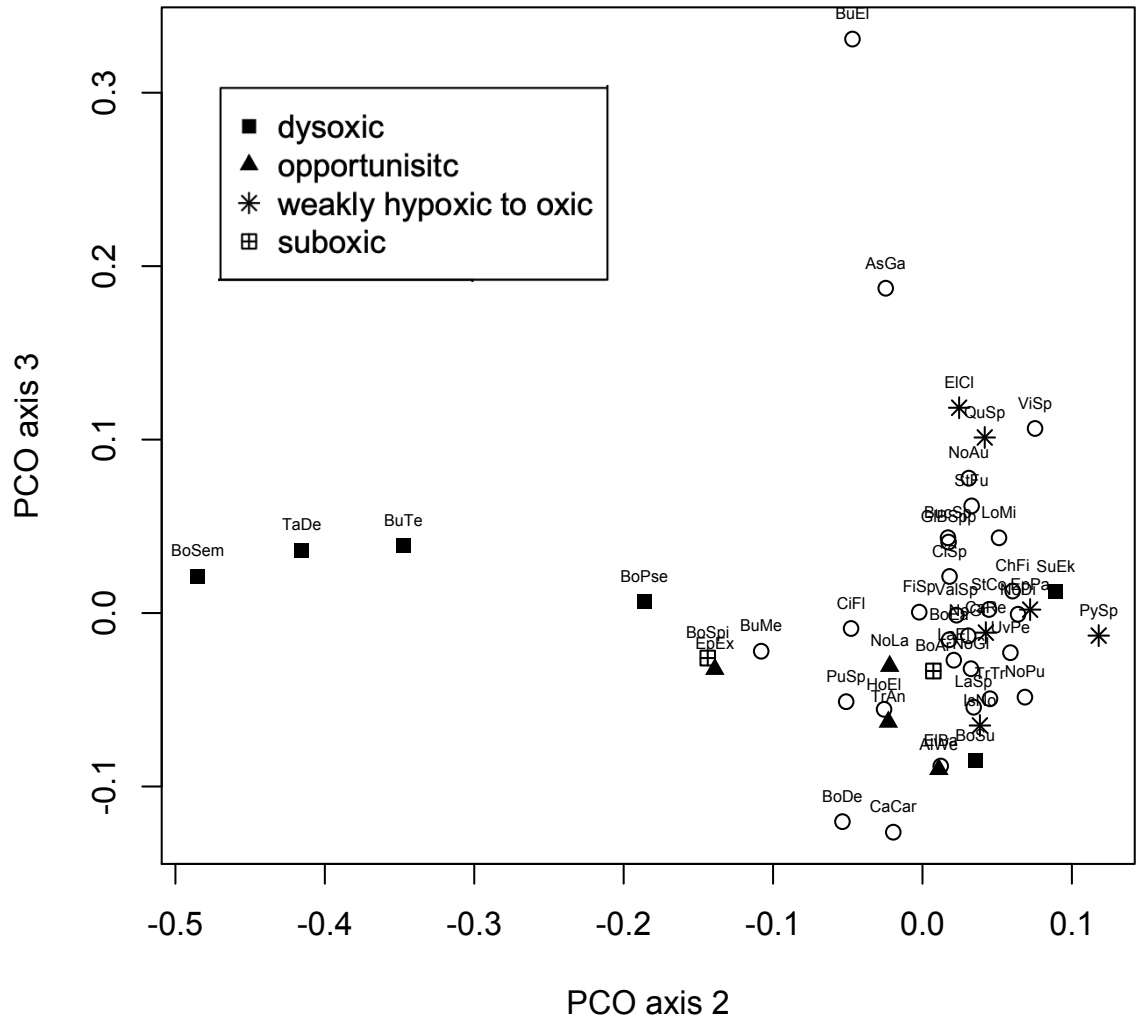

Figure 4.3 Top: The PCO Axis 1, 2 and 3 scores against age in years for the older subset from ~54- 14.8 ka. Middle: PCO Axis 2 species scores against PCO Axis 1 species scores. Bottom: PCO Axis 3 species scores against PCO Axis 2 species scores. Abbreviations as in Supplemental Table 4.2.

4.3.1.3. Deglacial Dysoxic Event thorough the Holocene: 14.7 ka – present (Younger Subset)

For the 14.7 ka to present subset, PCO Axis 1 summarized 52% of the faunal variation, followed by PCO Axis 2, which summarized 16% (Table 4.1). PCO Axis 3 and

PCO Axis 4 site scores were quite low being 7% and 5%, respectively, hence we do not discuss those further.

B. seminuda, T. delicata, B. subadvena, S. eckisi, B. pseudobeyrichi and *B. tenuata* have the most positive scores on PCO Axis 1 (Figure 4.4; Supplemental Table 4.2; Supplemental Table 4.4; Sharon et al., 2021). Suboxic species, such as *B. argentea* and *B. spissa,* have negative PCO Axis 1 scores. Species which are generally associated with opportunistic behavior, like *T. anglulosa, E. exigua* and *A. weddellensis,* have strong negative scores (Hayward et al., 2004; Sun et al., 2006). In addition, oxic-indicating species like *Quinqueloculina* spp. and *Pyrgo* spp. also have strong negative scores (Ohkushi et al., 2013). Furthermore, *C. reniforme, E. pacifica* and *E. clavatum, I. norcrossi* which are associated with glacial and oxic environments, have negative scores (Figure 4.4, Supplemental Table 4.4, Korsun and Hald, 2000; Ohkushi et al., 2003). Positive PCO Axis 1 scores were only seen between 14.7 ka to ~10.5 ka and after which all PCO Axis 1 scores are negative (Figure 4.4).

Dysoxic species like *B. tenuata, S. eckisi, B. seminuda* and oxic species like *Quinqueloculina* spp. and *Pyrgo* spp. have similar positive scores PCO Axis 2 species scores. Other oxic species like *I. norcrossi* and *C. reniforme* have similar positive scores to the dysoxia-tolerant *B. subadvena* and *T. delicata*. Furthermore, *T. anglulosa, E. exigua* have similar positive PCO Axis 2 scores whereas *A. weddellensis* and *N. labradorica* have negative PCO Axis 2 scores. Positive PCO Axis 2 scores occurred from 14.7 to ~13.5 ka

and more negative scores were noted from ~13.5- ~7.4 ka. From ~7.4 – 0 ka PCO Axis 2 scores were mostly positive (Figure 4.4).

On PCO Axis 3, *B. subadvena* and *B. seminuda* have strong negative scores and *I. norcrossi*, *E. clavatum, Quinqueloculina* spp*., S. eckisi, E. pacifica, B. argentea* also have weak negative scores. *B. tenuata, T. delicata, B. spissa* and *T. angulosa* have mor positive PCO Axis 3 scores. Strong positive scores were seen ~14.7 ka and early Holocene. PCO Axis 3 sample scores have low variation from ~8.6 ka to present and the scores are mostly close to zero (Figure 4.4).

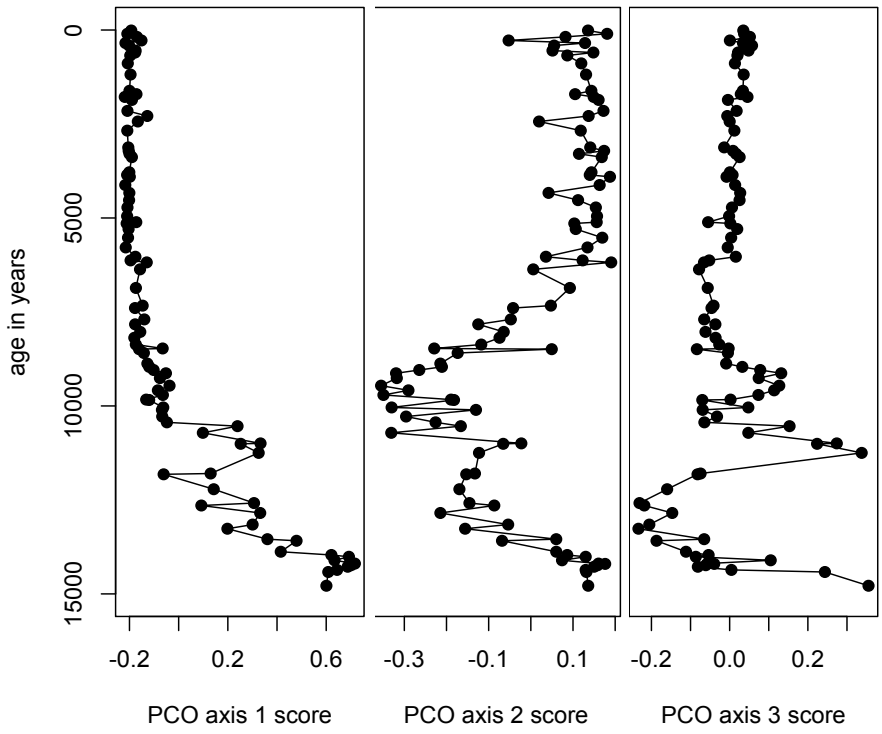

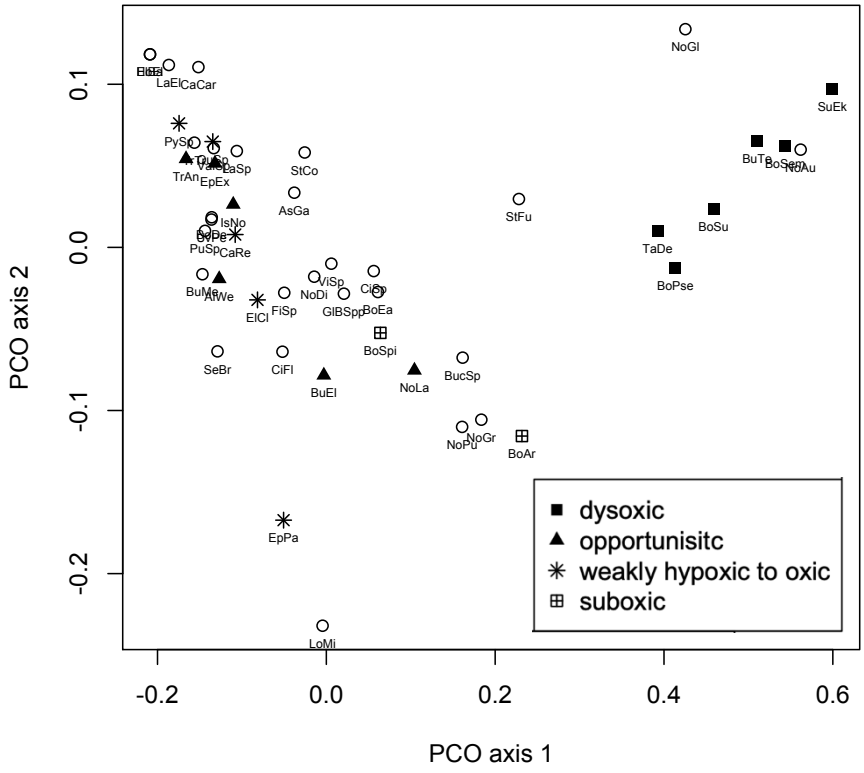
dysoxic
opportunisitc
weakly hypoxic to oxic
suboxic
PCO axis 1
PCO axis 2
-0.2
0.0
0.2
0.4
0.6
0.1
0.0
-0.1
-0.2
NoGl
SuEk
BuTe
BoSem
NoAu
StCo
AsGa
StFu
BoSu
TaDe
BoPse
CaRe
ViSp
NoDi
GlBSpp
BoEa
BoSpi
SeBr
CiFl
BuEl
NoLa
BucSp
NoPu
NoGr
BoAr
EpPa
LoMi

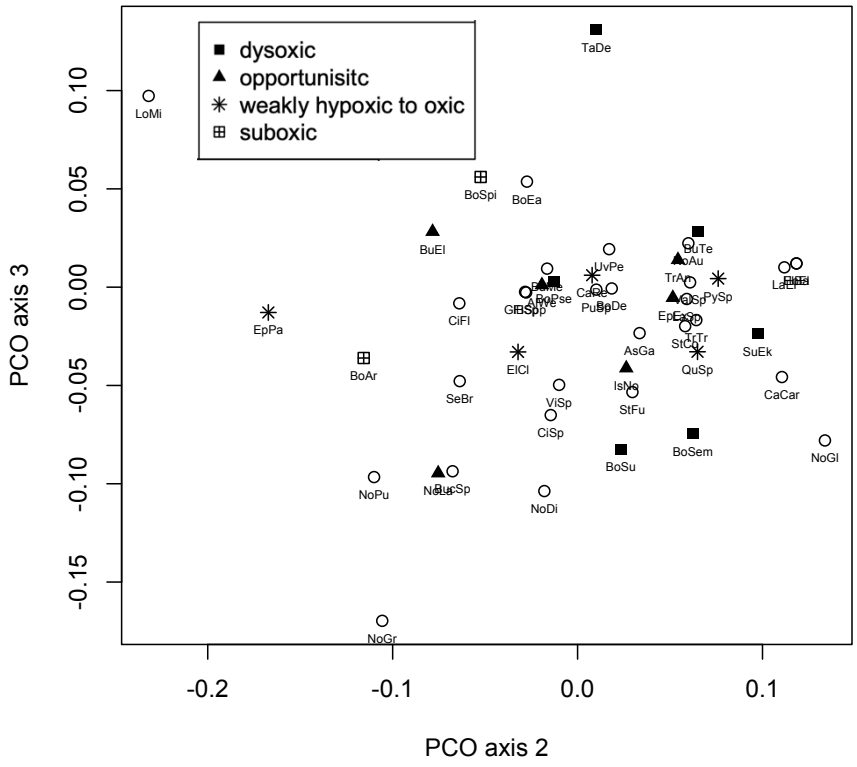
dysoxic
opportunisitc
weakly hypoxic to oxic
suboxic
PCO axis 2
PCO axis 3
-0.2
-0.1
0.0
0.1
0.10
0.05
0.00
-0.05
-0.10
-0.15
TaDe
LoMi
BoSpi
BoEa
BuEl
BuTe
UvPe
TrAn
PySp
LaEl
EpPa
CiFl
AsGa
SuEk
BoAr
ElCl
QuSp
CaCar
SeBr
IsNo
StFu
ViSp
CiSp
BoSu
BoSem
NoGl
NoPu
NoDi
NoGr

Figure 4.4 Top: PCO Axis 1, 2 and 3 sample scores against age in years for the younger data subset (14.7-0 ka). Middle: PCO Axis 2 versus PCO Axis 1 species scores. Bottom: PCO Axis 3 versus PCO Axis 2 species scores. Abbreviations as in Supplemental Table 4.2.

4.3.2. Paleoenvironmental Data

The range for $\delta^{18}O_{N.pachy}$ values was between 0.8‰ to 3.9‰ (Figure 4.5). Lower values of $\delta^{18}O_{N.pachy}$ occurred during MIS 3 (at ~29 ka, ~34 ka, ~36.9 ka, ~44 ka and ~46 ka), which corresponds well with high Mo/Al values and low mBDO values (Figure 4.5). At ~16.1 ka, $\delta^{18}O_{N.pachy}$ begins to gradually decline before an abrupt decline to 2.5‰ at 14.8 ka. The $\delta^{18}O_{N.pachy}$ values declined further to 1.5‰ at 14 ka and then increased to 3.4‰ at 13.3 ka. The $\delta^{18}O_{N.pachy}$ values were lower during the Bølling than during Allerød. Furthermore, a decline in $\delta^{18}O_{N.pachy}$ values was recorded during the early Holocene, these low values continued throughout the Holocene. The lowest $\delta^{18}O_{N.pachy}$ values occurred during B-A whereas values during early Holocene dysoxic event was 1.5‰. The range for $\delta^{18}O_{Uvi}$ values was lower as compared to the benthic $\delta^{18}O_{N.pachy}$ and was between 4.8‰ and 3‰. The $\delta^{18}O_{Uvi}$ starts declining to lower values at ~16 ka and remained below or ~3.5‰ from ~10.5 ka to present (Figure 4.5). The $\delta^{18}O_{N.pachy}$ and $\delta^{18}O_{Uvi}$ trends correspond well from ~13 ka to present and show lower values as compared to the rest of the record.

The maximum value for $\delta^{13}C_{N.pachy}$ was 1‰ and the minimum was -0.5‰; $\delta^{13}C_{Uvi}$ values ranged between -1.5‰ and -0.4‰. More negative values of $\delta^{13}C_{N.pachy}$ were seen during the MIS 2 and MIS 3 as compared to the younger subset (Figure 4.5). The negative $\delta^{13}C_{N.pachy}$ values corresponded to lower mBDO at ~23 ka, ~34 ka, ~ 36.6 ka, ~46 ka. The

Bølling had lower positive $\delta^{13}C_{N.pachy}$ as compared to the Allerød and early Holocene dysoxic event but at ~13.3 ka in Allerød the value was -0.13‰. The most positive values of $\delta^{13}C_{N.pachy}$ in the ~54 ka record are recorded during the Holocene. The trends in $\delta^{13}C_{Uvi}$ show no temporal trend and a wider range of values was seen during the MIS2 and MIS 3 as compared to the Holocene (Figure 4.5). More negative values of $\delta^{13}C_{Uvi}$ corresponding to lower mBDO were seen around 36 ka, ~41 ka, ~44 ka, ~46 ka. The most negative $\delta^{13}C_{Uvi}$ value of -1.5 was seen ~17.8 ka. More negative $\delta^{13}C_{Uvi}$ values were seen during B-A, in contrast they were less negative during early Holocene.

Faunal proxies like the proportion of dysoxic species, the proportion of opportunistic taxa and mBDO also show noticeable temporal changes (Figure 4.5). A sharp decrease in mBDO values and an increase in % dysoxic species correspond to negative PCO Axis 1 scores during events like B-A and early Holocene. Similar trends were also seen during the MIS 3. Furthermore, a strong increase in the % opportunistic species to >50 % of the total individuals in a sample occurred at ~53 ka, ~48.5 ka, ~46 ka, ~44 ka during MIS 3, at ~11.8 ka, and several times during the Holocene. Between ~42 ka and 13.5 ka, the relative abundance of opportunistic species was generally <30%, but from ~8.4 ka to present opportunists were consistently >40% of the total fauna (Figure 4.5).

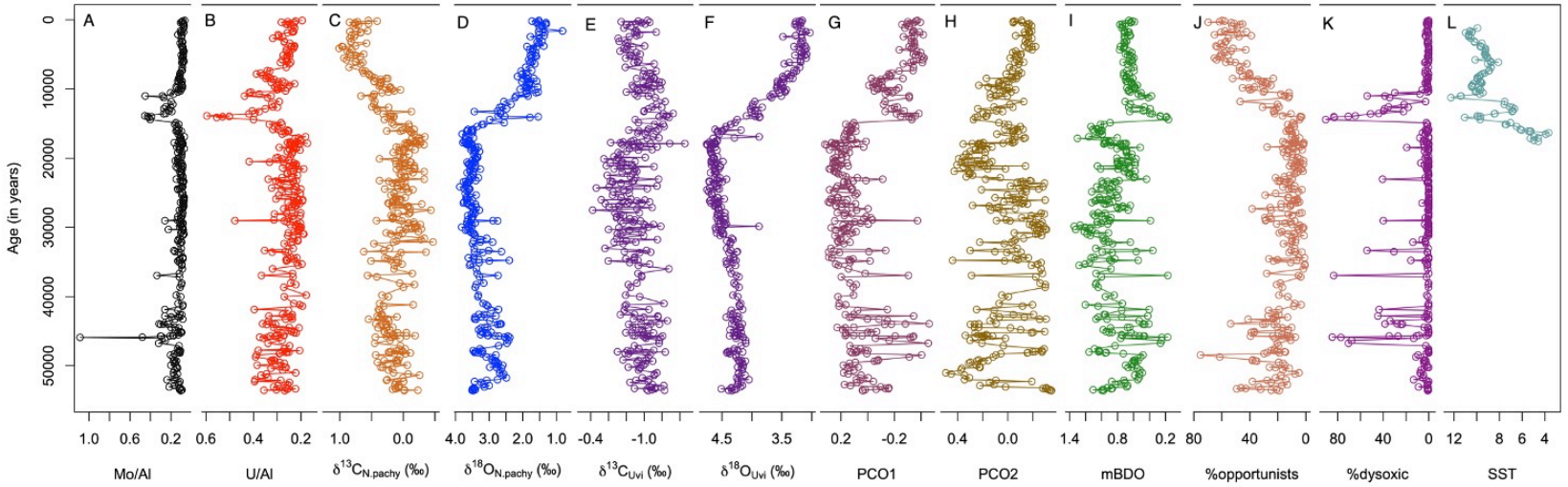

Figure 4.5 Environmental proxies over ~54,000 years for Site U1419. (A) Mo/Al, (B) U/Al, (C) $\delta^{13}C_{N.pachy}$, (D) $\delta^{18}O_{N.pachy}$, (E) $\delta^{13}C_{Uvi}$, (F) $\delta^{18}O_{Uvi}$, (G) PCO Axis 1 scores, (H) PCO Axis 2 scores, (I) mBDO, (J) and (K) proportional abundance of opportunistic taxa and dysoxic taxa, respectively, (L) SST interpolated from Praetorius et al. 2015.

4.3.3. Relationships among faunal gradients and environmental proxy timeseries

4.3.3.1. Before deglacial dysoxic event: ~54 - 14.8 ka (Older Subset)

In analyzing the relationships among variables, I performed 78 correlations for the older data subset, thus a Bonferroni correction was applied to the accepted significance level (α) of 0.05 to obtain a corrected significance level (α') of 6.4×10^{-4}; only correlations that meet this criterion are discussed below (see Supplemental Table 4.6 for all correlations). PCO Axis 1 scores have a negative association with $\delta^{18}O_{N.pachy}$ (Pearson r = -0.5) and mBDO (Pearson r = -0.8); when $\delta^{18}O_{Uvi}$ was partialled out, these associations with $\delta^{18}O_{N.pachy}$ were slightly weaker when $\delta^{18}O_{Uvi}$ was not partialled out (Figure 4.6). PCO Axis 2 shows strong negative association with Mo, U, %opportunists and % dysoxic even after partialling out $\delta^{18}O_{Uvi}$; of these the strongest relationship occurred with Mo (Pearson r = -0.6) and % dysoxic (Pearson r = -0.8). PCO Axis 2 scores have a weaker positive relationship with $\delta^{18}O_{N.pachy}$ (Pearson r = 0.4) and a weak negative relationship with $\delta^{13}C_{N.pachy}$ (Pearson r = -0.3) when $\delta^{18}O_{Uvi}$ is partialled out (Figure 4.6).

The mBDO has a positive association with $\delta^{18}O_{N.pachy}$ (Pearson r=0.7) and a weak negative relationship with $\delta^{13}C_{N.pachy}$ (Pearson r= -0.3). The correlation coefficients with mBDO were almost same with or without partialling out $\delta^{18}O_{Uvi.}$ Mo/Al has a negative association with $\delta^{18}O_{N.pachy}$ (Pearson r= -0.5), mBDO (Pearson r= -0.5), and PCO Axis 2 (Pearson r= -0.6) and positive relationship with %dysoxic (Pearson r=0.7); of these, the correlations with $\delta^{18}O_{N.pachy}$ and PCO Axis 2 were slightly stronger when $\delta^{18}O_{Uvi}$ was not

partialled out (Figure 4.6). In these partial correlations, U/Al produces similar, but slightly weaker correlations than does Mo/Al (Figure 4.6). A weak positive correlation was also seen between %opportunists and $\delta^{13}C_{N.pachy.}$ No significant correlations were seen with $\delta^{13}C_{Uvi}$ or %coarse when $\delta^{18}O_{Uvi}$ was partialled out (Figure 4.6).

4.3.3.2. Deglacial Dysoxic Event thorough the Holocene: 14.7 ka – present (Younger Subset)

In analyzing the relationships among variables, I performed 91 correlations for the younger data subset, thus a Bonferroni correction was applied to the accepted significance level (α) of 0.05 to obtain a corrected significance level (α') of 5.5×10^{-4}; only correlations that meet this criterion are discussed below (see Supplemental Table 4.7 for all correlations). Most of the correlations became insignificant once $\delta^{18}O_{Uvi}$ was partialled out and the ones that were retained became weaker (Figure 4.6). Therefore, to understand the correlations independent of glacial-interglacial changes we only present the results partialling out $\delta^{18}O_{Uvi.}$ PCO Axis 1 shows a strong positive association with Mo/Al (Pearson r= 0.8) and U/Al (Pearson r= 0.6) and % dysoxic (Pearson r= 0.9) whereas it was slightly stronger before partialling out $\delta^{18}O_{Uvi}$ (Figure 4.6). PCO Axis 1 also has a strong negative relationship with mBDO (Pearson r= -0.9) and % opportunists (Pearson r= -0.6). PCO Axis 2 shows very weak and insignificant correlations with most of the proxies except positive for relationships with Mo (Pearson r= 0.5), $\delta^{13}C_{N.pachy}$ (Pearson r= 0.5), and % dysoxic (Pearson r= 0.7).

The proxies for oxygenation have strong correlations with each other (Figure 4.6). The mBDO record has strong negative relationships with Mo/Al (Pearson r= -0.7), U/Al

(Pearson r= -0.6) and %dysoxic (Pearson r= -0.9) Mo/Al and U/Al also show strong positive relationships with %dysoxic (Pearson r= 0.9) and (Pearson r= 0.6), respectively.

SST showed no significant correlations with any proxy except for $\delta^{18}O_{N.pachy}$ when $\delta^{18}O_{Uvi}$ was not partialled out but upon partialling out $\delta^{18}O_{Uvi,}$ the correlations with SST became significant and stronger (Figure 4.7). In these partial correlations, SST has a negative association with both $\delta^{18}O_{N.pachy}$ and % opportunists (Pearson r= -0.5). SST also shows a negative relationship with mBDO (Pearson r= -0.4) and a positive relationship with Mo/Al (Pearson r= 0.4). In addition, upon partialling $\delta^{18}O_{Uvi,}$ a negative relationship was observed between % opportunists and Mo/Al, U/Al, % dysoxic (Pearson r= -0.4) and a positive association was observed with mBDO (Pearson r= 0.4).

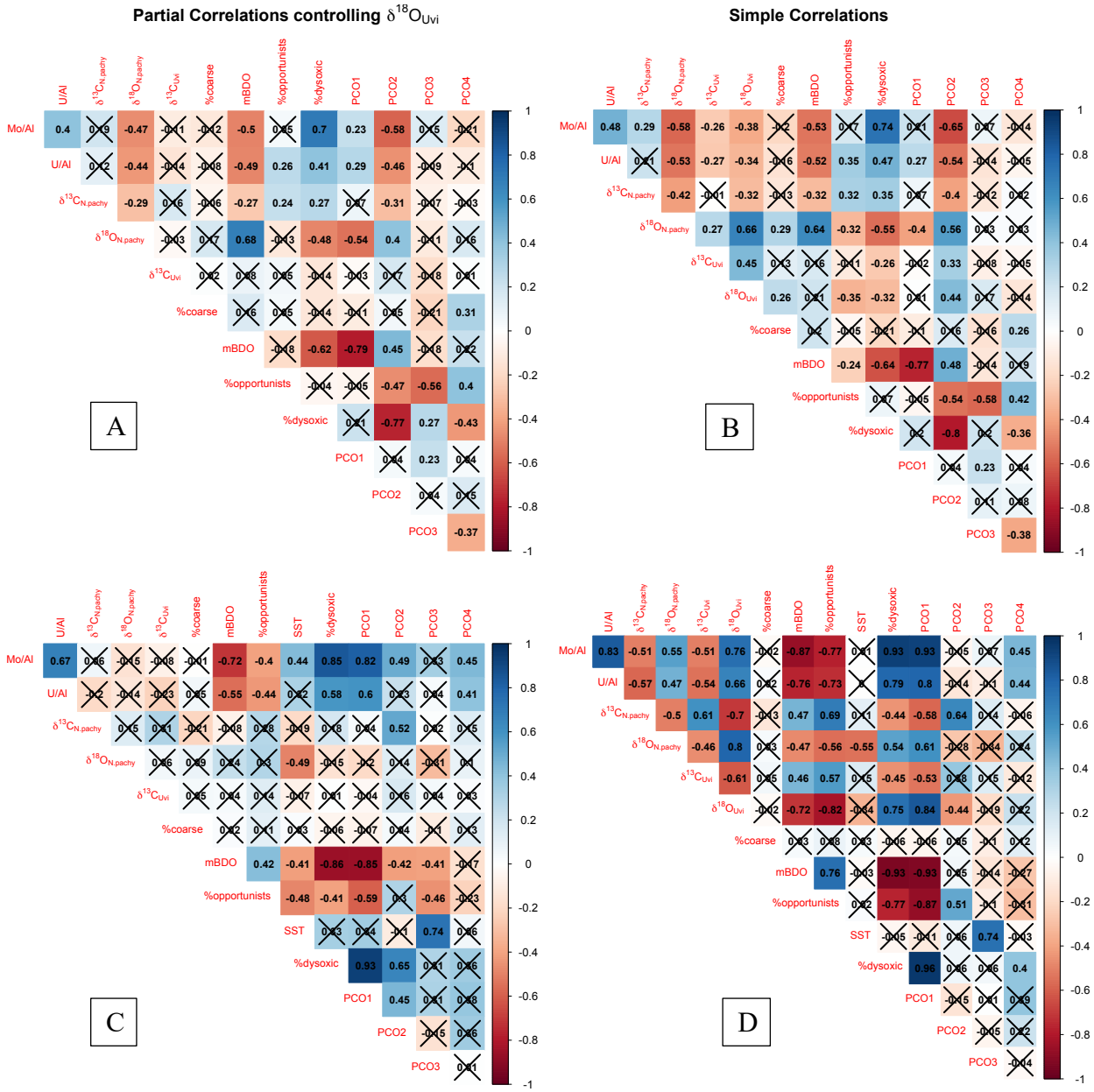

Figure 4.6 Bivariate Pearson correlations (A) and (B) older data subset; (C) and (D) younger dataset. (A) and (C) present partial correlations with $\delta^{18}O_{Uvi}$ partialled out and (B) and (D) show correlations without $\delta^{18}O_{Uvi}$ partialled out. Pearson correlations with p-values < α' were significant, and insignificant correlations with p-values > α' have been crossed out. Bonferroni corrected significance level (α') is 6.4×10^{-4} for correlations in (A); α'=5.5×10^{-4} for correlations in (B) and (C),

and $\alpha'=4.8\times10^{-4}$ for correlations in (D). Color scale and numbers in each cell reflect the strength and direction of the correlation.

4.3.4. Predicting oxygenation from other proxy variables

4.3.4.1. Before deglacial dysoxic events: 54-14.8 ka

The best supported multiple regression models for mBDO and PCO Axis 2 summarized >50% of their variance. The best supported model for other tested response variables were not as well predicted by the predictor variables included (Table 4.2).

PCO Axis 2 sample score is best predicted by a negative relationship with Mo/Al ($\beta = -0.07$), %opportunists ($\beta = -0.1$), U/Al ($\beta = -0.02$) and $\delta^{13}C_{N.pachy}$ ($\beta = -0.02$) and a positive relationship with $\delta^{13}C_{Uvi}$ ($\beta = 0.02$). Although r^2 values are lower, the best supported model for PCO Axis 1 retained negative relationships with $\delta^{18}O_{N.pachy}$ ($\beta - 0.2$) and %opportunists ($\beta = -0.03$) and positive relationships with U/Al ($\beta = 0.02$) and $\delta^{18}O_{Uvi}$ ($\beta = 0.1$). PCO Axis 3 is best predicted when all the predictors ($\beta < 0.1$) except $\delta^{13}C_{N.pachy}$ are included in the model (Table 4.2).

The best supported model for mBDO retains all four isotopic proxies and % opportunists as predictors and has an r^2 value of 0.5 (Table 4.2). Of these predictors, $\delta^{18}O_{N.pachy}$ has the strongest positive relationship ($\beta = 0.2$) whereas $\delta^{13}C_{N.pachy}$ ($\beta = -0.02$), $\delta^{18}O_{Uvi}$ ($\beta = -0.1$), and % opportunists ($\beta = -0.02$) have negative relationships. In addition, $\delta^{13}C_{Uvi}$ has a weaker ($\beta = 0.03$), positive relationship (Table 4.2). The best supported models for Mo/Al and U/Al have similar negative relationships with $\delta^{18}O_{N.pachy}$ ($\beta = -0.05$ and -0.03), and $\delta^{13}C_{Uvi}$ ($\beta = -0.1$), but the models have lower r^2 values (Table 4.2). In

addition, U/Al also has a positive relationship with $\delta^{18}O_{Uvi}$ and % opportunists ($\beta = 0.01$ for both). The % opportunists were best predicted by negative relationship with Mo/Al and $\delta^{18}O_{Uvi}$ and positive relationship with U/Al and $\delta^{13}C_{N.pachy}$ but this model had a low r^2 value (Table 4.2).

Table 4.2 Best supported multiple regression models for older subset (~54 – 14.8 ka). Significance levels: (***)=0.001, (**)= 0.01, (*)=0.5, (.)= 0.1, (ns)= not significant. Vif= variance inflation factor.

	Multiple R^2, Adjusted R^2	(p-value)	(Intercept-Estimate)	Mo/Al	U/Al	$\delta^{13}C_{N.pachy}$	$\delta^{18}O_{N.pachy}$	$\delta^{13}C_{Uvi}$	$\delta^{18}O_{Uvi}$	%Opportunistic	%coarse
PCO1	0.32, 0.31	$< 2.2 \times 10^{-16}$	0.02 (.)	-	0.02 (ns)	-	-0.15 (***)	-	0.10 (***)	-0.03 (*)	-
PCO1-vif					1.47		2.20		1.85	1.22	
PCO2	0.66, 0.65	$< 2.2 \times 10^{-16}$	0.02 (**)	-0.07 (***)	-0.02 (**)	-0.02 (**)	-	0.02 (***)	-	-0.06 (***)	-
PCO2-vif				1.41	1.47	1.20		1.12		1.23	
Mo/Al	0.34, 0.34	$< 2.2 \times 10^{-16}$	0.13 (***)	NA	NA	-	-0.05 (***)	-0.01 (.)	-	-	-
Mo/Al-vif							1.08	1.08			
mBDO	0.51, 0.5	$< 2.2 \times 10^{-16}$	0.83 (***)	NA	NA	-0.02 (ns)	0.20 (***)	0.03 (*)	-0.11 (***)	-0.02 (.)	-
mBDO-vif						1.30	1.95	1.28	2.15	1.21	
U/Al	0.35, 0.33	$< 2.2 \times 10^{-16}$	0.26 (***)	NA	NA	-	-0.03 (***)	-0.01 (**)	0.01 (*)	0.01 (***)	
U/Al-vif							1.81	1.25	2.13	1.16	
%Opportunistic	0.23, 0.21	1.27×10^{-11}	15.42 (***)	-1.26 (ns)	3.18 (***)	2.56 (***)	-	-	-2.57 (***)	NA	-
%Opportunistic-vif				1.43	1.35	1.16			1.28		
PCO3	0.43, 0.41	$< 2.2 \times 10^{-16}$	-0.03 (***)	0.01 (.)	-0.01 (ns)		-0.02 (*)	-0.02 (**)	0.02 (**)	-0.06 (***)	-0.02 (**)
PCO3-vif				1.62	1.62		2.61	1.31	2.19	1.24	1.11
PCO4	0.31, 0.30	$< 2.2 \times 10^{-16}$	-0.01 (ns)	-0.01 (*)	-0.01 (*)	-	-	-	-0.02 (*)	0.05 (***)	0.03 (***)
PCO4-vif				1.41	1.45				1.36	1.23	1.09

4.3.4.2. Deglacial Dysoxic Event thorough the Holocene: 14.7 ka – present

The best supported multiple regression models for all the response variables tested in the younger subset summarized >50% of their variance (Table 4.3). However, the VIF for $\delta^{18}O_{Uvi}$ in the best supported multiple regression model for PCO Axis 2, mBDO and Mo was >5.

In the younger portion of the time series, PCO Axis 1 sample scores were best predicted multiple regression model with a positive relationship with Mo/Al ($\beta = 0.15$), and negative relationships with %opportunists ($\beta = -0.09$) and SST ($\beta = -0.03$). PCO Axis 2 is best predicted by a positive relationship with $\delta^{13}C_{N.pachy}$ ($\beta = 0.07$) and % opportunists ($\beta = 0.1$) and negative relationships with $\delta^{18}O_{Uvi}$ ($\beta = -0.06$) and SST ($\beta = -0.02$). The best supported model for PCO Axis 3 retained negative relationship with U/Al and % opportunists and positive relationship with Mo/Al, $\delta^{13}C_{N.pachy}$ and SST (Table 4.3).

The mBDO is best predicted by a negative relationship with $\delta^{13}C_{N.pachy}$ and SST ($\beta = -0.03$) and $\delta^{18}O_{Uvi}$ ($\beta = -0.08$), and a positive relationship with % opportunists ($\beta = 0.06$). The best supported model for Mo/Al has a positive relationship with $\delta^{13}C_{N.pachy}$ and SST ($\beta = 0.02$) and $\delta^{18}O_{Uvi}$ ($\beta = 0.07$) and negative relationship with % opportunists ($\beta = -0.03$). The best supported model for U/Al has a negative relationship with $\delta^{13}C_{Uvi}$ ($\beta = -0.01$) and % opportunists ($\beta = -0.05$). U/Al was the only proxy which was predicted by $\delta^{13}C_{Uvi}$ in the 14.7 ka – present subset (Table 4.3).

The best supported model for % opportunists has negative relationships with U/Al (β = -3.94) and $\delta^{18}O_{Uvi}$ (β = -11.16), SST (β = -3.81) and positive relationships with $\delta^{13}C_{N.pachy}$ (β = 2.76) and % coarse (β = 1.8). In addition, the model using % opportunists as the response variable was the only model to retain % coarse as supported predictor in the younger subset (Table 4.3).

Table 4.3 Best supported multiple regression models for younger subset (14.7 – 0 ka). Significance levels: (***)=0.001, (**)= 0.01, (*)=0.5, (.)= 0.1, (ns)= not significant. Vif= variance inflation factor.

	Multiple R^2, Adjusted R^2	(p-value)	(Intercept-Estimate)	Mo/Al	U/Al	$\delta^{13}C_{N.pachy}$	$\delta^{18}O_{N.pachy}$	$\delta^{13}C_{Uvi}$	$\delta^{18}O_{Uvi}$	%Opportunistic	%coarse	SST
PCO1	0.93, 0.93	$< 2.2 \times 10^{-16}$	-0.03 (***)	0.15 (***)	-	-	-	-	-	-0.09 (***)	-	-0.03 (***)
PCO1-vif				2.49						2.50		1.00
PCO2	0.72, 0.70	$< 2.2 \times 10^{-16}$	-0.02 (*)	0.16 (***)	-	0.07 (***)	-	-	-0.06 (*)	0.11 (***)	-	-0.02 (ns)
PCO2-vif				3.28		2.30			6.58	4.63		1.65
Mo/Al	0.70, 0.67	2.2×10^{-16}	0.15 (***)	NA	NA	0.02 (*)	-	-	0.07 (***)	-0.03 (*)	-	0.02 (**)
Mo/Al-vif						2.17			5.02	4.23		1.48
mBDO	0.65, 0.63	5.3×10^{-15}	0.60 (***)	NA	NA	-0.03 (*)	-	-	-0.08 (***)	0.06 (**)	-	-0.03 (*)
mBDO-vif						2.17			5.02	4.23		1.48
U/Al	0.56, 0.55	3.4×10^{-13}	0.31 (***)	NA	NA	-	-	-0.015 (.)	-	-0.05 (***)	-	-
U/Al-vif								1.47		1.47		
%Opportunistic	0.80, 0.78	$< 2.2 \times 10^{-16}$	38.99 (***)	-	-3.94 (**)	2.76 (.)	-	-	-11.15 (***)	NA	1.77 (.)	-3.81 (***)
%Opportunistic-vif					2.04	2.20			3.21		1.05	1.28
PCO3	0.68, 0.65	2.7×10^{-15}	-0.005 (ns)	0.03 (.)	-0.05 (***)	0.02 (.)	-	-	-	-0.04 (**)	-	0.08 (***)
PCO3-vif				4.15	3.63	2.08				3.64		1.02
PCO4	0.35, 0.28	1.6×10^{-4}	0.02 (*)	0.04 (.)	0.02 (ns)	0.03 (.)	-	-	-0.03 (ns)	-0.03 (ns)	0.02 (.)	-0.02 (ns)
PCO4-vif				5.45	3.77	2.64			6.81	5.00	1.10	1.68

4.4. Discussion

4.4.1. Ordination analyses of the full time-series

In our previous study, we found that the faunal gradient on DCA Axis 1 primarily represented an oxygenation gradient (Sharon et al., 2021). For the analysis of the full 54 ka record, the temporal variation in faunal composition depicted on for PCO Axis 1 for the analyses herein were similar to that represented on DCA Axis 1 in the previous analysis between 54 ka and 10 ka (Figure 4.5). However, during the Holocene, DCA Axis 1 scores decline after the early Holocene, suggesting a transition from dysoxia to suboxia, whereas PCO Axis 1 scores do not change significantly after the B-A and early Holocene dysoxic events. This suggests that PCO axis 1 scores do not reflect a strong oxygenation gradient that clearly separates dysoxic, suboxic, and weakly-hypoxic fauna as did the DCA analysis. From the modern oxygen measurements and core-top faunal analyses, we know that GoA is suboxic in the present and not dysoxic as during the B/A and early Holocene (Sharon et al., 2021), further supporting that PCO Axis 1 does not represent a well-defined oxygen gradient like DCA Axis 1 (Sharon et al., 2021). Instead, PCO axis 1 may reflect the different faunal compositions typically observed during interglacial and interstadial times (negative values) and those observed during glacial times (positive values). This interpretation is supported by the more positive PCO Axis 1 scores for taxa like *E. pacifica, E. clavatum* and *C. reniforme* that are associated with glacial conditions and ice margin environments (Ohkushi et al., 2003; Murray, 2006). We also observe a strong influence of opportunistic taxa on PCO Axis 1 scores, reflecting strongly pulsed export production during interglacial times (Belanger et al., 2020). PCO axis 1 species scores for

species indicative of suboxic and dysoxic conditions and for species that indicate high productivity overlap, suggesting those conditions are either directly related or are indirectly associated with glacial-interglacial changes. The marked shift in PCO Axis 1 scores occurs at ~14.7 ka, coincident with the abrupt shift to dysoxic conditions reflected in DCA Axis 1 and PCO Axis 3 described below, thus partitioning our analyses before and after this boundary allows us to examine faunal responses and the drivers of dysoxic events separately in glacial and interglacial conditions.

In contrast to PCO Axis 1, PCO Axis 2 separates dysoxic taxa (positive values) from opportunist taxa (negative values), indicating that these ecological groups do not covary along all faunal axes. We also observe a separation of glacial-associated taxa along PCO Axis 2 in which species sometimes associated with low-oxygen conditions, such as *E. pacifica* (Jorissen et al., 2007), have more positive values than those associated with more productive environments, such as *C. reniforme* and *I. norcrossi* (Figure 4.2; Murray 2006; Usami et al., 2013).

Unlike the previous DCA analysis of the full time-series which captured the oxygenation gradient on the first ordination axis, the oxygenation gradient is more clearly reflected on PCO axis 3, which summarizes significantly less faunal variation. However, this axis primarily differentiates between samples dominated by dysoxic taxa (the most negative scores) and those dominated by other faunal groups. Extreme negative scores, such as those observed at ~36.8 ka and ~45.8 ka coincide with previously recognized dysoxic events (Sharon et al., 2021). All samples after the youngest dysoxic event have strongly positive PCO axis 3 scores, distinct from those samples older than the B-A,

further indicating that faunal differences associated with glacial vs interglacial times strongly influence the fauna. This strong influence could confound our interpretation of environmental drivers of faunal composition and of the drivers of dysoxic events within each climate state. Thus, we restrict correlation and multiple regression analyses to the time intervals before and after 14.7 ka, which are discussed below.

4.4.2. Geochemical Timeseries

Lower values of $\delta^{18}O_{N.pachy}$ were seen during MIS 3, which corresponded well with increased values of Mo/Al and lower mBDO, suggesting a relationship between warmer (or fresher) conditions and low-oxygen (Figure 4.5). Furthermore, lower values of $\delta^{18}O_{N.pachy}$ were also observed during the B-A and early Holocene. These low values continue throughout the Holocene in the younger subset. In addition, a return to more positive $\delta^{18}O_{N.pachy}$ values was also seen during the Y-D, which indicates cooler temperatures (and/or less freshening by meltwaters). Furthermore, the values of $\delta^{18}O_{N.pachy}$ during the Holocene were the lowest in the whole 54, 000 years record and remain low throughout the Holocene. The temporal patterns in $\delta^{18}O_{N.pachy}$ are similar to $\delta^{18}O_{Uvi}$ which starts declines at ~16 ka and is low throughout the Holocene. These changes in $\delta^{18}O_{Uvi}$ are primarily controlled by changes global ice volume and the strong correspondence with $\delta^{18}O_{N.pachy}$ suggests that $\delta^{18}O_{N.pachy}$ also primarily reflects global ice volume.

The most positive $\delta^{13}C_{N.pachy}$ values correspond to several dysoxic events in the MIS 2 and MIS 3, thus may reflect an association of high surface productivity with dysoxia (Figure 4.5). More positive $\delta^{13}C_{N.pachy}$ values were also recorded during early Holocene where the relative abundance opportunistic species is highest, further supporting an

association between high $\delta^{13}C_{N.pachy}$ and high productivity. In addition, Site U1419 was primarily suboxic during the Holocene, further suggesting a relationship between high surface productivity and low-oxygen.

4.4.3. Older Subset (~54-14.8 ka)

For the older subset, positive PCO Axis 1 scores correspond to dysoxic and suboxic species and negative scores correspond to weakly hypoxic to oxic species related to glacial conditions. *E. exigua* has a more positive Axis 1 score than *A. weddellensis* and both are near zero, suggesting little influence of pulsed carbon export on this axis. PCO Axis 1 may reflect an oxygen gradient, however it does not resolve the difference between dysoxic and suboxic faunas. This is further supported by the strong negative Pearson correlation between mBDO and PCO Axis 1 in which low mBDO are associated with positive PCO axis 1 scores.

PCO Axis 1 also has a strong negative correlation with $\delta^{18}O_{N.pachy}$ even when the effect of $\delta^{18}O_{Uvi}$ is partialled out, indicating that at least some of the covariation is representing temperature and/or freshening and is not entirely controlled by factors that covary with global ice volume. In the best supported regression model for PCO Axis 1, $\delta^{18}O_{N.pachy}$ is also retained and is the predictor with the strongest regression coefficient, although this model explains only about 30% of the variation in PCO Axis 1. However, the directionality of the relationship suggests that faunas with high abundances of suboxic and dysoxic species occur during times with warmer, or fresher, surface waters. This is consistent with the dysoxic events in the SBB and Baja California which were also related

to warmer and less ventilated periods corresponding to D/O events (Cannariato et al., 1999; Ohkushi et al., 2013; Tetard et al., 2017).

Samples with negative PCO Axis 2 scores have high abundances of four dysoxic species (*B. seminuda*, *B. tenuata*, *T. delicata, B. pseudobeyrichi*) whereas other dysoxic species have positive species scores along PCO Axis 2. These four dysoxic species with negative species scores are isolated from the rest of the fauna in PCO space (Figure 4.3), which may be indicative of a unique tolerance for extreme dysoxia. Strongly negative sample scores occur at ~46.5 ka, ~44 ka, 42.8 ka, ~36.9 ka, ~33 ka, ~29 ka consistent with earlier interpretations of dysoxic conditions from the DCA analysis (Sharon et al., 2021). Thus, negative PCO Axis 2 scores in the older subset may represent extreme dysoxia. Negative PCO Axis 2 scores are also associated with *E. exigua* whereas oxic species like *C. reniforme*, *Quinqueloculina* spp., *Pyrgo* spp., *I. norcrossi* and *E. pacifica* have positive scores (Figure 4.3, Supplemental Table 4.4), suggesting PCO Axis 2 summarizes an oxygen gradient ranging from severe dysoxia associated with pulsed productivity at the negative end of the gradient and suboxic to weakly hypoxic environments at the positive end of the gradient.

This interpretation is further supported by the negative correlation between PCO Axis 2 sample scores and Mo/Al and U/Al, both of which were retained as supported predictors of PCO axis 2 scores in the best supported multiple regression model. Of these, Mo/Al had the strongest relationship to PCO axis 2 in both analyses, supporting the interpretation that negative PCO Axis 2 scores reflect extreme dysoxia, or sulfidic

conditions. Correlations with these environmental variables were much weaker with PCO Axis 1 indicating that PCO Axis 2 represents a stronger oxygen gradient.

Furthermore, PCO Axis 2 has a weak negative correlation with $\delta^{13}C_{N.pachy}$ (higher abundance of dysoxic species with higher $\delta^{13}C_{N.pachy}$ values), suggesting higher surface productivity is associated with extreme low-oxygen conditions. A weak negative relationship between PCO Axis 2 and $\delta^{13}C_{N.pachy}$ was also retained in the best supported multiple regression model, however this relationship was not retained for PCO Axis 1 in either the best supported multiple regression model or the Pearson correlation. *E. exigua* covaries with the relative abundance of dysoxic taxa on both PCO Axis 1 and 2 and, thus, may indicate high seasonality in productivity is associated with the dysoxic events during the 54-14.8 ka period (Sun et al., 2006). However, the other opportunistic species, *A. weddellensis,* does not co-vary with the dysoxic events suggesting that these species may have different tolerances of low-oxygen conditions or may respond to different types of phytodetritus (Ohkushi et al., 2003).

Unlike PCO Axis 1, the best supported multiple regression model with PCO Axis 2 as the response variable has a good fit to the data and does not retain $\delta^{18}O_{N.pachy}$ as a predictor. Further, the positive correlation between PCO Axis 2 and $\delta^{18}O_{N.pachy}$ with $\delta^{18}O_{Uvi}$ is partialled out suggests extreme dysoxia was related to warmer/fresher conditions. Taking into account the strong negative relationship between PCO Axis 2 and Mo/Al, it appears that extreme dysoxia, to the exclusion of suboxic conditions, is not well predicted by $\delta^{18}O_{N.pachy}$ even though $\delta^{18}O_{N.pachy}$ has some predictive value when

considering the combined presence of the suboxia and dysoxia as on PCO Axis 1. This suggests that warmer, or fresher, conditions maybe a necessary background condition for the development of dysoxia but is not sufficient for the development severe dysoxia.

Furthermore, the influence of high seasonal productivity on PCO axis 2 scores is supported by its negative relationships with $\delta^{13}C_{N.pachy}$ and % opportunists in both the Pearson correlations and best supported model regression model. The lack of these relationships between $\delta^{13}C_{N.pachy}$, % opportunists and PCO Axis 1 scores further suggest that the combination of environmental variables associated with low $\delta^{18}O_{N.pachy}$ (warm, fresh surface waters) and high $\delta^{13}C_{N.pachy}$ (high productivity) is more important than either variable alone. For example, meltwater may have introduced nutrients related from melting of continental ice during the warmer seasons which may have led to an increase in *E. exigua* and other benthic opportunists. The respiration of exported organic carbon that allowed the opportunities to thrive would consume the bottom water oxygen, thus adding to any oxygen depletion caused by freshwater-induced stratification. Better-oxygenated conditions on PCO Axis 2 (positive values) might also be related to high annual surface productivity, evinced by covariance of *A. weddellensis* whereas dysoxic events may have been related to meltwater pulses which can lead to occasional increases in nutrients. Previous studies also related dysoxic events to poor ventilation, and respiration of organic matter by benthic organisms (Praetorius et al., 2015; Gray et al., 2018).

In the glacial subset, mBDO had a strong positive correlation with $\delta^{18}O_{N.pachy}$ when $\delta^{18}O_{Uvi}$ was partialled out and was also retained as the strongest predictor in the best

supported multiple regression model. This further suggests that the low-oxygen conditions (suboxic and dysoxia) are related to higher temperatures or meltwater pulses. The best supported regression models for other low-oxygen proxies (Mo/Al and U/Al) have low r^2 values but are still best predicted by a strong negative relationship with $\delta^{18}O_{N.pachy}$, consistent with their significant negative correlations with $\delta^{18}O_{N.pachy.}$ This relationship between low-oxygen proxies and $\delta^{18}O_{N.pachy}$ further supports the hypothesis that an increase in freshwater may have stratified the surface waters and caused a hinderance in proper ventilation or supply of oxygen from the atmosphere to these intermediate waters, thus leading to low-oxygen conditions (Praetorius et al. 2015). Furthermore, mBDO retains a weak negative relationship with $\delta^{13}C_{N.pachy}$ (higher surface productivity, the lower the oxygen) in both best supported multiple regression model and in the Pearson correlations, suggesting that surface productivity contributed to the low-oxygen conditions, but to a lesser extent than the higher temperature and freshwater pulses. The mBDO also has a positive relationship with $\delta^{13}C_{Uvi}$ and a strong negative relationship with $\delta^{18}O_{Uvi}$ in the best supported multiple regression model, however, the correlation with $\delta^{13}C_{Uvi}$ becomes insignificant once $\delta^{18}O_{Uvi}$ is partialled out. Furthermore, all correlations with $\delta^{13}C_{Uvi}$ become insignificant once $\delta^{18}O_{Uvi}$ is partialled out in both older and younger subset, which suggests a strong covariance between $\delta^{18}O_{Uvi}$ and $\delta^{13}C_{Uvi}$. Thus, changes in $\delta^{13}C_{Uvi}$ may not primarily reflect changes in the amount of organic matter remineralization in the porewaters and may instead be related to changes in bottom water masses. In addition, $\delta^{13}C_{Uvi}$ has a positive correlation with $\delta^{18}O_{Uvi}$ in the glacial whereas it is negative

during the younger subset, further suggesting different controls on $\delta^{13}C_{Uvi}$ in each climate state.

Interestingly, geochemical proxies for low-oxygen conditions are not as well predicted by other environmental proxies as are faunal proxies in the multiple regression models. This may reflect the threshold behavior of redox sensitive metals to redox conditions, which would hinder linear relationships with predictor variables as opposed to the more linear behavior of faunal composition along the oxygenation gradient.

Taken together, all the best supported multiple regression models predicting faunal gradients related to oxygenation and predicting proxies for low-oxygen conditions and the bivariate correlations among variables indicate that both meltwater and surface productivity likely impacted the oxygenation in GoA and led to the extreme dysoxia. However, the strength to the correlations and regression coefficients suggest that meltwater may have had a stronger role and indeed may have triggered the increase in surface productivity during the interstadials within the 54-14.8 ka period.

4.4.4. Younger subset (14.7 ka to present)

For the younger subset, PCO Axis 1 reflects an oxygen and productivity gradient, with dysoxic species having strong positive scores whereas oxic species and phytodetritus indicators having negative scores. Thus, high positive sample scores suggest dysoxia whereas negative scores suggest better oxygenation or suboxia. On PCO Axis 1, species indicative of high productivity covary with species associated with oxic conditions. Both opportunistic taxa, *A. weddellensis* and *E. exigua,* along with another the high productivity indicator *T. angulosa,* covary with oxic species including *Pyrgo* spp., *Quinqueloculina*

spp., *C. reniforme*, *E. pacifica*, *E. clavatum*. This is in contrast to the older subset where *E. exigua* was more closely associated with dysoxic species. This difference in the association of opportunistic taxa with the oxygenation gradient can be explained by very high proportional abundances of opportunistic taxa like *A. weddellensis* and *E. exigua* during the Holocene when suboxic conditions prevail whereas during the B-A and early Holocene the proportional abundances of dysoxic taxa exceeded 75% in most samples, which would mute the apparent response of the opportunists.

The best supported regression model for PCO Axis 1 included Mo/Al with a positive regression coefficient (dysoxic species increase as Mo/Al increases) consistent with the Pearson correlation (Table 4.3). In addition, PCO Axis 1 shows very strong positive and very strong negative correlations with % dysoxic and mBDO, respectively, which supports the interpretation that PCO axis 1 reflects oxygen. PCO Axis 1 was also predicted by a negative regression coefficient with % opportunists in the best supported regression model, consistent with the Pearson correlation (% opportunists are higher in with better oxygenated environments). This is consistent with the covariation of opportunists with oxic species and not with dysoxic species on PCO Axis 1 in the younger subset.

While PCO Axis 1 reflects faunal variation in response to an oxygen gradient in the younger subset, PCO Axis 2 summarizes faunal variation that may be associated with a gradient between seasonal and annual productivity in association with dysoxic and suboxic condition given the *E. exigua* and *A. weddellensis* PCO Axis 2 scores were very different. In addition, it may seem that the covariation between dysoxic species and

species associated with oxic environments in ordination space suggests PCO Axis 2 may not be strongly influenced by an oxygenation gradient (Figure 4.4; Supplemental Table 4.4). However, all dysoxic taxa have positive scores except for *B. pseudobeyrichi,* which has a score close to zero. Furthermore, PCO Axis 2 does retain a positive correlation with Mo and % dysoxic and negative correlation with mBDO and does show support for an oxygen gradient, however these correlations are weaker when compared with PCO Axis 1 correlations.

PCO Axis 2 was instead predicted by a positive regression coefficient with $\delta^{13}C_{N.pachy}$ which may explain the association between productivity suggested by positive species scores of *E. exigua* and dysoxic taxa. However, in this model the VIF for $\delta^{18}O_{Uvi}$ was 6.58, which suggests that the covariation between $\delta^{13}C_{N.pachy}$ and $\delta^{18}O_{Uvi}$ may inflate the importance of $\delta^{13}C_{N.pachy}$. Nevertheless, a positive correlation between PCO Axis 2 and $\delta^{13}C_{N.pachy}$ was retained even after partialling $\delta^{18}O_{Uvi.}$ out. This relationship also supports that an increase in productivity may be associated with positive scores on this faunal gradient, which largely reflects low-oxygen and high surface productivity.

Furthermore, the best supported multiple regression model for PCO axis 2 retained a strong positive relationship with the proportional abundance of opportunists whereas no such relationship was seen after partialling out $\delta^{18}O_{Uvi.}$ The regression model suggests that when the percentage of dysoxic taxa increases the percentage of opportunists also increases. However, during the Holocene a huge increase in proportion of opportunistic taxa was seen while dysoxic taxa comprised <4% of the total faunal abundances (Figure 4.5). In contrast, proportion of dysoxic was much higher during B-A and early Holocene

as compared to opportunistic taxa. However, *E exigua* does covary with dysoxic taxa on PCO Axis 2 suggesting association between dysoxic conditions and high pulsed productivity events (Figure 4.7). Furthermore, the contrast between the relative abundances of the dysoxic and opportunistic taxa can just be reflecting a situation where either of the species multiplied so rapidly to an extent that it muted the response of the other species. The associations between *E exigua* and dysoxia seen on PCO Axis 2 is also consistent with that seen in the older subset. Thus, the relationship between high surface productivity and dysoxia-suboxic conditions cannot be completely ruled out in the younger subset.

Unlike the glacial subset, none of the oxygenation proxies nor any of the PCO axes scores have supported correlations with $\delta^{18}O_{N.pachy}$ after partialling out $\delta^{18}O_{Uvi}$ in the younger subset. Similarly, for the 14.7- 0 ka record the best supported regression models do not retain $\delta^{18}O_{N.pachy}$ as a predictor and the VIF values of the predictor variable $\delta^{18}O_{Uvi}$ are > 5 for the best supported regression models for response variables including Mo/Al, mBDO, and PCO Axis 2. The strong covariation between planktonic and benthic oxygen isotopes for this subset may be an artifact of the short timeseries in which the transition from the glacial to the interglacial drives a decrease in global $\delta^{18}O$ and all dysoxic events in the older portion of the record occurred where $\delta^{18}O_{N.pachy}$ values are lower (Figure 4.5). Thus, the strong trends in global $\delta^{18}O$ may confound the ability to observe relationships between proxies for oxygenation and $\delta^{18}O_{N.pachy}$. Only SST has a correlation with $\delta^{18}O_{N.pachy}$ after $\delta^{18}O_{Uvi}$ is partialled out, which just indicates that the residual of $\delta^{18}O_{N.pachy}$ reflects temperature.

In the best supported multiple regressions models focused on predicting low-oxygen proxy values, $\delta^{18}O_{Uvi}$ had the strongest regression coefficient with Mo/Al and mBDO for younger subset. In the younger data subset, the partial correlations with $\delta^{18}O_{Uvi}$ had a greater effect on the apparent relationships than in the older subset. In the younger subset, 50% of the bivariate correlations were significant, but only 32% were significant after partialling out $\delta^{18}O_{Uvi}$. In the older subset, the percentage of significant correlations were 54% and 45% before and after partialling $\delta^{18}O_{Uvi}$ out, respectively, indicating little covariation with global changes $\delta^{18}O$ (Figure 4.6). Similarly, VIF for $\delta^{18}O_{Uvi}$ was <5 in all best models of the older subset indicating that the effect of the other predictor variables were not inflated by $\delta^{18}O_{Uvi}$ (Table 4.2). This further demonstrates the strong influence of glacial-interglacial changes on the younger subset. In addition, as we could clearly retain the relationships amongst proxies in the older subset, we suspect we would have retained them in the younger subset if the control of glacial-interglacial changes was not as strong a confounding factor.

SST had weak and insignificant correlations with most proxies when $\delta^{18}O_{Uvi}$ was not partialled out, but correlations became stronger and significant after partialling $\delta^{18}O_{Uvi}$ out, indicating that $\delta^{18}O_{Uvi}$ confounded relationship between SST and the other environmental variables. All of the best supported models for paleo-oxygenation proxies retained SST as a predictor except for the model predicting U/Al, which reflects suboxia rather than dysoxia (Klinkhammer and Palmer, 1991). The best supported model and Pearson correlations for mBDO and for Mo retained a negative and a positive relationship with SST, respectively, consistent with lower-oxygen conditions occurring during warmer

times (Table 4.3). The best supported model for PCO Axis 1 was also predicted by a negative relationship with SST, which suggests that higher temperatures are associated with higher abundances of dysoxic species and is consistent with previous studies in the GoA (Praetorius et al., 2015). However, the bivariate correlation between SST and PCO 1 was insignificant.

The proportion of opportunistic taxa had a positive relationship with mBDO (lower oxygenation less opportunists) whereas Mo/Al and SST had negative relationships with proportion of opportunists (lower the oxygen and higher temperature, the fewer the opportunists) in both the bivariate correlations and the multiple regression models, suggesting that opportunistic foraminifera are more abundant when conditions are better oxygenated and cooler. In the younger subset, the cooler conditions of the Holocene (more opportunists during suboxia) are relative to the warmer temperatures during early Holocene and B-A interval (more dysoxic taxa). While multiple regression models for mBDO and Mo retained $\delta^{13}C_{N.pachy}$ as a predictor, bivariate correlations revealed no significant correlations with $\delta^{13}C_{N.pachy}$ after partialling $\delta^{18}O_{Uvi}$ out. This can be explained by the influence of $\delta^{18}O_{Uvi}$, which had a VIF>5 in the best model, signifying that covariation between $\delta^{13}C_{N.pachy}$ and $\delta^{18}O_{Uvi}$ may inflate the importance of $\delta^{13}C_{N.pachy,}$ the same as seen in the best supported regression model for PCO Axis 2. This was also seen in the Pearson correlations where $\delta^{13}C_{N.pachy}$ showed strong and significant relationships with most proxies when $\delta^{18}O_{Uvi}$ was not partialled out, whereas upon partialling $\delta^{18}O_{Uvi}$ out all the correlations with $\delta^{13}C_{N.pachy}$ became weak and insignificant except for PCO Axis 2.

When the relative abundance of opportunistic taxa, proxy for phytodetritus fluxes to the seafloor, was used as a response variable, it was best predicted by a strong negative relationship with SST and positive relationship with $\delta^{13}C_{N.pachy}$, suggesting that times of higher surface productivity and lower temperatures were characterized by pulsed organic matter fluxes. Interestingly, relative abundance of opportunists is the only response variable in the younger subset that retains the percentage of coarse sediment as a predictor variable in the best supported multiple regression model. In that model, opportunists are more abundant when coarse sediment is more abundant, but this correlation coefficient had very low significance. In addition, no strong significant relationships were seen with % coarse with or without partialling out $\delta^{18}O_{Uvi}$. This means that the coarseness of sediment did not really influence the faunal assemblages.

Differences in the relationships amongst the variables in the older and younger subset may suggest different drivers controlling the oxygenation in the two subsets, however the relationships in the younger subset were difficult to extract given the strong influence of glacial-interglacial changes. In contrast to the older subset where multiple oxygen proxies show a relationship with $\delta^{18}O_{N.pachy}$, the only correlation that $\delta^{18}O_{N.pachy}$ showed in the younger subset was with SST. Consistently, none of the response variables were predicted by $\delta^{18}O_{N.pachy}$ in the best supported regression models in the younger subset. In contrast to older subset, where relationships with $\delta^{13}C_{N.pachy}$ were retained in both the statistical methods, in the younger subset the only significant bivariate correlation $\delta^{13}C_{N.pachy}$ had was with PCO Axis 2 suggesting that an increase in dysoxic taxa and *E.*

exigua was related to increase in surface productivity. Furthermore, *E. exigua* which dominates in the proportional abundance of opportunistic taxa covaries with dysoxic species but the proportion of dysoxic taxa becomes extremely dominant during relatively higher temperatures obscuring the response of opportunists. Hence, the effect of increased productivity on dysoxia cannot be completely ruled out in the younger subset. However, $\delta^{13}C_{N.pachy}$ was retained as a predictor in the best supported regression models for mBDO, Mo/Al and PCO Axis 2 scores in the younger subset its importance may have been inflated due to covariation with $\delta^{18}O_{Uvi.}$ Therefore, it can be inferred that the environmental changes in the younger subset were strongly influenced by glacial-interglacial changes, thus the relationships amongst the proxies could not be clearly explained. Although, a contrasting prolonged presence of high abundances of opportunistic taxa does indicate consistent presence of increased phytodetritus export to the bottom waters (Belanger et al., 2020). Furthermore, it can be implied if similar situations which drove dysoxia in the glacial interval like freshening/warming combined with high surface productivity occur in the future, there are chances of development of severe dysoxia in the GoA.

4.5. Conclusions: Unraveling the drivers

Dividing the data into subsets helped us understand the control of global changes related to transition from the glacial into interglacial conditions on the oxygenation of GoA. In the older subset, a combination of high temperatures, freshwater flux from melting glaciers, and high surface productivity together led to dysoxic conditions during the interstadials. The dysoxic events in the glacial correspond to the D/O events as also seen in the SBB (Cannariato et al., 1999; Ohkushi et al., 2013) suggesting that GoA was

also affected by surface productivity, warm temperatures and ventilation. In the younger subset, the increase of opportunists in the Holocene suggests an increase in pulsed productivity, but suboxic, as opposed to dysoxic conditions occur in the Holocene, suggesting that highly pulsed organic carbon export alone is not enough to drive dysoxia. Given the modern GoA has high seasonal productivity, future increasing temperatures could drive future dysoxia. This effect may be further amplified if there is sufficient melting of Alaskan glaciers to introduce freshwater stratification and further increase productivity, thus producing perfect conditions for the development of severe dysoxia (Keeling et al., 2010).

4.6. References

Anderson, D. R., Burnham, K. P., & Thompson, W. L. (2000). Null Hypothesis Testing: Problems, Prevalence, and an Alternative. *The Journal of Wildlife Management*, *64*(4), 912–923. Retrieved from http://www.jstor.org/stable/3803199

Beals, E. W. (1984). Bray-Curtis Ordination: An Effective Strategy for Analysis of Multivariate Ecological Data. In A. MacFadyen & E. D. Ford (Eds.) (Vol. 14, pp. 1–55). Academic Press. https://doi.org/10.1016/S0065-2504(08)60168-3

Belanger, C. L., Du, J., Payne, C. R., & Mix, A. C. (2020). North Pacific deep-sea ecosystem responses reflect post-glacial switch to pulsed export productivity, deoxygenation, and destratification. Deep Sea Research Part I: Oceanographic Research Papers, 103341. doi.org/10.1016/j.dsr.2020.103341

Bowerman, B. L., &. O'Connell, R. T. (1990). Linear statistical models: an applied approach. PWS-Kent, Boston.

Cannariato, K. G., Kennett, J. P., & Behl, R. J. (1999). Biotic response to late Quaternary rapid climate switches in Santa Barbara Basin: Ecological and evolutionary implications. *Geology*, *27*(1), 63–66.

Childers, A. R., Whitledge, T. E., & Stockwell, D. A. (2005). Seasonal and interannual variability in the distribution of nutrients and chlorophyll a across the Gulf of Alaska shelf: 1998–2000. Deep Sea Research Part II: Topical Studies in Oceanography, 52(1), 193–216. https://doi.org/10.1016/j.dsr2.2004.09.018

Crusius, J., Calvert, S., Pedersen, T., & Sage, D. (1996). Rhenium and molybdenum enrichments in sediments as indicators of oxic, suboxic and sulfidic conditions of deposition. *Earth and Planetary Science Letters*, *145*, 65–78. https://doi.org/10.1016/S0012-821X(96)00204-X

Davies, M. H., Mix, A. C., Stoner, J. S., Addison, J. A., Jaeger, J., Finney, B., & Wiest, J. (2011). The deglacial transition on the southeastern Alaska Margin: Meltwater input, sea level rise, marine productivity, and sedimentary anoxia. *Paleoceanography and Paleoclimatology*, *26*, PA2223. https://doi.org/10.1029/2010PA002051

Fox J, Weisberg S (2019). An R Companion to Applied Regression, Third edition. Sage, Thousand Oaks CA.

Gooday, A. J., & Jorissen, F. J. (2012). Benthic Foraminiferal Biogeography: Controls on Global Distribution Patterns in Deep-Water Settings. *Annual Review of Marine Science*, *4*(1), 237–262. https://doi.org/10.1146/annurev-marine-120709-142737

Gooday, A. J. (1993). Deep-sea benthic foraminiferal species which exploit phytodetritus: Characteristic features and controls on distribution. *Marine Micropaleontology*, *22*(3), 187–205. https://doi.org/10.1016/0377-8398(93)90043-W

Gray, W. R., Rae, J. W. B., Wills, R. C. J., Shevenell, A. E., Taylor, B., Burke, A., et al. (2018). Deglacial upwelling, productivity and CO2 outgassing in the North Pacific Ocean. Nature Geoscience, 11(5), 340–344. https://doi.org/10.1038/s41561-018-0108-6

Gulick, S. P. S., Jaeger, J. M., Mix, A. C., Asahi, H., Bahlburg, H., Belanger, C. L., et al. (2015). Mid-Pleistocene climate transition drives net mass loss from rapidly uplifting St. Elias Mountains, Alaska. *Proceedings of the National Academy of Sciences*, *112*(49), 15042 – 15047. https://doi.org/10.1073/pnas.1512549112

Hayward, B. W., Grenfell, H. R., Carter, R., & Hayward, J. J. (2004). Benthic foraminiferal proxy evidence for the Neogene palaeoceanographic history of the Southwest Pacific, east of New Zealand. *Marine Geology*, *205*(1), 147–184. https://doi.org/10.1016/S0025-3227(04)00022-2

Jaccard, S. L., & Galbraith, E. D. (2012). Large climate-driven changes of oceanic oxygen concentrations during the last deglaciation. *Nature Geoscience*, *5*(2), 151–156. https://doi.org/10.1038/ngeo1352

Jorissen, F. J., Fontanier, C., & Thomas, E. (2007). Paleoceanographical proxies based on deep-sea benthic foraminiferal assemblage characteristics. In C. Hillaire–Marcel & A. De Vernal (Eds.), *Proxies in Late Cenozoic Paleoceanography* (Vol. 1, pp. 263–325). Elsevier. https://doi.org/10.1016/S1572-5480(07)01012-3

Keeling, R. F., Körtzinger, A., & Gruber, N. (2010). Ocean deoxygenation in a warming world. *Annual Review of Marine Science*, *2*(1), 199–229. https://doi.org/10.1146/annurev.marine.010908.163855

Kim, S. (2015) ppcor: An R Package for a Fast Calculation to Semi-partial Correlation Coefficients. Communications for Statistical Applications and Methods, 22(6), 665-674.

Korsun, S., & Hald, M. (2000). Seasonal dynamics of benthic foraminifera in a glacially fed fjord of Svalbard, European Arctic. *Journal of Foraminiferal Research*, *30*(4), 251–271. https://doi.org/10.2113/0300251

Legendre, P., & Legendre, L. (2012). *Numerical Ecology*. Elsevier Science. Retrieved from https://books.google.com/books?id=6ZBOA-iDviQC

McCune, B., Grace, J. B. J. B., & Urban, D. L. (2002). Analysis of Ecological Communities. *MjM Software Design* (Vol. 28). Gleneden Beach, OR.

McManus, J., Berelson, W., Severmann, S., Poulson, R., Hammond, D., Klinkhammer, G., & Holm, C. (2006). Molybdenum and uranium geochemistry in continental margin sediments: Paleoproxy potential. *Geochimica et Cosmochimica Acta*, *70*, 4643–4662. https://doi.org/10.1016/j.gca.2006.06.1564

Moffitt, S. E., Moffitt, R. A., Sauthoff, W., Davis, C. V, Hewett, K., & Hill, T. M. (2015). Paleoceanographic insights on recent oxygen minimum zone expansion: Lessons for modern oceanography. PLOS ONE, 10(1), e0115246. https://doi.org/10.1371/journal.pone.0115246

Ohkushi, K., Thomas, E., & Kawahata, H. (1999). Abyssal benthic foraminifera from the northwestern Pacific (Shatsky Rise) during the last 298 kyr. *Marine Micropaleontology*, *38*(2), 119–147. https://doi.org/https://doi.org/10.1016/S0377-8398(99)00040-7

Ohkushi, K., Itaki, T., & Nemoto, N. (2003). Last Glacial–Holocene change in intermediate-water ventilation in the Northwestern Pacific. *Quaternary Science Reviews*, *22*(14), 1477–1484. https://doi.org/10.1016/S0277-3791(03)00082-9

Ohkushi, K., Kennett, J. P., Zeleski, C. M., Moffitt, S. E., Hill, T. M., Robert, C., et al. (2013). Quantified intermediate water oxygenation history of the NE Pacific: A new benthic foraminiferal record from Santa Barbara basin. *Paleoceanography*, *28*(3), 453–467. https://doi.org/10.1002/palo.20043

Oksanen, J., Blanchet, F. G., Friendly, M., Kindt, R., Legendre, P., McGlinn, D., et al. (2017). Vegan: Community ecology package. Retrieved from cran.r-project.org/package=vegan

Paulmier, A., & Ruiz-Pino, D. (2009). Oxygen minimum zones (OMZs) in the modern ocean. Progress in Oceanography, 80(3), 113–128. https://doi.org/10.1016/j.pocean.2008.08.001

Payne, C. R., & Belanger, C. L. (2021). Enhanced Carbonate Dissolution Associated with Deglacial Dysoxic Events in the Subpolar North Pacific. *Paleoceanography and Paleoclimatology*, *36*(4), e2020PA004206. https://doi.org/https://doi.org/10.1029/2020PA004206

Praetorius, S. K., Condron, A., Mix, A. C., Walczak, M. H., McKay, J. L., & Du, J. (2020). The role of Northeast Pacific meltwater events in deglacial climate change. *Science Advances*, *6*(9). https://doi.org/10.1126/sciadv.aay2915

Praetorius, S. K., Mix, A. C., Walczak, M. H., Wolhowe, M. D., Addison, J. A., & Prahl, F. G. (2015). North Pacific deglacial hypoxic events linked to abrupt ocean warming. *Nature*, *527*, 362–366. https://doi.org/10.1038/nature15753

Sakai, K., Ohkushi, K., & Shibahara, A. (2021). Biotic response of benthic foraminifera to OMZ variations in the northwestern Pacific since the last deglaciation. *Geo-Marine Letters*, *41*. https://doi.org/10.1007/s00367-020-00671-7

Sharon, Belanger, C., Du, J., & Mix, A. (2021). Reconstructing paleo-oxygenation for the last 54,000 years in the Gulf of Alaska using cross-validated benthic foraminiferal and geochemical records. *Paleoceanography and Paleoclimatology*, 36, e2020PA003986. https://doi.org/10.1029/2020PA003986

Stabeno, P. J., Bond, N. A., Hermann, A. J., Kachel, N. B., Mordy, C. W., & Overland, J. E. (2004). Meteorology and oceanography of the Northern Gulf of Alaska. *Continental Shelf Research*, *24*(7–8), 859–897.

Sun, X., Corliss, B. H., Brown, C. W., & Showers, W. J. (2006). The effect of primary productivity and seasonality on the distribution of deep-sea benthic foraminifera in the North Atlantic. *Deep Sea Research Part I: Oceanographic Research Papers*, *53*(1), 28–47. https://doi.org/10.1016/j.dsr.2005.07.003

Tetard, M., Licari, L., & Beaufort, L. (2017). Oxygen history off Baja California over the last 80 kyr: A new foraminiferal-based record. *Paleoceanography*, *32*. https://doi.org/10.1002/2016PA003034

Tribovillard, N., Algeo, T. J., Lyons, T., & Riboulleau, A. (2006). Trace metals as paleoredox and paleoproductivity proxies: An update. *Chemical Geology*, *232*(1), 12–32. https://doi.org/10.1016/j.chemgeo.2006.02.012

Walczak, M. H., Mix, A. C., Cowan, E. A., Fallon, S., Fifield, L. K., Du, J., et al. (2020). Phasing of millennial-scale climate variability in the pacific and Atlantic oceans. Science, 370, 716–720. https://doi.org/10.1126/science.aba7096

Wie, T. and Simko, V. (2017). R package "corrplot": Visualization of a Correlation Matrix (Version 0.84).

Venables, W. N. and Ripley, B. D. (2002) Modern Applied Statistics with S. Fourth edition. Springer

Zheng, Y., Anderson, R. F., van Geen, A., & Kuwabara, J. (2000). Authigenic molybdenum formation in marine sediments: a link to pore water sulfide in the Santa Barbara Basin. *Geochimica et Cosmochimica Acta*, *64*(24), 4165–4178. https://doi.org/10.1016/S0016-7037(00)00495-6/10.1016/S0016-7037(00)00495-6

4.7. Supplemental Figures and Tables

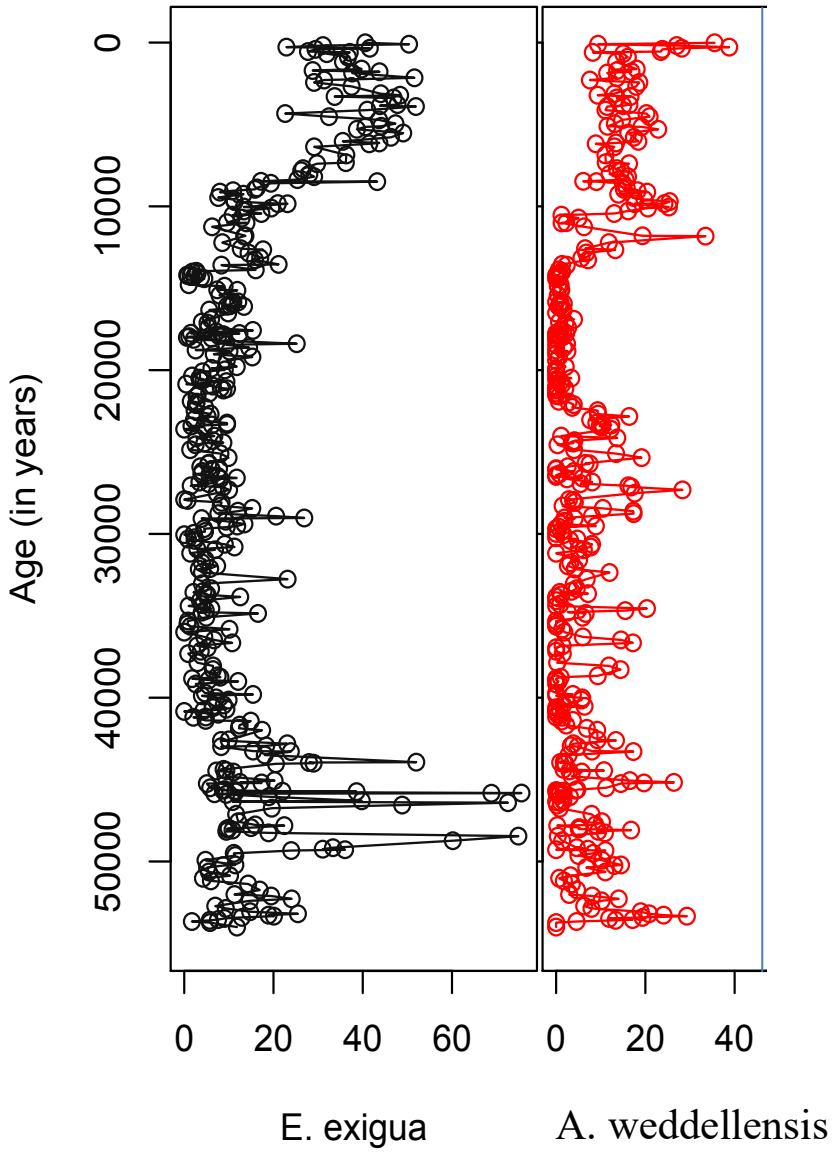

Figure 4.7 Proportional abundances of E. exigua and A. weddellensis which when summed have been called %opportunists.

Supplemental Table 4.1= Species data same as Chapter 2.

Supplemental Table 4.2= Species oxygen preferences same as Chapter 2 and 3.

Supplemental Table 4.3= PCO site scores full data, older subset, younger subset.

Supplemental Table 4.4= PCO species scores full data, older subset, younger subset.

Supplemental Table 4.5= All proxy data (isotopes, metals, %dysoxic, %opportunists, SST).

Supplemental Table 4.6= Older subset p values for Pearson correlations.

Supplemental Table 4.7= Younger subset p values for Pearson correlations.

5. CONCLUSIONS

In Chapter 2, I found that both the benthic foraminifera and geochemical trace sensitive metals show several dysoxic events during the ~54, 000 years record in the Gulf of Alaska (GoA). Dysoxic events were not only restricted to the deglacial but were also found during the glacial interval. Moreover, two dysoxic events during the glacial were as severely dysoxic as the Bølling-Allerød dysoxic event. On using different size fractions, I found that using >125 μm size fraction produces similar trends of oxygenation as seen when the whole >63 μm size fraction data was used. However, excluding the 63 -125 μm size fraction can lead to loss of opportunistic taxa which comprised high relative abundances in several samples and can be indicative of productivity which is a possible driver of dysoxia. On modifying Behl Dissolved Oxygen (BDO) index, I figured that using only a few index taxa to reconstruct estimated paleo-oxygen value does not produce accurate estimated oxygen values as compared to using all the taxa in the dataset. Furthermore, using a few index taxa produced biased results producing lower oxygen values. Many low-oxygen events were brief suggesting that transitions between the suboxic to dysoxic conditions could occur in less than 100 years, which can be detrimental for the regional ecosystem.

In Chapter 3, on reconstructing oxygenation histories across several sites in the eastern North Pacific on the same scale using taxonomically standardized benthic foraminifera data, I found that the dysoxic events occurred around similar time intervals at distant sites at similar depths like GoA and Santa Barbara Basin, Baja Sur California.

This suggests that the dysoxic events were not just regional events but occurred basinwide and may have been linked to large scale global climatic changes. However, differences in the relative severities of dysoxia may have been enhanced due to regional influences. Furthermore, dysoxia as severe as the southern sites of SBB site (MD02-2303 and MD02-2304) and Baja California site MD02-2508 was found at GoA which is generally a better oxygenated site given its proximity to North Pacific Intermediate Waters production source. The southern sites may be more dysoxic due to the impact of low oxygen water masses from the south. The deeper sites like ODP 1017 and ODP Hole890B did not show much variation in oxygenation throughout the record. I also found that it is important for these oxygen comparisons to be among sites at a similar water depth such that faunal differences due to bathymetric gradients have limited influence; geographic distance imposed less faunal dissimilarity.

In Chapter 4, on dividing the 54,000 years data into two subsets I found that the dysoxic events in the GoA during the glacial interval may have been associated with increased temperatures or meltwater pulses along with high surface productivity. For the deglacial subset, the associations between the drivers and oxygen could not be clearly understood as they were strongly influenced by glacial-interglacial changes. However, it was implied that drivers similar to the ones that caused dysoxia during the glacial interval may have been responsible for the development in dysoxia during the deglacial as well. Furthermore, huge relative abundances of opportunistic benthic foraminifera in the Holocene suggest high surface productivity. If large amounts of freshwater due to melting of glaciers caused by global warming gets added into the GoA, it may produce the perfect

environment for development of severe dysoxia which can be devastating for the regional marine life and fisheries industry.

In conclusion, dysoxic events of similar severity occurred in the GoA during the glacial and deglacial intervals. Dysoxia as severe as the southern sites developed in the generally well-oxygenated GoA during the deglacial and interstadial events during the glacial. The dysoxic events in the GoA during the glacial were likely caused by both high productivity and warm temperatures. If conditions similar to the dysoxic events of the glacial interval occur in the of GoA, dysoxia as severe as the B-A may develop which can be detrimental for the regional ecosystem and affect the fisheries that local communities highly depend on. High seasonal productivity that contributed to past dysoxic events currently occur in the modern GoA and increase in meltwater due to rising temperatures in this glaciated margin may produce the perfect conditions for development of dysoxia which can be devastating. Finally, complete benthic foraminiferal assemblages can be efficiently utilized to understand paleoenvironmental conditions and therefore help forecast the future of our oceans and marine ecosystem.